Lemos, June

From: Jacob Patterson <jacob.patterson.esq@gmail.com>
Sent: Wednesday, July 21, 2021 11:08 AM
To: Lemos, June; Munoz, Cristal
Subject: Public Comment -- 7/26/21 City Council Meeting, Item No. 7A
Attachments: MND Attachment 7 - KASL Water Model Study for 1250 Del Mar Drive.pdf; Thompson_et_al-2021-Nature_Climate_Change.pdf; Updates to Limits of Growth.pdf; 20210714 Vice MIT Predicted in 1972 That Society Will Collapse This Century. New Research Shows We're on Schedule_.pdf; 20210719 Specktor Article.pdf; 20210628 Water and Housing Needs Collide in California's Severe Drought.pdf; 20210615 The West's Water Restriction Nightmare Is Just Beginning.pdf; 20210623 California water shortages_ Why some places are running out _ CalMatters.pdf

City Clerk's Office,

Here are a few more documents for the administrative record for the Grocery Outlet appeal scheduled for Monday the 26th. Please include this email and the attachments as public comments. Although I am not fully re-explaining them here, the attachments contain additional supporting evidence for positions raised in prior public comments or the appeals themselves, and are intended to bolster the record regarding those positions. Such concerns include but are not limited to the impact of climate change and sea level rise on the City's available water supply and other public services, which were not accounted for in the City's water supply analysis.

The "moon wobble" study relates to this issue as well and it will compound the projected impacts of sea-level rise and tidal variations on the City's current raw water sources. Since it is new and in addition to the prior comments and objections, this presents a fresh reason to question the validity of the City's purportedly complete and adequate analysis for this project. This project's contribution to these issues will be cumulatively considerable because the water supply and system are so stressed based on current and projected future conditions (also not factored into the City's existing and now outdated water model) that the City's water supply is insufficient for current development. In a situation like this, even relatively small additional water use amounts to a considerable contribution to the existing dire situation. Many communities have completely stopped additional development because of the dire drought situation that is predicted to be the new norm rather than an unusual outlier.

The KASL water study for the prior proposed project involving a Grocery Outlet in a different location is submitted in relation to the City's new, dramatically lower projections for expected water use by the newer proposed Grocery Outlet of a similar size as in the prior application, which appear to be based on projected water use figures without any discernable source or citation (i.e., an asserted but unsupported alleged "fact").

The limits to growth study update materials relate to the same issues because the staff recommendations mirror the issues and serve as local examples of the unintended consequences of local planning decisions that the 1972 MIT model predicts will lead to societal collapse in the 2040s (interestingly the decade following the predicted catastrophic changes to the moon's orbit that will likely result in massive coastal flooding and disruption of coastal environments like our own.

Thanks,

--Jacob

EXTREME WEATHER

The West's Water Restriction Nightmare Is Just Beginning

Oakley, Utah placed a moratorium on any new construction projects that would tap into the city's water system.

By Dharna Noor 6/15/21 12:56PM | Comments (4) | Alerts

Photo: Ethan Miller (Getty Images)

A small city in Utah is taking an unprecedented step to adapt to megadrought conditions in the West: halting any new construction projects that would tap into the local water. It's the first municipal ordinance of its kind.

Last month, officials from Oakley, Utah—a city of 1,500—finalized a moratorium on new development extending through November. The ordinance prohibits the "erection, construction, re-construction or alteration of any structure" that needs new water connections.

"The city is concerned that the current drought conditions will result in critical water shortages and require further drastic curtailment measures that would be detrimental to the entire city and cause significant public harm," it says.

Oakley is hardly alone, though. The West's water resources have come under increasing pressure from rising temperatures tied to the climate crisis. Heat can both melt out snowpack early and cause water stored in reservoirs to evaporate. It can also affect groundwater recharge, particularly in years with low snowfall. Explosive growth in the region has made matters worse since more homes and businesses with more lawns and more farmers with water-needy crops put extra pressure on the water system. What's happening in Oakley is a sign of what could come in other communities if the West is to stave off an even bigger water crisis.

Related Stories

- The Worst European Floods in 100 Years Have Left 120 Dead, 1,300 Missing
- In Biden's America, You'll Turn on the Shower and Nothing Comes Out, Just Drip Drip, Can't Get the Soap Off
- Red Tide Has Killed at Least 791 Tons of Fish in Florida

The measure to stop building passed amid a historic drought in Utah that has led to, among other things, the state's governor asking residents to literally pray for rain. Oakley is currently in an "extreme drought," according to the Drought Monitor, while more than 60% of the state sits in the worst category, dubbed exceptional drought.

By taking this dramatic step now, Eric Jones, a regional engineer at Utah's Division of Water Rights, said officials could help ward off the need for more "draconian measures," like restrictions on individual water usage.

"Oakley has a good understanding of their sources and is ahead of the curve," he wrote in an email.

Conserving water will be particularly important since Utah's drought is also creating conditions for catastrophic wildfires, which is shaping up to potentially be the state's worst on record. Low reservoir levels and impacts on pressure could be particularly dangerous.

“If a fire broke out in town, and the fire department came to hook into a fire hydrant to put it out, they would have no water,” Oakley Mayor Wade Woolstenhulme told a local ABC affiliate.

Even locations that are dependent on groundwater face issues. Oakley’s water sources, which include two springs and a well, are performing at lower levels than average amid the drought.

“Groundwater integrates the effects of temperature and precipitation over multiple years, so as drought conditions persist, [the] water table drops and water becomes more limited,” Paul Brooks, a hydrologist at the University of Utah, said in an email. “That makes the current exceptional heat and dry conditions a challenge for utility managers.”

The city is scheduled to bring a new well online next year as its first new source in 20 years, which could help ensure residents have more access to water. But the need for water may still outstrip the new additions. The town has seen its population grow in recent years, and it reopened an old school this year. A local city councilperson told local outlet the Park Record that the city received triple its usual number of building permits this year. The moratorium on new water connections could help ensure Oakley has enough for current residents, buying it time.

“Community leaders have a responsibility to ensure that all residents have access to safe, reliable sources of water,” Robert Adler, a law professor at University of Utah’s S.J. Quinney College of Law with expertise in environmental and water law, wrote in an email. “When growth outstrips water supply, that’s not possible, and the responsible response is to curtail growth until the balance between supply and demand can be addressed.”

Oakley’s new measure is the latest in a string of new drought adaptation policies being considered and passed by Western states and municipalities. Earlier this month, Nevada banned developers from planting new grass on street medians, traffic circles, office parks, and apartment complex entrances. In April, Oakley itself passed another ordinance to stop homeowners from installing water-intensive elements like ponds, outdoor pools, and waterfalls.

Oakley is the first town to put a moratorium in place on new building, but Adler expected more will follow suit as more growing Western cities are forced to grapple with persistent water scarcity. In fact, he said, those future policies could make Oakley’s new policy look like kid stuff, especially as they become necessary in cities with more extreme rates of growth.

“The Oakley moratorium is on the mild side of the spectrum. It is temporary, and is supposed to be lifted once a new well comes online. It also does not apply to

development permits that have already been issued, and is coupled with stricter water conservation requirements for existing users," he said.

City councilors in Oakley have said just a handful of new development proposals have been affected by the moratorium, which seems like a small price to pay to keep people safe during punishing heat and drought.

Conditions are expected to worsen this summer. This week, a heat wave has sent temperatures soaring in the West. On Tuesday, Salt Lake City—located about an hour west of Oakley—had its hottest day ever recorded when the mercury hit 107 degrees Fahrenheit (41.7 degrees Celsius). (That's also now the city's all-time high temperature for June.) Water resources will surely suffer in the blast furnace, and they'll only become more precarious as we get further into the dry season.

"Human-caused climate change has absolutely worsened drought conditions in Utah," William Anderegg, an assistant professor of biology at the University of Utah, said in an email. "A study from last year found that climate change is responsible for about half of the long-term mega-drought severity in the southwest since the early 2000s, and that is absolutely influencing the severe summer drought this year in Utah."

The West is expected to continue to dry out as the climate crisis worsens. These recent years, then, are a preview of what could come.

“No one wants to be in a situation where water supply is so limited that it needs to be rationed during times of year, especially the hottest, driest times of the year,” said Brooks.

MORE FROM GIZMODO

- Verizon Finally Embraces RCS, Now the Lone Holdout Is Apple
- *Masters of the Universe: Revelation* Is a He-Man Fan's Dream*
- *Cyberpunk 2077*'s Retrofuturistic World Is Worth Exploring Beneath the Flaws
- For the First Time Ever, Scientists Witness Chimps Killing Gorillas

EARTHER » EXTREME WEATHER

DISCUSSION

By Dense Non Aqueous Phase Liquid

I mentioned this before on Earther and I’ll mention it again. The USGS has an awesome new interactive national water data dashboard for its water information system here:

https://waterdata.usgs.gov/nwis?

The new dashboard link is at the top of the web page. The new dashboard is experimental or in beta. There’s a whole bunch of surface (lakes and rivers) and well water (groundwater) data for the entire country a mouse click away. It use to take awhile, like a long while, to see earth science data.

What's cool is one can find the city of Oakley, UT on the map. Then realize it's not too far west of Salt Lake City. Maybe it's becoming suburbanized. Maybe it's not. There's a rodeo there. Then zoom in and see that the Weber River runs through it. Then one can click to see river flow data

See all replies

CALMATTERS

ENVIRONMENT

Water shortages: Why some Californians are running out in 2021 and others aren't

BY RACHEL BECKER , JUNE 23, 2021 UPDATED JULY 14, 2021

Stevens Creek Reservoir near Cupertino is one of the reservoirs that supplies water to Santa Clara County. It is only 17% full. This photo was shot on June 7, near the beginning of the long dry season. Photo by Nhat V. Meyer, Bay Area News Group

IN SUMMARY

Drought resilience depends on location but also extraordinary engineering — determining which California places are running out of water this year and which remain in good shape.

In Los Angeles, people have been hearing about the dangers of drought for decades. But in this land of infinity pools and backyard putting greens — better suited for rattlesnakes and scrub — water never seems to run out.

Yet little Redwood Valley in Mendocino County, which gets a bountiful **38 inches** of rain in an average year and sits **near the headwaters of the Russian River**, has been devastated by this year's drought. Each resident has been told to use no more than 55 gallons per day — enough to **fill a bathtub** and flush a toilet six times.

And in San Jose, where less than half of its usual rain has fallen this year, people have been asked to cut water use by 15% — a target that could become mandatory if locals fail to comply.

When it comes to the impact of drought, location is key. Rain and snow vary greatly across California's myriad microclimates, leaving some towns, mostly in the north, accustomed to yearly refills of their rivers, reservoirs and aquifers. Others farther south have fewer natural supplies of their own, and in parts of the Central Valley, **the drought never really left**.

But drought resilience is manufactured, too. Decades of planning and extraordinary

Running out of water and time: How unprepared is California for 2021's drought?

Tulare County's never-ending drought brings dried up wells and plenty of misery

engineering and technology keep the water flowing to arid places.

As drought intensifies, state warns users to stop pumping water from major rivers

"There is, of course, no single Northern California or Southern California when it comes to water," said **Peter Gleick,** founder of the Pacific Institute, a global water think tank. "Water is a very local phenomenon. And every region and every water district has a different mix of water supply options and water demands.

This satellite image shows how full Lake Oroville, which supplies much of the state's drinking water, was in June 2019 and how shallow and dry it is in June 2021. It's currently holding only 41% of its historic average for this time of year. Credit: NASA Credit: **NASA**

During the last drought, in 2015, Californians were ordered to cut their water use by an average **of 25% statewide**. This time, there is **no statewide emergency**, no universal mandate and no standardized water waste rules.

Instead, residents are facing a patchwork of restrictions. Bracing for a crisis, towns relying on the hard-hit Russian River have imposed stringent mandates on residents and coastal communities may have to truck in water to make it through the year. At the same time, most of California's urban hubs are prepared to weather the summer with only voluntary cuts and limited restrictions that in many cases are holdovers from previous droughts.

A CalMatters survey of the state's 10 largest water agencies found only one — in San Jose — has issued **new limits** on watering yards, washing cars and other outdoor uses. Eight, including **Sacramento**, already had rules curbing irrigation and water waste on the books. And four, including water agencies in the **East Bay** and **Riverside**, have asked people to voluntarily cut back between 10% and 25%.

Even though Southern California is more arid, it's better hydrated, too: That's because it has largely relied on water transported from elsewhere, dating back more than 100 years in Los Angeles and 50 years in neighboring cities and counties. About half of the water that flows from **taps in the region is imported**, while half comes from carefully nurtured groundwater reserves and recycled sewage.

As a result, Los Angeles residents are unlikely to face new water restrictions this summer. After a soggy 2019 plus declines in water use since the last drought, the Metropolitan Water District, which supplies imported water to 19 million people in six counties, **entered 2021** with record levels of water in storage.

The grip of drought even varies within single counties. For instance, one Mendocino County town is flush with recycled water and groundwater stores, but in another, residents are ordered to reduce use.

"We have a patchwork in part because (water) is managed locally," said **Felicia Marcus**, who led the state's response to the 2012-2016 drought under former Gov. Jerry Brown.

"The situation is dire in some places, and those places are making calls for higher levels of conservation," Marcus said. "In other places, they may be prepared, or they may be dreaming."

Southern California's manufactured resilience

Southern California goes to extraordinary lengths to **take water from elsewhere**. This nature-defying engineering keeps the region replete with water even when little falls from the sky. (Downtown Los Angeles averages **about 14 inches per year**, about a third as much as Mendocino.)

First came the city of **Los Angeles' aqueduct** — backed by **San Fernando Valley investors** and approved by voters in 1905 — sucking up mountain-fed streams and lakes in the Owens Valley and transporting it 137 miles.

But it wasn't enough.

Then came the Metropolitan Water District's aqueduct, drawing from California's share of the Colorado River, snaking through the desert and tunneling through mountains to deliver water to the Los Angeles basin in 1941.

But that wasn't enough, either.

Finally, the state in **the 1960s began building** a massive system to carry river water from Northern California, pumping it over the Tehachapi Mountains and through **700 miles** of pipelines and channels to deliver it to San Joaquin Valley farmland and 27 million people, **mostly in Southern California**.

And that is enough — for now.

These three extraordinary engineering feats have made much of Southern California able to pull water from a variety of places all at once, transforming its landscape and satisfying the region's thirst.

Los Angeles County also pioneered recycled water, building the nation's **first reclamation plant in 1962** to treat sewage and use it to replenish its aquifers. Neighboring Orange County has been a world leader in recycling

water, **purifying its own sewage** and capturing the Inland Empire's to feed its groundwater.

San Diego, too, has built up its resilience since the last drought. For decades it was almost **totally reliant on Metropolitan Water District's imported** water. But since the 1990s, the San Diego County Water Authority has added desalinated and recycled water, built one dam and raised another, pumped groundwater and cut a deal to get Colorado River water from Imperial County. The water authority announced the region is "drought-safe this summer" with "no shortages or mandates in the forecast."

Stephanie Pincetl, director of UCLA's California Center for Sustainable Communities, who has **studied Southern California's reliance on distant water sources**, said the decisions had far-reaching, if unintended, consequences: Los Angeles' **water grab from the Owens Valley** exploited distant ecosystems, and urban sprawl was fueled by the Metropolitan Water District's imports.

"It's really the growth machine of Southern California … by providing all this water to inland places, and allowing the sense that there's unlimited water and the sense that you can build as far as the eye can see," Pincetl said.

Construction of the 137-mile Los Angeles Aqueduct, which brought water from the Owens River to the San Fernando Valley, began in 1907 and took six years.

Still, she said, "You can point fingers a lot, but you can also be reassured that you can actually turn the tap on and have water come out of it, most of the time."

But is it enough to weather droughts aggravated by climate change?

This year, California regulators announced that they **would deliver only 5%** of the State Water Project's supplies because of extreme drought conditions.

Metropolitan, flush with funds from the cities and agencies it supplies, has spent billions to store water, nearly doubling its reservoir capacity with the completion of the **$1.9 billion** reservoir at **Diamond Valley Lake in 2000**.

Between stowing water in reservoirs, pouring it into aquifers and banking it in Lake Mead, Metropolitan Water District's storage has increased **13-fold since 1980**, shoring up supplies for residents from Ventura to San Diego to San Bernardino.

Los Angeles also doesn't anticipate issuing new water use restrictions, at least not yet.

"We don't see any need right now, because storage levels are still very good," said Delon Kwan, the Los Angeles Department of Water and Power's assistant director of water resources. "If you still have water in storage, why are you asking customers to do more?"

> **"Maybe Southern California is happy this year and jumping up and down. But if this drought continues for two more years, what will happen? Would they be as happy in two years?".**
>
> – NEWSHA AJAMI, STANFORD UNIVERSITY'S WATER IN THE WEST PROGRAM

But water experts caution about the potential for more dry days ahead, exacerbated by climate change, so a gallon of water used now is one less

saved for later.

“Maybe Southern California is happy this year and jumping up and down. But if this drought continues for two more years, what will happen? Would they be as happy in two years?” said **Newsha Ajami**, director of urban water policy at Stanford University’s Water in the West program.

Deven Upadhyay, Metropolitan’s chief operating officer, said that it could take several dry years in a row before the district imposes mandatory reductions in Southern California. “If we just continue to get dry year after dry year after dry year, there’s going to come a time where we’re going to be wrapping up messaging and asking for mandatory reductions. But that’s not where we are right now,” he said.

Imported water, recycled wastewater and collected stormwater runoff are used for irrigation and fountains at Los Angeles County’s Descanso Gardens in La Cañada Flintridge. Photo by Pablo Unzueta, CalMatters

Still, some parts of Los Angeles County are already struggling.

Palmdale, an aerospace hub in the Mojave Desert north of Los Angeles, draws water from snowmelt off the San Gabriel Mountains, taps into the State Water Project directly and pumps groundwater to supply more than 120,000 people.

The Palmdale Water District doesn't have enough storage to bank water during wet years or enough money to easily increase its supply.

"We're not as financially nimble as some of the really big players," said **Peter Thompson**, Palmdale's director of resource and analytics. "We're just getting to the point where we can start investing in those projects that have already benefited places like Metropolitan."

Residents of this desert city, where **less than an inch of rain** has fallen this year, were asked in the spring to **voluntarily cut water use** by 15%. In July, the water district's board may consider making it mandatory.

"Out in the desert, you need more water to keep things alive. So when we experience drought, then you also experience increased demand," Thompson said. "That's one of those double-edged swords that we deal with out here."

Mendocino County's isolation means no resilience

Water is much more precarious in Mendocino County, which is isolated from state and federal aqueducts. Instead, residents rely on patchy aquifers and water that's stored in **Lake Mendocino** and released into the Russian River.

Properties for sale along the oak-lined roads of Redwood Valley boast their water sources in the listings. One **$675,000 home** touts a water district hook-up and a seasonal spring. **Another $699,000** listing flaunts its "elaborately designed 22,000 gallon water storage system."

Known for its wine, weed and wild coast, Mendocino County was one of the first places where California Gov. Gavin Newsom **declared a drought emergency**.

In other parts of the state, "when there's a problem, there's a pipe and there's a canal, and you can connect one water system to the next," said Mendocino County Supervisor **Glenn McGourty** in a **June meeting** of the county's drought task force. "We don't have things like that in Mendocino County, so we're going to have to be really creative in our solutions."

This year's drought is the most dire situation they've faced in decades. At the end of May, Lake Mendocino **hit a record low of just 40% capacity**. Earlier this month, the county faced projections that the reservoir could be dry by the end of the year. In response, the state adopted **emergency regulations** that could stop 2,400 water right holders from diverting water from the Russian River as early as July 5.

Lake Mendocino in January 2020. Photo by Anne Wernikoff, CalMatters

Lake Mendocino in January 2021. Photo by Bobby Cochran Photography

Although Redwood Valley lies just north of Lake Mendocino, its water supply is never guaranteed. Residents rely on sales from a nearby water agency and any surplus left in the reservoir by nearby communities.

But at this point, there's no surplus. Agricultural connections have been shut off in Redwood Valley and residents **are limited** to 55 gallons per person per day — enough **for just a 22-minute shower** and nothing else.

"My dream was to garden," said Darrell Carpenter, a 61-year-old artist and handyman whose family has lived in Redwood Valley for three generations. Carpenter moved back full time after his partner died six years ago. When the water restrictions and rate changes were announced, he wondered, "Do I sell and move?"

Carpenter was lucky, able to restart an inactive well on his property and keep his garden alive, which he has slowly been converting to native plants and succulents. Still, he worries that his luck and the water will run out as more people stick straws into the ground.

“It might be a false sense of security,” he said.

Darrell Carpenter is converting his garden in Redwood Valley to native and drought-resistant plants. Photo courtesy of Carpenter

The water district’s cuts have left the reservation for the Redwood Valley Band of Pomo Indians with nothing to refill its tank for irrigating a community garden and filling its fire truck. Hydrants are still operating, but outdoor water use is banned and rancheria officials are investigating whether they can draw water from an old well.

“We don’t have any access to any other water,” said tribal administrator Mary Camp. “We’re really concerned.”

Farther out along the coast, in the town of Mendocino, residents depend on private wells pumping from rain-fed groundwater stores. The town declared **a stage 4 water shortage emergency** in May requiring residents to use 40% less water than allotted.

"I'm nervous. I'm definitely nervous," said Mendocino City Community Services District Superintendent Ryan Rhoades. "I'm sure that some wells will run dry this year, probably more than last year."

McGourty, the Mendocino County supervisor, blamed the county's predicament on its limited water storage.

"We've been lulled into the idea maybe that we have lots and lots of water. And we do have lots and lots of water. The problem is that we don't store lots and lots of water," McGourty told water officials across the region. "We're in a different world now, because of climate change."

"We don't have any access to any other water…We're really concerned."

– MARY CAMP, REDWOOD VALLEY BAND OF POMO INDIANS

Ukiah, just ten miles from hard-hit Redwood Valley, is weathering the drought much better because of steps taken after the last dry spell.

Five decades ago, the Doobie Brothers **described Ukiah** as a land where "mountain streams that rush on by show the fish a jumpin.'" Today the city is facing extremely dry conditions in the Russian River, which typically makes up about half of the supply for its 16,000 residents.

Ukiah will lean more heavily on groundwater, bolstered after the last drought with a state grant that helped pay for three new wells. The city also built a $34 million recycled water plant that pumps out irrigation water, making up a third of its supply.

"The city saw the writing on the wall, and was looking to improve our drought resiliency, before it was cool," said Sean White, director of water resources for the city of Ukiah.

"It's kind of a disparate tale. If you live in the city of Ukiah, (the drought) is really not that big of a deal … If you live in some of the adjoining ones, it's either bad or terrible."

Silicon Valley's perfect storm

In Silicon Valley, aging dams and drought have collided this year, making Santa Clara County among the hardest hit in the Bay Area. Storage in reservoirs has dwindled by 74%. And supplies from state and federal aqueducts have dropped far below expected levels.

Making matters worse, the area's largest reservoir is all but empty, drained last year to retrofit it for earthquakes. Without it, the amount of water stored locally for 2 million people in **San Jose and nearby communities** has been cut by more than half.

"We're seeing the perfect storm building up and it's right in front of us," said **Rick Callender**, Valley Water's CEO, at a June board meeting. "We're indeed in a dire situation."

If dry conditions persist through next year, land could sink and wells could go dry. In the southern part of Santa Clara County, groundwater is the only drinking water source.

"The aggressiveness and the severity of this drought, the way the drought is increasing is much greater than the previous drought," **Aaron Baker**, chief operating officer at Valley Water, said at the hearing. "Conditions will be far worse in 2022 if drought conditions continue and no action is taken."

Valley Water's board this month **ordered a mandatory 33% cut** in residential water use from 2013 levels — a 15% reduction from 2019. Individual water providers will enforce it, which means rules for residents could vary depending on who sends water to their taps.

> **"Conditions will be far worse in 2022 if drought conditions continue and no action is taken."**
>
> **– AARON BAKER, VALLEY WATER**

Cupertino's director of public works, **Roger Lee**, warns that if water providers fail to coordinate, it could lead to a patchwork of restrictions in neighborhoods served by multiple retailers.

"We can have customers with one set of rules on one side of the street and different sets of rules on the other side of the street," Lee said at the hearing. "It gets very difficult with messaging."

Marin County's largest water provider, too, has been hit hard by shortages in its own reservoirs and those in Mendocino and Sonoma counties. Marin Water, which aims to cut use across the county by 40%, has banned watering plants during the day and limited sprinklers to two days a week, among other **mandatory restrictions**,

Most of the Bay Area isn't in such dire straits — at least not yet. Residents of the East Bay were asked to reduce water use by 10%, and San Francisco golf courses, parks and other irrigation customers were asked to cut back. Both water districts already prohibit wasteful use, like washing down sidewalks.

And both, like Los Angeles, pipe water from far away.

The East Bay's aqueducts snake about 90 miles from **the Pardee Reservoir in the Sierra foothills**, delivering the vast majority of the utility's supply.

"Our forefathers (thought) to create this massive infrastructure that has been our source, our lifeline to the East Bay and has positioned us well during these dry times," said Tracie Morales, an East Bay Municipal Utility

District spokesperson. Still, Morales said, "We're concerned about what another dry year will bring."

San Francisco, where residential use per person falls well below the state average, draws **about 85%** of its water from Yosemite's Hetch Hetchy, which was **dammed in 1923**, flooding the territory of **the Tuolumne Me-Wuk people**. San Francisco's reservoirs remain in decent shape **at 75% of maximum storage**, said spokesperson Will Reisman.

"The Santa Clara Valley used to be orchards here, but we didn't have the population that San Francisco had and we didn't have the impetus of the 1906 quake and the resulting fires to go grab the Hetch Hetchy water," said **Gary Kremen**, vice chair of Valley Water's board of directors. "They were there first, so they got the better deal."

Counties urgently seeking state help

Some areas, like Santa Clara, are looking for Newsom to expand drought emergencies that could unleash greater enforcement powers and reduce regulations to speed construction products and ease pricey purchases of emergency water supplies.

Compared to the counties already under drought emergencies, "we're in just as bad shape as them, if not worse," Kremen said at a press briefing.

Palmdale spokesperson Judy Shay also said her water district is looking for stronger messaging from the state as it ramps up its drought response.

"We also don't want to be the ones making all those strict rules," Shay said. "We also need direction from the state."

An oak woodland is among the lush features at Descanso Gardens in La Cañada Flintridge. The Los Angeles region was transformed with the use of imported water and recycled wastewater. Pablo Unzueta for CalMatters

The Pacific Institute's Gleick calls for urgent collective action throughout the West.

"The speed with which the western drought is accelerating and worsening makes it urgent that the governors of the western states declare water conservation mandates and targets and provide resources to help cities and farms cut water use," Gleick said.

The issue is bigger than simply responding to the current drought, said UCLA's Pincetl. Californians will need to reimagine what the future could look like and rethink their relationship to water.

"We don't actually know where we live ... we live in this kind of irrigated bubble that insulates us from the actual California," Pincetl said. "And having easily accessible water is part of that story."

Rachel Becker

rachel@calmatters.org

Rachel Becker is a reporter with a background in scientific research. After studying the links between the brain and the immune system, Rachel left the lab bench with her master's degree to become a journalist... **More by Rachel Becker**

Environment & Energy

Water and Housing Needs Collide in California's Severe Drought

By Emily C. Dooley

June 28, 2021, 3:00 AM

- 85% of California is experiencing extreme drought
- Hundreds of thousands of homes need building each year

Housing advocates and developers are warily watching California's intensifying drought and what it may mean in a state that needs millions of new homes to house its residents.

Eighty-five percent of the state is in extreme drought. And in coastal Marin County, north of San Francisco, rainfall is at its lowest levels since records began 140 years ago.

It's here where the state's twin issues of housing stock and water availability are colliding. But it could be a harbinger of things to come for the rest of the state.

Additional housing puts more stress on water supplies. The housing and water conflict "piles one major policy crisis on top of another," said Richard Frank, director of the California Environmental Law & Policy Center at University of California, Davis.

Gov. Gavin Newsom (D) signed executive orders in April and May declaring 41 counties in a drought state of emergency, giving water regulators more authority to manage water use and diversions.

At the same time, an estimated 120,000 affordable homes need to be built each year through 2030 to meeting housing needs, particularly for extremely low-income residents, according to a 2021 report from the California Housing Partnership, a nonprofit affordable housing group.

"I'm afraid I do think it's going to become a bigger issue," Partnership CEO and President Matt Schwartz said.

Stalled Project

Consideration of a moratorium on new water connections by the Marin Municipal Water District has already stalled one affordable housing project and could hurt another one 10 years in the making. The district has scheduled a July 6 meeting to discuss the moratorium.

Vivalon, a nonprofit in Marin County, is working on its final permits to build what's called an healthy aging center, with support services for older county residents on two floors and 66 affordable apartments on four higher floors. The wait list has more than 400 names.

"The last moratorium was four to five years," Vivalon Chief Executive Anne Grey said in an interview. "That's just time we don't have."

The $48 million project will have trouble getting financing without water.

"It could stop the project dead in the tracks," she said. "People are counting on this housing for the future of the community."

A 74-unit multifamily complex already approved by the county for low- and extremely low-income residents is also in limbo, said Alexis Gevorgian, a managing member for AMG & Associates, a developer.

The project in Marin City was the first development proposal submitted to the county under new state laws meant to streamline housing developments. Gevorgian was hoping to break ground in three to four months.

But he needs a letter from the water district promising service. Without that, he said, "we can't get our state and federal subsidies to build our project."

'Dire Situation'

Marin Water District held off on approving the moratorium after a lengthy meeting, where board members considered exempting affordable housing projects. A new vote hasn't been scheduled.

"It's important we not be increasing demand on a system that is already taxed," Marin Water District President Cynthia Koehler said in an interview. "We just need to send a pretty clear signal this is a dire situation."

Grey and Gevorgian are hoping affordable housing will get a pass or special consideration.

"I'm hoping the water district is sympathetic to our need," Grey said.

During the 2012 to 2106 drought, California water regulators issued 21 orders barring water districts from allowing new connections and ordering existing promises of water availability null and void if building permits weren't in place before certain deadlines.

The orders were issued in northern, central, and coastal California and targeted districts that had water rights that were junior to other users, such as agriculture and irrigation districts.

The same could happen during this drought, though it would likely affect smaller water systems and not large, urban suppliers where housing developments are typically based, said Darrin Polhemus, deputy director for drinking water programs at the State Water Resources Control Board.

“I don’t see a big impact on the state housing stock,” he said.

Legal Remedy?

During the last drought, the Hidden Valley Lake Community Services Water District west of Sacramento sued to overturn a state order prohibiting it from adding new connections beyond the more than 2,400 already in operation.

The district eventually won because they argued their supply came from groundwater and not surface water, over which the State Water Resources Control Board has regulatory power. The 2014 moratorium wasn’t lifted until July 2020.

Developers who secure water availability agreements from a local government like a county that then issues a moratorium could have some legal recourse, otherwise the cases are hard to fight, said a water rights and real estate attorney who spoke on condition of anonymity due to ongoing client representations.

Developers could, however, get special agreements in advance that they’re exempt from moratoriums, as a development in Half Moon Bay south of San Francisco was able to do several years ago, the California Housing Partnership’s Schwartz said.

For Grey, a lawsuit wouldn’t be possible for the nonprofit.

“We wouldn’t have the bandwidth to do that because it would be too expensive,” she said. “We can’t put our other services in jeopardy for an unknown outcome. It’s too risky.”

New NIMBY Threat

Housing is needed throughout the state. Where housing opponents usually cite traffic concerns, water concerns could become one more way to thwart development.

“Frankly, I think they’re looking for new bullets to tie things up,” Schwartz said. “I think the next one will be water.”

He is considering sponsoring a bill in the state legislature that would exempt affordable housing projects from moratoriums. Unlike single-family homes, affordable housing developments rarely have elaborate landscaping and come with water-efficient appliances and plumbing.

“We’ve got to get out in front of this,” Schwartz said.

Whether there’s a formal moratorium or not , developers could see pushback at the local level when it comes to building permits and NIMBY residents, said Steve Cruz, a consultant on water and resource issues for the California Building Industry Association.

Prohibiting new connections also won’t solve a problem and could force people into older homes that are less water-efficient.

“It’s not really addressing the problem,” Cruz said. “You’re not going to take us out of drought because you’re taking away new development.”

To contact the reporter on this story: Emily C. Dooley at edooley@bloombergindustry.com

To contact the editor responsible for this story: Chuck McCutcheon at cmccutcheon@bloombergindustry.com

Documents

Document
California Housing Partnership report

Related Articles

California Drought Is So Bad Almond Farms Are Ripping Out Trees — June 23, 2021, 4:00 AM

Drought Complicates California’s Tight Housing Market — Sept. 10, 2015, 4:35 PM

MOTHERBOARD
TECH BY VICE

MIT Predicted in 1972 That Society Will Collapse This Century. New Research Shows We're on Schedule.

A 1972 MIT study predicted that rapid economic growth would lead to societal collapse in the mid 21st century. A new paper shows we're unfortunately right on schedule.

NA By Nafeez Ahmed

July 14, 2021, 6:00am

IMAGE: GETTY

A remarkable new study by a director at one of the largest accounting firms in the world has found that a famous, decades-old warning from MIT about the risk of industrial civilization collapsing appears to be accurate based on new empirical data.

As the world looks forward to a rebound in economic growth following the devastation wrought by the pandemic, the research raises urgent questions about the risks of attempting to simply return to the pre-pandemic 'normal.'

In 1972, a team of MIT scientists got together to study the risks of civilizational collapse. Their system dynamics model published by the Club of Rome identified impending 'limits to growth' (LtG) that meant industrial civilization was on track to collapse sometime within the 21st century, due to overexploitation of planetary resources.

The controversial MIT analysis generated heated debate, and was widely derided at the time by pundits who misrepresented its findings and methods. But the analysis has now received stunning vindication from a study written by a senior director at professional services giant KPMG, one of the 'Big Four' accounting firms as measured by global revenue.

Limits to growth

The study was published in the *Yale Journal of Industrial Ecology* in November 2020 and is available on the KPMG website. It concludes that the current business-as-usual trajectory of global civilization is heading toward the terminal decline of economic growth within the coming decade—and at worst, could trigger societal collapse by around 2040.

The study represents the first time a top analyst working within a mainstream global corporate entity has taken the 'limits to growth' model seriously. Its author, Gaya Herrington, is Sustainability and Dynamic System Analysis Lead at KPMG in the United States. However, she decided to undertake the research as a personal project to understand how well the MIT model stood the test of time.

The study itself is not affiliated or conducted on behalf of KPMG, and does not necessarily reflect the views of KPMG. Herrington performed the research as an extension of her Masters thesis at Harvard University in her capacity as an

Tech

New Report Suggests 'High

explaining her project on the GNHC website as follows:

Civilization Coming to an End' Starting in 2050

NAFEEZ AHMED

06.03.19

"Given the unappealing prospect of collapse, I was curious to see which scenarios were aligning most closely with empirical data today. After all, the book that featured this world model was a bestseller in the 70s, and by now we'd have several decades of empirical data which would make a comparison meaningful. But to my surprise I could not find recent attempts for this. So I decided to do it myself."

Titled 'Update to limits to growth: Comparing the World3 model with empirical data', the study attempts to assess how MIT's 'World3' model stacks up against new empirical data. Previous studies that attempted to do this found that the model's worst-case scenarios accurately reflected real-world developments. However, the last study of this nature was completed in 2014.

The risk of collapse

Herrington's new analysis examines data across 10 key variables, namely population, fertility rates, mortality rates, industrial output, food production,

ecological footprint. She found that the latest data most closely aligns with two particular scenarios, 'BAU2' (business-as-usual) and 'CT' (comprehensive technology).

"BAU2 and CT scenarios show a halt in growth within a decade or so from now," the study concludes. "Both scenarios thus indicate that continuing business as usual, that is, pursuing continuous growth, is not possible. Even when paired with unprecedented technological development and adoption, business as usual as modelled by LtG would inevitably lead to declines in industrial capital, agricultural output, and welfare levels within this century."

Study author Gaya Herrington told *Motherboard* that in the MIT World3 models, collapse "does not mean that humanity will cease to exist," but rather that "economic and industrial growth will stop, and then decline, which will hurt food production and standards of living… In terms of timing, the BAU2 scenario shows a steep decline to set in around 2040."

THE 'BUSINESS-AS-USUAL' SCENARIO (SOURCE: HERRINGTON, 2021

In the comprehensive technology (CT) scenario, economic decline still sets in around this date with a range of possible negative consequences, but this does not lead to societal collapse.

THE ‘COMPREHENSIVE TECHNOLOGY’ SCENARIO (SOURCE: HERRINGTON, 2021

Unfortunately, the scenario which was the least closest fit to the latest empirical data happens to be the most optimistic pathway known as ‘SW’ (stabilized world), in which civilization follows a sustainable path and experiences the smallest declines in economic growth—based on a combination of technological innovation and widespread investment in public health and education.

)THE ‘STABILIZED WORLD’ SCENARIO (SOURCE: HERRINGTON, 2021)

Although both the business-as-usual and comprehensive technology scenarios point to the coming end of economic growth in around 10 years, only the BAU2 scenario “shows a clear collapse pattern, whereas CT suggests the possibility of future declines being relatively soft landings, at least for humanity in general.”

Both scenarios currently “seem to align quite closely not just with observed data,” Herrington concludes in her study, indicating that the future is open.

A window of opportunity

While focusing on the pursuit of continued economic growth for its own sake will be futile, the study finds that technological progress and increased investments in public services could not just avoid the risk of collapse, but lead to a new stable and prosperous civilization operating safely within planetary boundaries. But we really have only the next decade to change course.

indicate a slowdown and eventual halt in growth within the next decade or so, but World3 leaves open whether the subsequent decline will constitute a collapse," the study concludes. Although the 'stabilized world' scenario "tracks least closely, a deliberate trajectory change brought about by society turning toward another goal than growth is still possible. The LtG work implies that this window of opportunity is closing fast."

In a presentation at the World Economic Forum in 2020 delivered in her capacity as a KPMG director, Herrington argued for 'agrowth'—an agnostic approach to growth which focuses on other economic goals and priorities.

"Changing our societal priorities hardly needs to be a capitulation to grim necessity," she said. "Human activity can be regenerative and our productive capacities can be transformed. In fact, we are seeing examples of that happening right now. Expanding those efforts now creates a world full of opportunity that is also sustainable."

She noted how the rapid development and deployment of vaccines at unprecedented rates in response to the COVID-19 pandemic demonstrates that we are capable of responding rapidly and constructively to global challenges if we

"The necessary changes will not be easy and pose transition challenges but a sustainable and inclusive future is still possible," said Herrington.

The best available data suggests that what we decide over the next 10 years will determine the long-term fate of human civilization. Although the odds are on a knife-edge, Herrington pointed to a "rapid rise" in environmental, social and good governance priorities as a basis for optimism, signalling the change in thinking taking place in both governments and businesses. She told me that perhaps the most important implication of her research is that it's not too late to create a truly sustainable civilization that works for all.

TAGGED: CLIMATE CHANGE,DYSTOPIA

MORE FROM VICE

World News

Two Clubs from Doomed Super League Received Millions in Taxpayer

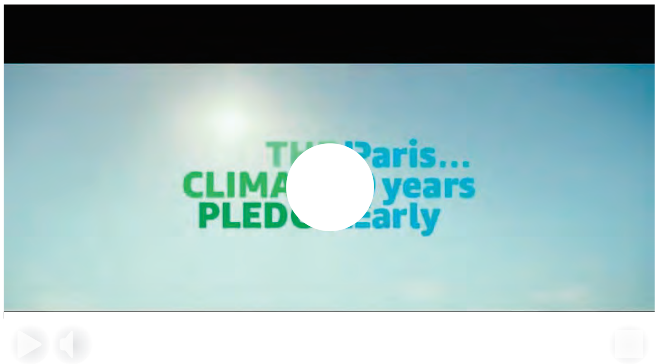

Society is right on track for a global collapse, new study of infamous 1970s report finds

By Brandon Specktor - Senior Writer 2 days ago

A steep downturn in human population and quality of life could be coming in the 2040s, the report finds.

Human society is on track for a collapse in the next two decades if there isn't a serious shift in global priorities, according to a new reassessment of a 1970s report, Vice reported

In that report — published in the bestselling book "The Limits to Growth" (1972) — a team of MIT scientists argued that industrial civilization was bound to collapse if corporations and governments continued to pursue continuous economic growth, no matter the costs. The researchers forecasted 12 possible scenarios for the future, most of which predicted a point where natural resources would become so scarce that further economic growth would become impossible, and personal welfare would plummet.

The report's most infamous scenario — the Business as Usual (BAU) scenario — predicted that the world's economic growth would peak around the 2040s, then take a sharp downturn, along with the global population, food availability and natural resources. This imminent "collapse" wouldn't be the end of the human race, but rather a societal turning point that would see standards of living drop around the world for decades, the team wrote.

Related: How much time does humanity have left?

So, what's the outlook for society now, nearly half a century after the MIT researchers shared their prognostications? Gaya Herrington, a sustainability and dynamic system analysis researcher at the consulting firm KPMG, decided to find out. In the November 2020 issue of the Yale Journal of Industrial Ecology, Herrington expanded on research she began as a graduate student at Harvard University earlier that year, analyzing the "Limits to Growth" predictions alongside the most current real-world data.

Herrington found that the current state of the world — measured through 10 different variables, including population, fertility rates, pollution levels, food production and industrial output — aligned extremely closely with two of the scenarios proposed in 1972, namely the BAU scenario and one called Comprehensive Technology (CT), in which technological advancements help reduce pollution and increase food supplies, even as natural resources run out.

While the CT scenario results in less of a shock to the global population and personal welfare, the lack of natural resources still leads to a point where economic growth sharply declines — in other words, a sudden collapse of industrial society.

"[The BAU] and CT scenarios show a halt in growth within a decade or so from now," Herrington wrote in her study. "Both scenarios thus indicate that continuing business as usual, that is, pursuing continuous growth, is not possible."

The good news is that it's not too late to avoid both of these scenarios and put society on track for an alternative — the Stabilized World (SW) scenario. This path begins as the BAU and CT routes do, with population, pollution and economic growth rising in tandem while natural resources decline. The difference comes when humans decide to deliberately limit economic growth on their own, before a lack of resources forces them to.

and a deliberate choice to limit industrial output and prioritize health and education services.

On a graph of the SW scenario, industrial growth and global population begin to level out shortly after this shift in values occurs. Food availability continues to rise to meet the needs of the global population; pollution declines and all but disappears; and the depletion of natural resources begins to level out, too. Societal collapse is avoided entirely.

This scenario may sound like a fantasy — especially as atmospheric carbon dioxide levels soar to record highs. But the study suggests a deliberate change in course is still possible.

RELATED CONTENT

Images of melt: Earth's vanishing ice
The reality of climate change: 10 myths busted
Top 10 ways to destroy Earth

Herrington told Vice.com the rapid development and deployment of vaccines during the COVID-19 pandemic is a testament to human ingenuity in the face of global crises. It's entirely possible, Herrington said, for humans to respond similarly to the ongoing climate crisis — if we make a deliberate, society-wide choice to do so.

"It's not yet too late for humankind to purposefully change course to significantly alter the trajectory of [the] future," Herrington concluded in her study. "Effectively, humanity can either choose its own limit or at some point reach an imposed limit, at which time a decline in human welfare will have become unavoidable."

Read more about the report at Vice.com.

Climate Change Is Triggering Eco-Anxiety
When news about the environment becomes grim, you might be overcome by an urge to hide or collapse.

PLAY SOUND

Originally published on Live Science.

Water Model Study for 1250 Del Mar Drive Proposed Retail Shopping Center

Fort Bragg Water Model

Proposed Project Description

PROJECT NAME: Hare Creek Center

DESCRIPTION: The purpose of the proposed project is to develop a shopping mall to accommodate the retailer Discount Grocery, four unidentified retail tenants, and one unidentified restaurant. New shopping center consisting of three buildings, including: Building A at 15,000 square feet, Building B at 10,000 square feet and Building C at 4,500 square feet of retail space. The project would be served by a new access road, proposed for the west edge of the development that would connect Bay View Avenue (CR #439A) to the southwest to Ocean View Drive at the intersection of Ocean View and Harbor Avenue. The project also includes a new 99 space parking lot, loading zones, pedestrian improvements, rainwater storage tanks, utilities, drainage improvements and associated landscaping.

The project includes a boundary line adjustment between parcels 018-450-40 and 018-450-41, adding 32,586 square feet (0.75 acres) to parcel 018-450-40 (currently 2.42 acres), the combined parcel would be 3.16 acres. The boundary line adjustment is proposed so that the proposed development is on one parcel.

LOCATION: The proposed 3.16 acre project site is located at 1250 Del Mar Drive on Todd Point within the City of Fort Bragg city limits just north and west of the Highway 20/Highway 1 intersection. The parcel is located within the coastal zone. APN 018-450-40 & 018-450-41. The site is bounded to the north by a hotel and mini-golf course, to the east by Highway 1 and to the south and west by undeveloped property. The Project is approximately three quarters of a mile west of the existing Highway 20 water tank.

Figure 1: Project Site

Estimated Water Demands

Estimated water demands for the Project were determined by comparing four different resources. See Table 1: Estimated Water Demands for Proposed 1250 Del Mar Drive Retail Center. Estimated demands applied to the node closest to the Project are as follows:

Average Day Demand:	8,260 gpd (5.7 gpm)
Maximum Day Demand:	16,520 gpd (11.5 gpm)
Peak Hour Demand:	23,128 gpd (16.1 gpm)

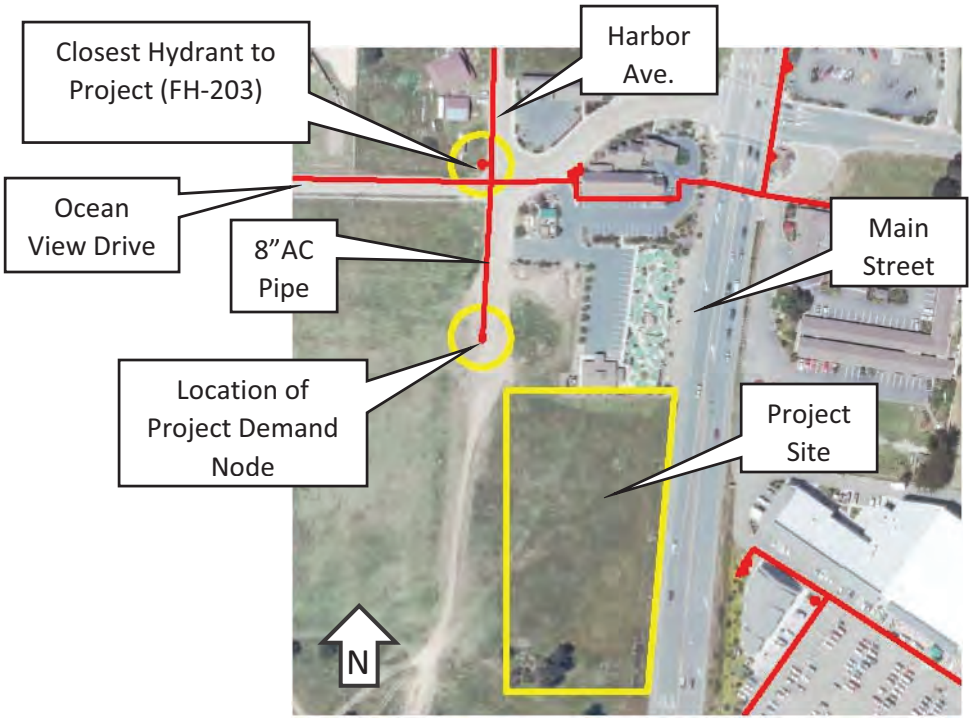

Figure 2: Existing Water System Near Project

Existing system demands were taken from the City of Fort Bragg, Phase 1 Water Facilities Study: Existing Water Collection, Distribution and Capacity, Nov. 2013 (Phase 1 Water Study). The existing system was modeled with the projected demands for 2022.

Model Results

To determine the impact of the Project on the City's water system, six different scenarios were modeled:

1) 2022 Maximum Day Demands, Existing System without Project
2) 2022 Maximum Day Demands, Existing System plus Project
3) 2022 Peak Hour Demands, Existing System without Project
4) 2022 Peak Hour Demands, Existing System plus Project
5) Fire Flow Analysis, 2022 Maximum Day Demands, Existing System without Project

6) Fire Flow Analysis, 2022 Maximum Day Demands, Existing System plus Project

See model results in Table 2, Water Model Results and Comparison. Results are shown for Scenarios 1) through 4) as the difference between the pressure at each hydrant of the existing system before the Project and the existing system plus the Project. Similarly, fire flow analysis results for 5) and 6) results are shown as the difference in available fire flow. Available fire flow is defined in the appendix titled "Description of Fire Flows in Hydraulic Modeling". Also see the Phase 1 Water Study referenced above for a further explanation of available fire flow as well as detailed explanations of the water model developed for the City of Fort Bragg.

2022 MAXIMUM DAY DEMANDS PRESSURE DIFFERENCE

Results from the hydraulic model show no significant difference in pressure between the existing water system with and without the Project. A maximum difference of 0.1 psi is observed. These results are presented in Table 2.

2022 PEAK HOUR DEMANDS PRESSURE DIFFERENCE

Similar to the 2022 maximum day demands comparison, results from the hydraulic model show no significant difference in pressure between the existing water system with and without the Project. A maximum difference of 0.1 psi is observed. These results are also presented in Table 2.

2022 MAXIMUM DAY DEMANDS FIRE FLOW ANALYSIS, AVAILABLE FIRE FLOW DIFFERENCE

Per the Phase 1 Water Study, the required minimum fire flow is 1,500 gpm. As explained in the Phase 1 Water Study, not all of the existing Fort Bragg hydrants meet minimum fire flow requirements. Improvements to the water system were recommended in the Phase 1 Water Study to improve the system's fire flows.

Results from the hydraulic model show no significant difference in pressure between the existing water system with and without the Project. For hydrants with available fire flow less than 1,500 gpm, the maximum flow difference is 3 gpm. For hydrants with available fire flows above 1,500 gpm, the maximum flow difference is 16 gpm, or less than 1% change. These results are presented in Table 2.

Summary

Using the calibrated Fort Bragg network hydraulic model and with input from the water system staff at the City of Fort Bragg, no significant changes to the existing water system are anticipated with the addition of the proposed project at 1250 Del Mar Drive.

Table 1: Estimated Water Demands for Proposed 1250 Del Mar Drive Retail Center

Fort Bragg Water Model

Building Area	29,500	SF
Parcel Size (After LLA)	3.16	AC
Assumed Building Frontage	200	ft

Resource 1: Phase 1 Water Study [1]

Ave. Day Demand / SF	0.28	gpd/SF, Table 1
Ave. Day Demand	**8,260**	**gpd**
Max. Day Factor	2	
Max. Day Demand / SF	0.56	gpd/SF
Max. Day Demand	**16,520**	**gpd**

Resource 2: West Yost Study [2]

Ave. Day Demand / AC	2,520	gpd/AC, p.4
Ave. Day Demand	**7,963**	**gpd**
Max. Day Factor	2	, p.5
Max. Day Demand / AC	5,040	gpd/AC, p.4
Max. Day Demand	**15,926**	**gpd**

Resource 3: Water Capital Improvement Fee Study [3]

Ave. Day Demand / SF	0.11	gpd/SF
Ave. Day Demand	**3,245**	**gpd**
Assumed Max. Day Factor	2	
Assumed Max. Day Demand / SF	0.22	gpd/SF
Max. Day Demand	**6,490**	**gpd**

Resource 4: Wastewater Engineering, Metcalf & Eddy [4]

Ave. Day Demand	450	gpd for first 25' of frontage
	400	gpd for each additional 25' of frontage
Ave. Day Demand	**3,250**	**gpd**
Assumed Max. Day Factor	2	
Max. Day Demand	**6,500**	**gpd**

Water Demands Selected for 1250 Del Mar Drive Retail Center

Average Day Demand	8,260	gpd	5.7	gpm
Maximum Day Demand	16,520	gpd	11.5	gpm
Peak Hour Demand (1.4 * MDD)	23,128	gpd	16.1	gpm

(1) City of Fort Bragg, Phase 1 Water Facilities Study: Existing Water Collection, Distribution and Capacity, Nov. 2013, KASL Engineers

(2) Technical Memorandum No. 1, Georgia-Pacific Fort Bragg Mill Site Redevelopment Project - GP and City of Fort Bragg Potable Water Demand and Supply Projections, Jan. 10, 2011, West Yost

(3) Water Capital Improvement Fee Study, 2000, Bartle Wells Associates

(4) Wastewater Engineering, Metcalf & Eddy, Inc. McGraw-Hill, Table 2-6, 1972

Table 2: Water Model Results and Comparison for Proposed 1250 Del Mar Dr. Retail Center

Fort Bragg Water Model

Minimum Desired Available Fire Flow (gpm): 1,500

Model Hydrant Label	Max Day 2022 (926 gpm) Pressure (psi)	Max Day 2022 Plus 1250 Del Mar Dr. (937 gpm) Pressure (psi)	Max Day 2022 Press. Difference Pressure (psi)	Peak Hour 2022 (1296 gpm) Pressure (psi)	Peak Hour 2022 1250 Del Mar Dr. (1313 gpm) Pressure (psi)	Peak Hour 2022 Pressure Difference Pressure (psi)	Max Day 2022 Available Fire Flow Flow (gpm) [1][3]	Max Day 2022 + 1250 Del Mar Dr. Available Fire Flow Flow (gpm) [1][3]	Max Day 2022 Available Fire Flow Difference Flow (gpm) [2]
FH-1	21.4	21.4	0	21.4	21.4	0	2,500	2,500	0
FH-2	51.1	51.1	0	51.1	51.1	0	**538**	**538**	0
FH-2A	52	52	0	51.9	51.9	0	**538**	**538**	0
FH-3	53.2	53.2	0	53.2	53.2	0	**877**	**877**	0
FH-4	53.1	53.1	0	53.1	53.1	0	**877**	**877**	0
FH-5	52.9	52.9	0	52.8	52.8	0	**509**	**509**	0
FH-5A	55.8	55.8	0	55.8	55.8	0	**547**	**547**	0
FH-6	57.4	57.4	0	57.4	57.4	0	**549**	**549**	0
FH-7	57.7	57.7	0	57.7	57.7	0	**833**	**833**	0
FH-8	35.3	35.3	0	35.2	35.2	0	2,376	2,368	-8
FH-8A	60.8	60.8	0	60.8	60.8	0	**943**	**943**	0
FH-9	58.2	58.2	0	58.2	58.2	0	**1,423**	**1,423**	0
FH-10	59.1	59.1	0	59	59	0	1,971	1,970	-1
FH-11	57.8	57.8	0	57.8	57.8	0	1,715	1,715	0
FH-12	55.9	55.9	0	55.9	55.9	0	**1,388**	**1,388**	0
FH-13	54	54	0	54	54	0	**1,222**	**1,222**	0
FH-14	52.7	52.7	0	52.6	52.6	0	**1,150**	**1,150**	0
FH-15	52	52	0	52	52	0	**1,123**	**1,123**	0
FH-16	53.1	53.1	0	53.1	53.1	0	**1,291**	**1,291**	0
FH-17	56.4	56.4	0	56.4	56.4	0	**1,468**	**1,468**	0
FH-18	57.3	57.3	0	57.3	57.3	0	1,603	1,603	0
FH-19	57.4	57.4	0	57.3	57.3	0	1,650	1,650	0
FH-20	50.6	50.6	0	50.5	50.5	0	**978**	**978**	0
FH-21	50.1	50.1	0	50.1	50.1	0	**994**	**994**	0
FH-22	60.4	60.4	0	60.4	60.4	0	1,583	1,583	0
FH-23	51.5	51.5	0	51.5	51.5	0	**1,436**	**1,436**	0
FH-24	50.5	50.5	0	50.4	50.4	0	**939**	**939**	0
FH-25	39.2	39.2	0	39	39	0	**668**	**668**	0
FH-26	39.4	39.4	0	39.2	39.2	0	**851**	**849**	**-2**
FH-26A	38.1	38.1	0	37.9	37.9	0	**800**	**798**	**-2**
FH-27	62.2	62.2	0	62.2	62.2	0	2,035	2,035	0
FH-28	61.7	61.7	0	61.7	61.7	0	2,035	2,035	0
FH-29	61.6	61.6	0	61.6	61.6	0	2,007	2,007	0
FH-30	60.4	60.4	0	60.4	60.4	0	2,023	2,023	0
FH-31	60.3	60.3	0	60.2	60.2	0	2,028	2,027	-1
FH-32	61	61	0	61	61	0	1,992	1,991	-1
FH-33	59.5	59.5	0	59.5	59.5	0	2,009	2,009	0

Model Hydrant Label	Max Day 2022 (926 gpm) Pressure (psi)	Max Day 2022 Plus 1250 Del Mar Dr. (937 gpm) Pressure (psi)	Max Day 2022 Press. Difference Pressure (psi)	Peak Hour 2022 (1296 gpm) Pressure (psi)	Peak Hour 2022 1250 Del Mar Dr. (1313 gpm) Pressure (psi)	Peak Hour 2022 Pressure Difference Pressure (psi)	Max Day 2022 Available Fire Flow Flow (gpm) [1][3]	Max Day 2022 + 1250 Del Mar Dr. Available Fire Flow Flow (gpm) [1][3]	Max Day 2022 Available Fire Flow Difference Flow (gpm) [2]
FH-34	58.5	58.5	0	58.4	58.4	0	1,991	1,991	0
FH-35	53.4	53.4	0	53.4	53.4	0	1,879	1,879	0
FH-35A	51.4	51.4	0	51.4	51.4	0	1,758	1,757	-1
FH-36	52.3	52.3	0	52.3	52.3	0	**892**	**892**	0
FH-37	55.7	55.7	0	55.7	55.7	0	**1,261**	**1,261**	0
FH-38	55.2	55.2	0	55.2	55.2	0	**1,367**	**1,367**	0
FH-39	39.5	39.5	0	39.4	39.4	0	**612**	**612**	0
FH-40	40.7	40.7	0	40.6	40.6	0	**691**	**690**	**-1**
FH-41	38.4	38.4	0	38.3	38.3	0	2,087	2,080	-7
FH-42	61.5	61.5	0	61.5	61.5	0	1,973	1,973	0
FH-43	41.1	41.1	0	40.9	40.9	0	**991**	**989**	**-2**
FH-44	63	63	0	63	63	0	2,099	2,098	-1
FH-45	61.6	61.6	0	61.6	61.6	0	**1,023**	**1,023**	0
FH-46	56.5	56.5	0	56.5	56.5	0	1,893	1,892	-1
FH-47	58.2	58.2	0	58.1	58.1	0	1,582	1,582	0
FH-48	41.4	41.4	0	41.2	41.2	0	**1,136**	**1,133**	**-3**
FH-49	40.6	40.6	0	40.4	40.4	0	**1,220**	**1,219**	**-1**
FH-50	41	41	0	40.8	40.8	0	**1,237**	**1,236**	**-1**
FH-51	65.4	65.4	0	65.4	65.4	0	**1,171**	**1,171**	0
FH-52	64.5	64.5	0	64.5	64.5	0	1,980	1,980	0
FH-53	41.9	41.9	0	41.7	41.7	0	1,805	1,803	-2
FH-54	67.8	67.8	0	67.8	67.8	0	**1,378**	**1,378**	0
FH-55	61.6	61.6	0	61.6	61.6	0	2,109	2,101	-8
FH-56	58.9	58.9	0	58.9	58.9	0	2,109	2,101	-8
FH-57	58.4	58.4	0	58.3	58.3	0	2,109	2,101	-8
FH-58	33.8	33.8	0	33.5	33.5	0	**986**	**984**	**-2**
FH-59	68.2	68.2	0	68.2	68.2	0	1,685	1,685	0
FH-60	43.7	43.7	0	43.5	43.5	0	2,105	2,098	-7
FH-61	42.4	42.4	0	42.1	42.1	0	1,833	1,828	-5
FH-62	43.1	43.1	0	42.8	42.8	0	**1,360**	**1,358**	**-2**
FH-63	42.2	42.2	0	41.9	41.9	0	**638**	**638**	0
FH-64	43.2	43.2	0	42.8	42.8	0	**1,349**	**1,347**	**-2**
FH-65	41.2	41.2	0	40.9	40.9	0	**808**	**807**	**-1**
FH-66	43.9	43.9	0	43.6	43.6	0	**1,081**	**1,080**	**-1**
FH-66A	41.8	41.8	0	41.5	41.5	0	**927**	**925**	**-2**
FH-67	42.5	42.5	0	42.3	42.2	-0.1	**573**	**572**	**-1**
FH-68	37.9	37.9	0	37.6	37.6	0	**554**	**554**	0
FH-69	45.3	45.3	0	45	44.9	-0.1	2,160	2,152	-8
FH-70	44.4	44.4	0	44.1	44.1	0	**1,244**	**1,243**	**-1**
FH-71	38.8	38.8	0	38.5	38.5	0	**1,231**	**1,228**	**-3**

Model Hydrant Label	Max Day 2022 (926 gpm) Pressure (psi)	Max Day 2022 Plus 1250 Del Mar Dr. (937 gpm) Pressure (psi)	Max Day 2022 Press. Difference Pressure (psi)	Peak Hour 2022 (1296 gpm) Pressure (psi)	Peak Hour 2022 1250 Del Mar Dr. (1313 gpm) Pressure (psi)	Peak Hour 2022 Pressure Difference Pressure (psi)	Max Day 2022 Available Fire Flow Flow (gpm) [1][3]	Max Day 2022 + 1250 Del Mar Dr. Available Fire Flow Flow (gpm) [1][3]	Max Day 2022 Available Fire Flow Difference Flow (gpm) [2]
FH-72	40.8	40.8	0	40.4	40.4	0	**893**	**891**	**-2**
FH-73	43.8	43.8	0	43.5	43.4	-0.1	**1,093**	**1,091**	**-2**
FH-74	52	52	0	51.7	51.7	0	**1,105**	**1,103**	**-2**
FH-75	45.4	45.4	0	45.1	45.1	0	2,129	2,122	-7
FH-76	45.1	45.1	0	44.7	44.7	0	2,137	2,131	-6
FH-77	44.2	44.2	0	43.8	43.8	0	2,145	2,138	-7
FH-78	45.5	45.5	0	45.1	45.1	0	2,149	2,142	-7
FH-79	48.8	48.8	0	48.5	48.5	0	1,575	1,574	-1
FH-80	38.8	38.8	0	38.5	38.5	0	**1,153**	**1,151**	**-2**
FH-81	46.1	46.1	0	45.8	45.8	0	**1,255**	**1,252**	**-3**
FH-82	41.1	41	-0.1	40.7	40.7	0	**953**	**951**	**-2**
FH-83	45.3	45.3	0	45	44.9	-0.1	**1,128**	**1,126**	**-2**
FH-84	48.9	48.9	0	48.6	48.5	-0.1	2,006	1,999	-7
FH-85	47.2	47.2	0	46.9	46.9	0	1,625	1,624	-1
FH-86	46.3	46.3	0	46	46	0	2,145	2,138	-7
FH-87	46.7	46.7	0	46.4	46.4	0	**1,368**	**1,366**	**-2**
FH-88	46.5	46.5	0	46.2	46.2	0	**1,387**	**1,386**	**-1**
FH-89	44.7	44.7	0	44.3	44.3	0	2,144	2,135	-9
FH-90	49.1	49.1	0	48.8	48.7	-0.1	**1,491**	**1,490**	**-1**
FH-91	44.6	44.6	0	44.3	44.2	-0.1	**804**	**802**	**-2**
FH-92	40.2	40.2	0	39.9	39.8	-0.1	**625**	**624**	**-1**
FH-93	47.7	47.7	0	47.4	47.3	-0.1	1,546	1,541	-5
FH-94	48.8	48.8	0	48.4	48.4	0	1,604	1,600	-4
FH-95	49.8	49.8	0	49.5	49.4	-0.1	1,821	1,820	-1
FH-96	47.5	47.5	0	47.2	47.2	0	2,146	2,137	-9
FH-97	49.1	49.1	0	48.8	48.8	0	1,513	1,511	-2
FH-98	51	51	0	50.6	50.6	0	1,616	1,615	-1
FH-99	51.2	51.2	0	50.9	50.9	0	1,952	1,944	-8
FH-100	43.9	43.9	0	43.6	43.6	0	**852**	**850**	**-2**
FH-101	51	51	0	50.7	50.7	0	1,754	1,748	-6
FH-102	51	51	0	50.6	50.6	0	2,134	2,125	-9
FH-103	50.5	50.5	0	50.2	50.2	0	1,755	1,754	-1
FH-104	53.6	53.6	0	53.3	53.3	0	1,879	1,878	-1
FH-105	49	49	0	48.7	48.6	-0.1	**1,383**	**1,381**	**-2**
FH-106	45	45	0	44.7	44.7	0	**1,083**	**1,082**	**-1**
FH-107	50.2	50.2	0	49.9	49.9	0	1,717	1,714	-3
FH-108	51.9	51.9	0	51.6	51.6	0	1,813	1,806	-7
FH-109	51.7	51.7	0	51.3	51.3	0	1,894	1,887	-7
FH-110	51.5	51.4	-0.1	51.1	51.1	0	1,908	1,906	-2
FH-111	50.8	50.8	0	50.5	50.5	0	1,566	1,565	-1

Model Hydrant Label	Max Day 2022 (926 gpm) Pressure (psi)	Max Day 2022 Plus 1250 Del Mar Dr. (937 gpm) Pressure (psi)	Max Day 2022 Press. Difference Pressure (psi)	Peak Hour 2022 (1296 gpm) Pressure (psi)	Peak Hour 2022 1250 Del Mar Dr. (1313 gpm) Pressure (psi)	Peak Hour 2022 Pressure Difference Pressure (psi)	Max Day 2022 Available Fire Flow Flow (gpm) [1][3]	Max Day 2022 + 1250 Del Mar Dr. Available Fire Flow Flow (gpm) [1][3]	Max Day 2022 Available Fire Flow Difference Flow (gpm) [2]
FH-112	54.2	54.2	0	53.9	53.9	0	1,745	1,744	-1
FH-113	53.6	53.6	0	53.3	53.3	0	2,003	1,995	-8
FH-114	49.6	49.6	0	49.2	49.2	0	2,139	2,131	-8
FH-115	55.4	55.4	0	55	55	0	2,118	2,110	-8
FH-116	54.2	54.2	0	53.9	53.9	0	2,119	2,111	-8
FH-117	55.1	55.1	0	54.8	54.8	0	2,059	2,058	-1
FH-118	50.9	50.9	0	50.6	50.6	0	**1,446**	**1,445**	**-1**
FH-119	51.6	51.6	0	51.3	51.2	-0.1	**1,299**	**1,298**	**-1**
FH-120	53.9	53.9	0	53.6	53.6	0	1,949	1,942	-7
FH-121	57.3	57.3	0	56.9	56.9	0	1,954	1,947	-7
FH-122	57.7	57.7	0	57.4	57.4	0	1,954	1,946	-8
FH-123	53.9	53.9	0	53.6	53.5	-0.1	2,004	2,003	-1
FH-124	50.8	50.8	0	50.5	50.5	0	2,074	2,065	-9
FH-125	53.3	53.3	0	53	53	0	1,702	1,701	-1
FH-126	56.5	56.5	0	56.2	56.1	-0.1	1,860	1,859	-1
FH-127	56.4	56.4	0	56.1	56.1	0	2,028	2,019	-9
FH-128	56.9	56.9	0	56.6	56.5	-0.1	1,676	1,674	-2
FH-129	56.6	56.6	0	56.3	56.3	0	1,942	1,934	-8
FH-130	58.9	58.9	0	58.6	58.6	0	2,107	2,099	-8
FH-131	54.5	54.5	0	54.1	54.1	0	2,074	2,065	-9
FH-132	55.4	55.4	0	55	55	0	2,088	2,079	-9
FH-133	58	58	0	57.6	57.6	0	2,093	2,084	-9
FH-134	57.3	57.3	0	57	57	0	2,038	2,030	-8
FH-135	59.8	59.8	0	59.5	59.5	0	1,818	1,817	-1
FH-136	62.1	62.1	0	61.8	61.7	-0.1	1,768	1,767	-1
FH-137	61.8	61.8	0	61.4	61.4	0	2,020	2,012	-8
FH-138	59	58.9	-0.1	58.6	58.6	0	2,008	1,999	-9
FH-139	55.1	55.1	0	54.8	54.8	0	2,005	1,997	-8
FH-140	50.5	50.5	0	50.2	50.1	-0.1	2,036	2,028	-8
FH-141	48.1	48.1	0	47.8	47.8	0	**1,407**	**1,405**	**-2**
FH-142	47.4	47.4	0	47.1	47.1	0	**1,343**	**1,341**	**-2**
FH-143	48.7	48.7	0	48.4	48.4	0	2,129	2,120	-9
FH-144	50.5	50.5	0	50.1	50.1	0	2,021	2,012	-9
FH-145	48.9	48.9	0	48.6	48.6	0	2,010	2,002	-8
FH-145A	47	47	0	46.7	46.6	-0.1	1,633	1,631	-2
FH-146	48.1	48.1	0	47.8	47.8	0	1,708	1,705	-3
FH-147	50.6	50.6	0	50.3	50.3	0	1,502	1,500	-2
FH-148	53.4	53.4	0	53.1	53.1	0	1,613	1,611	-2
FH-149	57.6	57.6	0	57.3	57.3	0	1,747	1,744	-3
FH-150	50.8	50.7	-0.1	50.4	50.4	0	1,647	1,644	-3

Model Hydrant Label	Max Day 2022 (926 gpm) Pressure (psi)	Max Day 2022 Plus 1250 Del Mar Dr. (937 gpm) Pressure (psi)	Max Day 2022 Press. Difference Pressure (psi)	Peak Hour 2022 (1296 gpm) Pressure (psi)	Peak Hour 2022 1250 Del Mar Dr. (1313 gpm) Pressure (psi)	Peak Hour 2022 Pressure Difference Pressure (psi)	Max Day 2022 Available Fire Flow Flow (gpm) [1][3]	Max Day 2022 + 1250 Del Mar Dr. Available Fire Flow Flow (gpm) [1][3]	Max Day 2022 Available Fire Flow Difference Flow (gpm) [2]
FH-151	45.6	45.6	0	45.3	45.3	0	1,558	1,555	-3
FH-152	45.1	45.1	0	44.8	44.7	-0.1	1,500	**1,497**	**-3**
FH-153	46.4	46.4	0	46	46	0	1,808	1,805	-3
FH-153A	48.6	48.6	0	48.3	48.2	-0.1	2,021	2,013	-8
FH-154	45	45	0	44.7	44.7	0	1,792	1,788	-4
FH-155	45.4	45.4	0	45.1	45.1	0	1,660	1,659	-1
FH-156	44.9	44.8	-0.1	44.5	44.5	0	1,513	1,510	-3
FH-157	46.5	46.5	0	46.2	46.2	0	**1,317**	**1,315**	**-2**
FH-158	45.6	45.6	0	45.3	45.3	0	**1,424**	**1,422**	**-2**
FH-159	45.2	45.2	0	44.9	44.9	0	2,069	2,064	-5
FH-160	45.8	45.7	-0.1	45.4	45.4	0	1,510	1,508	-2
FH-161	48.6	48.6	0	48.3	48.3	0	1,942	1,939	-3
FH-162	47.4	47.4	0	47.1	47.1	0	1,765	1,762	-3
FH-163	57.3	57.3	0	57.1	57.1	0	2,500	2,500	0
FH-163A	76	76	0	75.8	75.8	0	2,500	2,500	0
FH-164	90.4	90.4	0	90.2	90.2	0	2,500	2,500	0
FH-165	90.4	90.4	0	90.2	90.2	0	2,500	2,500	0
FH-166	90.1	90.1	0	89.9	89.9	0	2,500	2,500	0
FH-167	89.9	89.9	0	89.6	89.6	0	2,500	2,500	0
FH-168	89.9	89.9	0	89.6	89.6	0	2,500	2,500	0
FH-169	56.4	56.4	0	56	56	0	2,072	2,064	-8
FH-170	60.1	60.1	0	59.7	59.7	0	2,095	2,086	-9
FH-171	60.8	60.8	0	60.5	60.4	-0.1	1,905	1,904	-1
FH-172	61	60.9	-0.1	60.6	60.5	-0.1	**1,441**	**1,441**	0
FH-173	62.3	62.3	0	61.9	61.9	0	**1,449**	**1,449**	0
FH-174	63.6	63.6	0	63.3	63.2	-0.1	1,836	1,835	-1
FH-175	54.5	54.5	0	54.2	54.2	0	2,031	2,022	-9
FH-176	48.6	48.6	0	48.3	48.3	0	2,194	2,185	-9
FH-177	62.2	62.2	0	61.9	61.9	0	2,043	2,035	-8
FH-178	64.5	64.5	0	64.2	64.1	-0.1	2,037	2,028	-9
FH-179	60	60	0	59.7	59.7	0	2,022	2,014	-8
FH-180	52	52	0	51.6	51.6	0	2,040	2,032	-8
FH-181	47.6	47.6	0	47.3	47.3	0	2,090	2,081	-9
FH-182	49.3	49.3	0	49	49	0	**1,258**	**1,257**	**-1**
FH-183	51.4	51.4	0	51.1	51.1	0	**887**	**886**	**-1**
FH-184	59.7	59.7	0	59.4	59.4	0	2,271	2,255	-16
FH-185	49.9	49.9	0	49.6	49.6	0	1,832	1,819	-13
FH-185A	59.8	59.8	0	59.5	59.5	0	1,868	1,855	-13
FH-186	51.3	51.3	0	51	51	0	1,758	1,745	-13
FH-187	44.5	44.5	0	44.2	44.2	0	1,618	1,609	-9

Model Hydrant Label	Max Day 2022 (926 gpm) Pressure (psi)	Max Day 2022 Plus 1250 Del Mar Dr. (937 gpm) Pressure (psi)	Max Day 2022 Press. Difference Pressure (psi)	Peak Hour 2022 (1296 gpm) Pressure (psi)	Peak Hour 2022 1250 Del Mar Dr. (1313 gpm) Pressure (psi)	Peak Hour 2022 Pressure Difference Pressure (psi)	Max Day 2022 Available Fire Flow Flow (gpm) [1][3]	Max Day 2022 + 1250 Del Mar Dr. Available Fire Flow Flow (gpm) [1][3]	Max Day 2022 Available Fire Flow Difference Flow (gpm) [2]
FH-188	44.1	44.1	0	43.8	43.8	0	1,579	1,568	-11
FH-189	43.2	43.2	0	43	43	0	1,605	1,600	-5
FH-190	44.8	44.7	-0.1	44.6	44.5	-0.1	1,846	1,839	-7
FH-191	47.6	47.6	0	47.4	47.4	0	2,029	2,022	-7
FH-192	46.6	46.5	-0.1	46.4	46.4	0	**1,494**	**1,491**	**-3**
FH-193	45.3	45.3	0	45.1	45.1	0	1,655	1,652	-3
FH-194	54	54	0	53.9	53.9	0	2,432	2,423	-9
FH-194A	53.5	53.5	0	53.3	53.3	0	2,500	2,500	0
FH-194B	53	53	0	52.9	52.9	0	2,500	2,500	0
FH-195	51.7	51.7	0	51.5	51.5	0	2,500	2,500	0
FH-196	75.3	75.3	0	75.1	75	-0.1	1,979	1,979	0
FH-198	45.4	45.4	0	45.2	45.2	0	2,500	2,500	0
FH-198A	43.4	43.4	0	43.2	43.2	0	**1,371**	**1,368**	**-3**
FH-199	37.5	37.5	0	37.4	37.4	0	2,500	2,500	0
FH-200	26.7	26.7	0	26.6	26.6	0	2,500	2,500	0
FH-201	19.3	19.3	0	19.3	19.3	0	2,500	2,500	0
FH-202	46.5	46.5	0	46.2	46.1	-0.1	1,544	1,533	-11
FH-203 [4]	48.6	48.6	0	48.3	48.3	0	1,584	1,573	-11
FH-204	51.5	51.5	0	51.2	51.2	0	1,744	1,731	-13
FH-205	53.7	53.7	0	53.4	53.3	-0.1	1,578	1,566	-12
FH-205A	59.2	59.2	0	59	58.9	-0.1	1,578	1,566	-12
FH-206	63.6	63.6	0	63.2	63.2	0	2,057	2,048	-9
FH-207	59.4	59.4	0	59.1	59.1	0	2,073	2,064	-9
FH-208	58	58	0	57.6	57.6	0	2,082	2,073	-9
FH-209	58.8	58.8	0	58.4	58.4	0	2,087	2,078	-9
FH-210	60	60	0	59.6	59.6	0	2,092	2,084	-8
FH-211	63.7	63.7	0	63.3	63.3	0	1,708	1,707	-1
FH-212	61.7	61.7	0	61.3	61.3	0	1,755	1,754	-1
FH-213	68.5	68.5	0	68.1	68.1	0	2,052	2,044	-8
FH-214	65.2	65.2	0	64.9	64.8	-0.1	2,010	2,009	-1
FH-215	68	68	0	67.7	67.6	-0.1	2,057	2,048	-9
FH-216	65.5	65.5	0	65.2	65.2	0	2,062	2,054	-8
FH-217	61.8	61.8	0	61.5	61.4	-0.1	2,069	2,060	-9
FH-218	59.6	59.6	0	59.3	59.2	-0.1	2,036	2,034	-2
FH-219	59.4	59.4	0	59	59	0	2,086	2,078	-8
FH-220	60.4	60.4	0	60.1	60.1	0	2,092	2,084	-8
FH-221	60.7	60.7	0	60.4	60.4	0	2,092	2,084	-8
FH-222	62.3	62.3	0	61.9	61.9	0	1,915	1,914	-1
FH-223	63.7	63.7	0	63.3	63.3	0	1,763	1,762	-1
FH-224	65.5	65.5	0	65.1	65.1	0	**1,027**	**1,027**	0

Model Hydrant Label	Max Day 2022 (926 gpm) Pressure (psi)	Max Day 2022 Plus 1250 Del Mar Dr. (937 gpm) Pressure (psi)	Max Day 2022 Press. Difference Pressure (psi)	Peak Hour 2022 (1296 gpm) Pressure (psi)	Peak Hour 2022 1250 Del Mar Dr. (1313 gpm) Pressure (psi)	Peak Hour 2022 Pressure Difference Pressure (psi)	Max Day 2022 Available Fire Flow Flow (gpm) [1][3]	Max Day 2022 + 1250 Del Mar Dr. Available Fire Flow Flow (gpm) [1][3]	Max Day 2022 Available Fire Flow Difference Flow (gpm) [2]
FH-225	67.2	67.2	0	66.8	66.8	0	1,547	1,547	0
FH-226	80.1	80.1	0	79.6	79.6	0	**793**	**793**	0
FH-227	75.6	75.6	0	75.1	75.1	0	**866**	**865**	**-1**
FH-228	76.7	76.7	0	76.1	76.1	0	**783**	**783**	0
FH-229	82.8	82.8	0	82.3	82.3	0	**608**	**608**	0
FH-230	80.8	80.8	0	80.3	80.2	-0.1	**578**	**578**	0
FH-231	79.1	79.1	0	78.5	78.5	0	**568**	**568**	0
FH-232	74.4	74.4	0	73.8	73.8	0	**553**	**552**	**-1**
FH-232A	73.4	73.4	0	72.8	72.8	0	**542**	**542**	0
FH-232B	70.3	70.3	0	69.8	69.7	-0.1	**568**	**568**	0
FH-233	74.2	74.2	0	73.7	73.7	0	**1,055**	**1,055**	0
FH-234	61.2	61.2	0	60.8	60.8	0	2,089	2,081	-8
FH-235	67.5	67.5	0	67.1	67.1	0	1,729	1,728	-1
FH-236	66.3	66.3	0	65.9	65.9	0	1,746	1,746	0
FH-237	69.3	69.3	0	68.9	68.9	0	1,646	1,645	-1
FH-238	67.9	67.9	0	67.5	67.5	0	1,686	1,685	-1
FH-239	68.8	68.7	-0.1	68.3	68.3	0	1,657	1,656	-1
FH-240	69.6	69.6	0	69.2	69.2	0	1,664	1,663	-1
FH-241	69.7	69.7	0	69.3	69.3	0	1,798	1,797	-1
FH-242	69.8	69.8	0	69.4	69.4	0	1,726	1,725	-1
FH-243	71.8	71.8	0	71.4	71.4	0	1,738	1,737	-1
FH-244	71.3	71.3	0	70.9	70.9	0	1,724	1,724	0
FH-245	70	70	0	69.6	69.6	0	1,680	1,679	-1
FH-246	70.9	70.9	0	70.5	70.5	0	1,564	1,564	0
FH-247	72.6	72.6	0	72.2	72.2	0	**1,469**	**1,469**	0
FH-248	64.4	64.4	0	64	64	0	2,003	2,002	-1
FH-249	67.1	67.1	0	66.7	66.7	0	2,092	2,084	-8
FH-250	62.6	62.6	0	62.2	62.2	0	2,091	2,082	-9
FH-251	64.1	64.1	0	63.8	63.7	-0.1	2,092	2,083	-9
FH-252	65.3	65.3	0	64.9	64.9	0	1,953	1,952	-1
FH-253	67.4	67.4	0	67	67	0	2,048	2,047	-1
FH-500	50.3	50.3	0	50	50	0	1,986	1,984	-2
FH-501	61.1	61.1	0	60.7	60.7	0	1,624	1,623	-1
FH-WARF1-2.5	67.9	67.9	0	67.5	67.5	0	2,055	2,047	-8

Notes:
(1) Values highlighted in red indicate hydrants whose available fire flow is less than the desired 1,500 gpm.
(2) Values highlighted in red indicate hydrants whose available fire flow is less than the desired 1,500 gpm, and the difference between pre-project vs. post-project is greater than 0.
(3) Tank levels conservatively estimated at 0 volume for fire flow tests.
(4) FH-203 is the closest hydrant to the Project. See Figure 2.

Appendix: Description of Fire Flows in Hydraulic Modeling

1. Field measured fire flow

- Hydrant flow is measured with flow meter
- 2.5” opening vs. 4.5” opening will give different flow results

2. Modeled Automated Fire Flow Analysis (Available fire flow)

- Available flow values indicate the maximum flow at each hydrant such that residual pressures at the hydrant stay above 20 PSI and all system components stay above 35 PSI during maximum day demands
- Available fire flows are computed by iteratively assigning demands and computing system pressures at each demand increment. For example:

  Hydrant A is being tested.

  1. 1 GPM is added to Hydrant A.
  2. All other pressures in the system are checked to see if they are above 35 PSI.
  3. Hydrant A is checked to see if its own pressure is above 20 PSI.
  4. If both 2. and 3. pass the test, then another 1 GPM is added to Hydrant A, and the system pressures are checked again.
  5. If both 2. and 3. do not pass the test, the available flow total is stopped and reported.

- All hydrants can be checked at once using the automated fire flow analysis.
- Automated Fire Flow Analysis does not take into account losses in the hydrant.

3. Modeled discharge to atmosphere fire flow (Simulates field measured fire flow)

- Emitter coefficient is assumed for each hydrant type. Assumed emitter coefficients:
  - 150 - 180 for 2.5” outlets
  - 167 - 185 for 2 - 2.5” outlets
  - 380 - 510 for the 4.5” outlets
- Pressure head is converted to velocity at outlet
- Each hydrant needs to be modeled separately
- Discharge to atmosphere fire flow does take into account losses in the hydrant.

ARTICLES
https://doi.org/10.1038/s41558-021-01077-8

nature climate change

Check for updates

Rapid increases and extreme months in projections of United States high-tide flooding

Philip R. Thompson[1,2]✉, Matthew J. Widlansky[2], Benjamin D. Hamlington[3], Mark A. Merrifield[4], John J. Marra[5], Gary T. Mitchum[6] and William Sweet[7]

Coastal locations around the United States, particularly along the Atlantic coast, are experiencing recurrent flooding at high tide. Continued sea-level rise (SLR) will exacerbate the issue where present, and many more locations will begin to experience recurrent high-tide flooding (HTF) in the coming decades. Here we use established SLR scenarios and flooding thresholds to demonstrate how the combined effects of SLR and nodal cycle modulations of tidal amplitude lead to acute inflections in projections of future HTF. The mid-2030s, in particular, may see the onset of rapid increases in the frequency of HTF in multiple US coastal regions. We also show how annual cycles and sea-level anomalies lead to extreme seasons or months during which many days of HTF cluster together. Clustering can lead to critical frequencies of HTF occurring during monthly or seasonal periods one to two decades prior to being expected on an annual basis.

The impact of high-tide flooding (HTF) accumulates over numerous seemingly minor occurrences, which can exceed the impact of rare extremes over time[1–3]. These impacts are subtle—for example, the loss of revenue due to recurrent road and business closures[4]—compared with the physical damage of property and infrastructure associated with extreme storm-driven events. As sea-level rise (SLR) increases the frequency of HTF in the United States[5–11], coastal communities will need to adapt. However, developing adaptation pathways for recurrent coastal flooding is challenging and requires knowledge of environmental and social tipping points at which current actions and policies become ineffective[12–14].

Here we characterize projected increases in US HTF (including the impact of the 18.6-year nodal cycle in tidal amplitude[15–17]) in a way that can be used to establish planning horizons and develop adaptation pathways. First, we focus on the rate of flooding-frequency increase, which is not well understood despite being critical to establishing SLR impact timelines[18]. More specifically, we examine acute inflections, or tipping points, in the rate of increase that mark transitions from periods of gradual (and potentially imperceptible) change to rapid increase in HTF frequency. Second, we focus on the tendency of HTF episodes to cluster in time[19]. Scientists, engineers and decision-makers are accustomed to the statistics and impacts of isolated extreme events[20–23], but given the cumulative nature of HTF impacts[1–3], we describe extreme months or seasons during which the number of flooding episodes, rather than the magnitude, is exceptional.

Projections of HTF frequency

Ensemble projections of twenty-first-century HTF frequency (Methods) are generated for 89 tide-gauge locations across the contiguous United States and US-affiliated Pacific and Caribbean islands (Supplementary Data). HTF frequencies are represented as counts of days in monthly and annual windows for which at least one hourly sea-level value exceeds the flooding threshold of interest. US National Oceanic and Atmospheric Administration (NOAA) SLR scenarios[24] and derived HTF thresholds[10], which are ubiquitous in US coastal planning, are used to produce the projections. NOAA minor and moderate flooding thresholds correspond to levels 50–60 cm and 80–90 cm, respectively, above the local mean higher high water tidal datum[10] (Supplementary Data). Here we focus on the NOAA Intermediate Low and Intermediate SLR scenarios corresponding to 0.5 m and 1.0 m, respectively, of global mean SLR by 2100. At present, it is not possible to assess which of the NOAA SLR scenarios the observations are tracking due to decadal variability in global and local sea level[25–27] and the lack of divergence in the scenarios (<2 cm) during 2000–2020. However, these two scenarios bracket the bulk of global and local SLR possibilities during the twenty-first century, being roughly equivalent to the 4th and 83rd percentiles[24] of probabilistic local sea-level projections[28] based on IPCC Fifth Assessment Report Representative Concentration Pathway 8.5 (ref. [29]).

Under the Intermediate scenario, annual projections of HTF days from different regions of the US coastline show dramatic increases in HTF frequency over the next 30–40 years (Fig. 1). The 10th–90th percentile range of each ensemble projection represents the degree to which the count in any given year can vary due to local sea-level variability across a variety of processes and timescales from high-frequency surge to decadal climate variability. Including the effect of local sea-level variability is essential for producing useful HTF projections, as SLR and astronomical tides alone will underestimate HTF frequency (Extended Data Fig. 1)[10]. Note that the range of projections over the ensemble at each location should not be interpreted as a true uncertainty, because uncertainty in anthropogenic SLR is excluded in this case by using a discrete NOAA SLR scenario. Incorporating uncertainty in SLR (as in the probabilistic projection[28] from which the NOAA scenarios are extracted[24]) would produce a much wider range of possibilities.

Rapid transitions in the frequency of HTF

The projections in Fig. 1 exhibit an important commonality: pronounced inflections in HTF frequency before mid-century. Such

[1]Department of Oceanography, University of Hawai'i at Mānoa, Honolulu, HI, USA. [2]Joint Institute for Marine and Atmospheric Research, University of Hawai'i at Mānoa, Honolulu, HI, USA. [3]NASA Jet Propulsion Laboratory, Pasadena, CA, USA. [4]Scripps Institution of Oceanography, University of California, San Diego, La Jolla, CA, USA. [5]Inouye Regional Center, NOAA/NESDIS/National Centers for Environmental Information, Honolulu, HI, USA. [6]College of Marine Science, University of South Florida, St. Petersburg, FL, USA. [7]NOAA/National Ocean Service, Silver Spring, MD, USA. ✉e-mail: philiprt@hawaii.edu

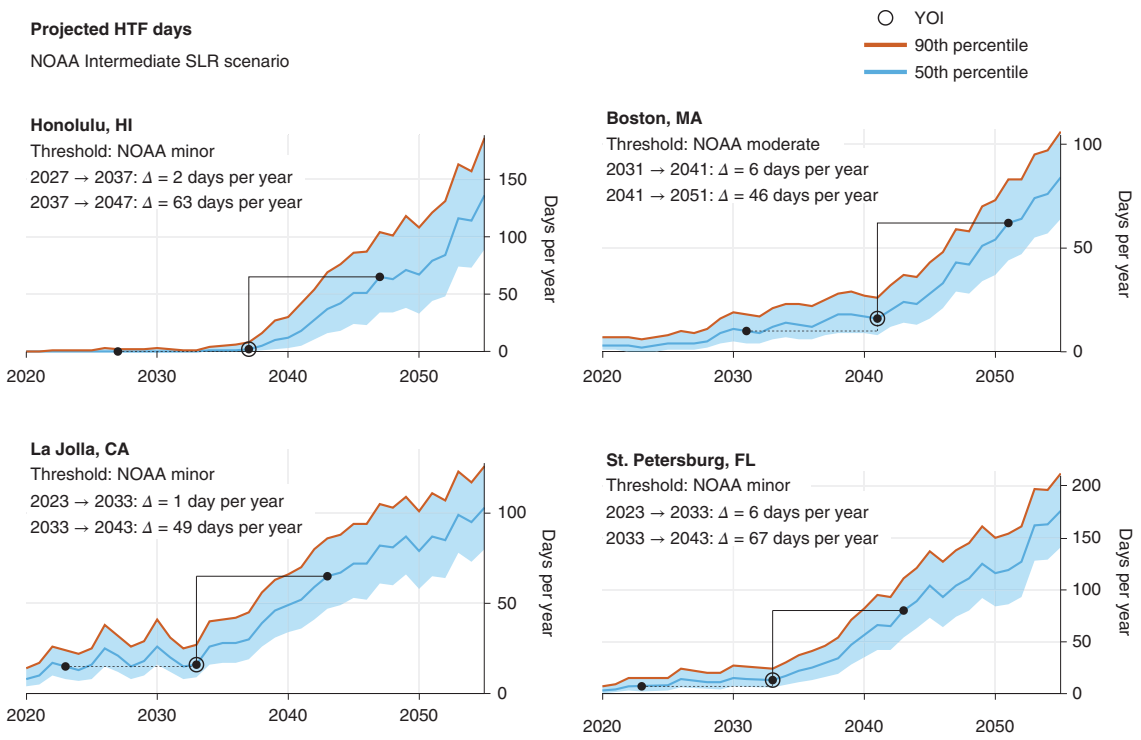

Fig. 1 | Projections of annual counts of HTF days for the NOAA Intermediate SLR scenario. The NOAA minor flooding threshold is used for Honolulu, San Diego and St. Petersburg. The NOAA moderate flooding threshold is used for Boston to highlight a threshold that is not yet routinely exceeded, which is not the case for the Boston minor threshold[11]. The 50th percentile from the ensemble of projections (blue line) and the 10th–90th percentile range (blue shading, with the 90th percentile highlighted in orange) show increasing numbers of HTF days per year. The YOI (open black circle) for each projection corresponds to abrupt increases in the frequency of HTF days, which are highlighted by comparing the projected increases (Δ) over two adjacent ten-year periods (dashed and solid black lines).

inflections, or tipping points, are essential for planning, because they represent transitions from regimes of gradual—and in some cases almost imperceptible—change to regimes of rapid increase in HTF frequency. These transitions can produce acute impacts in unsuspecting and underprepared communities if not identified in advance and communicated to stakeholders and decision-makers. The timing and severity of inflections are related to multiple factors. First, present-day HTF in most locations occurs during only the highest astronomical tides of the year. With SLR, increasing moderate (and more common) high tides will reach flood thresholds, resulting in a rapid increase in the number of HTF days. Second, high-tide amplitudes vary predictably in space and time due to astronomical forcing over timescales from monthly (that is, spring–neap cycles) to decadal (that is, the 18.6-year nodal cycle; see below). The interplay between SLR elevating increasing numbers of high tides towards the threshold and modulations of the tidal amplitude by astronomical forces dictates the timing and nature of inflections in HTF frequency.

To investigate contributions to projected rapid HTF increases, we identify a year of inflection (YOI) for each combination of tide-gauge location, scenario and threshold (Methods). In practice, a continuum of YOIs exists at each location corresponding to the range of possibilities for threshold height and evolution of twenty-first-century SLR. While the YOIs here are specific to the scenarios and thresholds used, they indicate the approximate timing at which rapid transitions will occur for similar scenarios and thresholds. For the four highlighted cases (Fig. 1), the YOI marks the end of a decade experiencing little increase in the expected number of HTF days per year, while decades following the YOIs experience a quadrupling or more.

YOI timing at the four locations is linked to modulations of tidal amplitude associated with the 18.6-year nodal cycle[15,16]. For example, in St. Petersburg, the nodal cycle range is 4.7 cm, representing the peak-to-trough difference in the height of the highest (annual 99th percentile) astronomical tides over a nodal cycle (Fig. 2, left). While not large compared with nodal cycle ranges exceeding 20 cm in other parts of the world[30], the range in St. Petersburg is sufficient to impact the evolution of increasing HTF. During 2024–2033, the Intermediate scenario projects 8.9 cm of SLR in St. Petersburg (Fig. 2, left). The height of the highest tides, however, is projected to increase by just 4.3 cm due to decreasing tidal amplitude associated with the nodal cycle. The opposite occurs during the following decade, and the increase in the height of the highest tides (14.1 cm) is enhanced relative to SLR (9.4 cm). Importantly, the decadal difference in high-tide height increase in St. Petersburg (14.1 − 4.3 = 9.8 cm) is larger than a decade of projected SLR (~9 cm per decade for the Intermediate scenario).

In St. Petersburg, the ratio of the nodal cycle range to a decade of projected SLR is roughly 0.5. Calculating this ratio across the United States highlights locations and regions where the nodal cycle is of sufficient magnitude to contribute to rapid inflections in HTF frequency (Fig. 2, right). Ratios in many locations, including 73% along the Pacific and Gulf of Mexico coastlines, exceed 0.4. In the near term, such locations are most susceptible to rapid inflections in HTF frequency due to the confluence of SLR and nodal cycle modulations of tidal amplitude.

The projection algorithm employed here (Methods) explicitly incorporates twenty-first-century predictions of astronomical tides and captures the effects of long-period tidal modulation on HTF frequency. The nonlinear relationship between the height of the

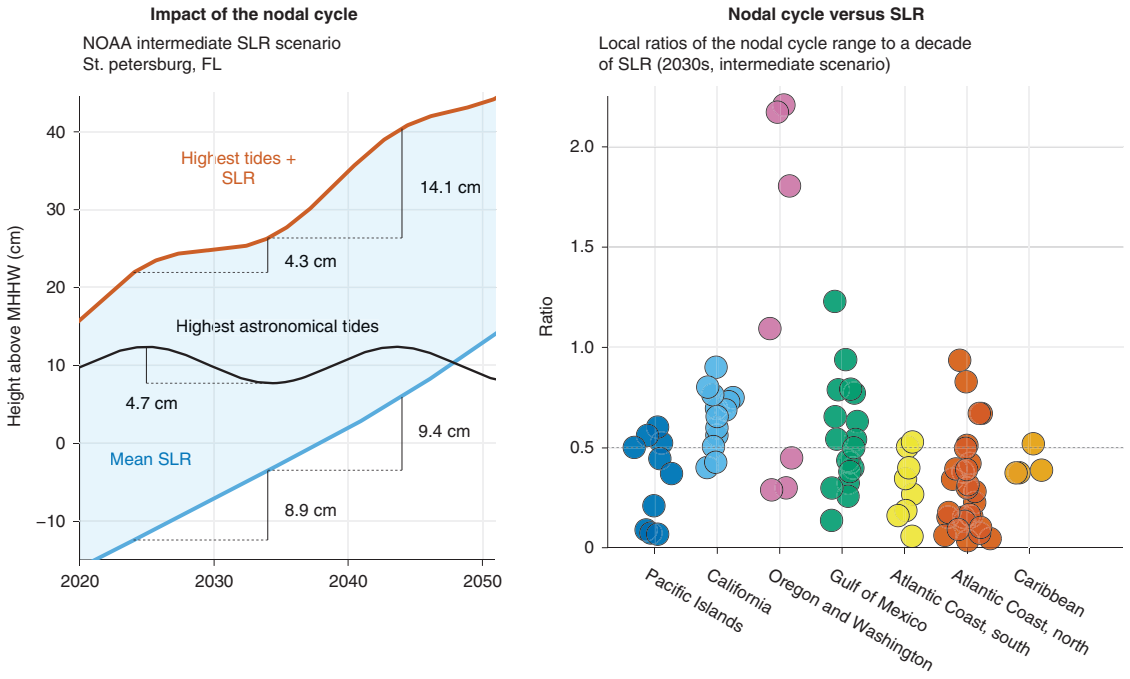

Fig. 2 | Impact of the nodal cycle. Left, projected heights of the highest tides in St. Petersburg, Florida (red), due to the combination of projected mean SLR (blue, NOAA Intermediate SLR scenario) and the 18.6-year nodal cycle expressed in the annual 99th percentile of astronomical tidal height (black). All time series are relative to the current mean higher high water (MHHW) tidal datum. Right, ratios at each US tide-gauge location of nodal cycle peak-to-trough range to ten years of projected SLR (2030s, NOAA Intermediate SLR scenario). The dot colours correspond to US coastal regions.

highest tides and HTF frequency (Methods) further amplifies the inflection in the HTF projection, which manifests in a rapid increase from 13 to 80 HTF days per year on average in St. Petersburg over the decade following the YOI in 2033 (Fig. 1, lower right). Not coincidentally, the YOI for St. Petersburg also corresponds to the nodal cycle minimum in tidal amplitude, marking the transition between suppression and enhancement of increasing high-tide height by the nodal cycle.

YOI timing around the United States tends to be similar (though not uniform) within regions (Fig. 3 and Supplementary Data). Timing generally depends on (1) threshold height, (2) local rates of relative SLR and (3) the timing of nodal cycle minima in tidal amplitude. Higher rates of relative SLR and/or lower thresholds lead to earlier YOIs. Glacial isostatic adjustment[31] can offset absolute SLR, leading to YOIs later in the century (for example, in Oregon and Washington). The relative importance of the nodal cycle varies with the ratios in Fig. 2. For locations and regions where the nodal cycle is a leading order contribution to changes in HTF, YOIs tend to occur near minima in tidal amplitude. We note, however, that the timing of minima in tidal amplitude varies regionally depending on the tidal constituent for which nodal cycle modulations are most prominent. For Hawai'i, the Pacific Coast and the Gulf of Mexico, the nodal cycle is most prominent in modulations of the lunar diurnal (K1) tidal constituent, which has amplitude minima in the mid-2030s, mid-2050s and early 2070s. For northern portions of the Atlantic coast, the nodal cycle is most prominent in modulations of the lunar semidiurnal (M2) tidal constituent, which has amplitude minima in the mid-2020s, mid-2040s and early 2060s. Hence, the YOI for Boston in Fig. 1 occurs in the mid-2040s, while YOIs for the other three cases occur in the mid-2030s.

The purpose of the YOI calculation is to provide a marker for the potential onset of rapid HTF increases. The severity of the increase following YOIs is indicated in two ways in Fig. 3. The values along the vertical axis correspond to absolute increases in the expected number of HTF days per year during the decade following each YOI. The sizes of the markers correspond to relative increases (that is, ten-year multipliers) in HTF days per year over the decade following the YOI. The most acute inflections occur where the ten-year period following the YOI experiences both large absolute (that is, the upper portion of the vertical-axis domain) and large relative (that is, large marker) changes.

Under the Intermediate scenario, many Atlantic locations will experience modest inflections in the frequency of minor HTF in the mid-2020s (Fig. 3, top), which in some cases correspond to minima in nodal cycle modulations of the M2 tidal constituent. The relative ten-year increases for Atlantic locations are generally modest compared with those for other regions, because the minor threshold is already routinely exceeded for many of these sites[11]. Around the mid-2030s, locations along the Pacific and Gulf of Mexico coastlines will experience rapid increases in HTF frequency (Fig. 3, top). The timing and severity of inflections in these regions are influenced by nodal cycle modulations of the K1 tidal constituent and are generally associated with large ten-year multipliers, indicating transitions from few to many HTF days per year. Under the Intermediate SLR scenario, 71% of Pacific Island, California and Gulf of Mexico locations will experience at least a tripling, and 59% at least a quadrupling, of minor HTF days per year over a ten-year period beginning in the 2030s.

NOAA moderate flooding thresholds are rarely exceeded at present[11]. For the Intermediate SLR scenario, rapid transitions in moderate HTF tend to begin in the mid-2040s along the Atlantic coast and during the 2050s for the Pacific and Gulf coasts (Fig. 3, bottom). Exceptions include Gulf of Mexico locations (for example, Grand Isle, Louisiana, and Galveston, Texas) where YOIs occur during the mid-2030s due to high subsidence rates and substantially larger relative SLR. In general, YOIs for moderate thresholds occur later in the century than those for minor thresholds. Since the projected rate of SLR accelerates during the twenty-first century, YOIs

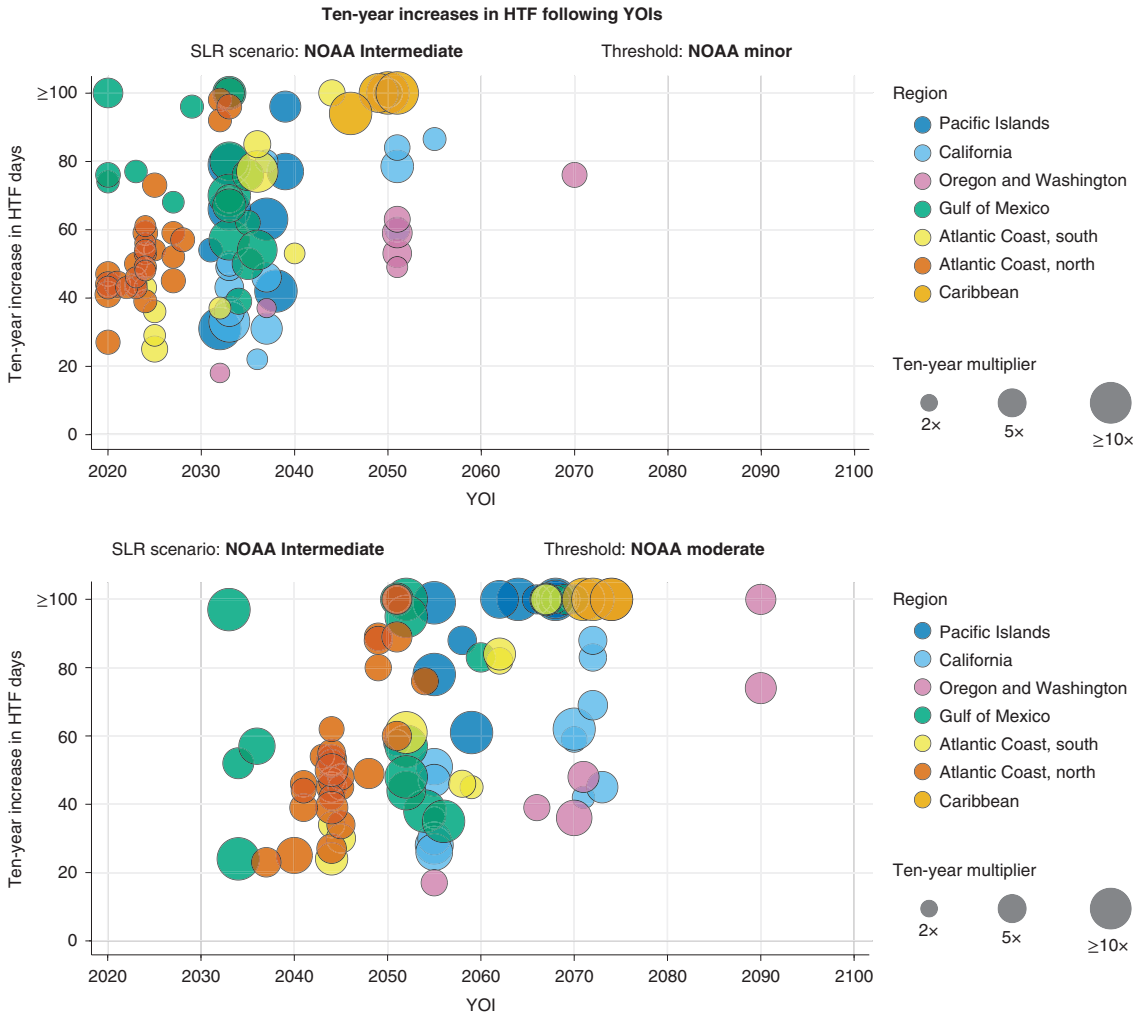

Fig. 3 | YOIs for the NOAA Intermediate SLR scenario. The upper and lower panels correspond to the NOAA minor and moderate flooding thresholds, respectively. The position along the horizontal axis corresponds to the timing of the YOI. The vertical axis indicates projected ten-year increases in annual counts of HTF days following YOIs. The dot sizes correspond to ten-year multipliers following the YOIs. The colours denote geographic regions. See Extended Data Fig. 2 for an analogous figure assuming the NOAA Intermediate Low SLR scenario.

for moderate thresholds tend to occur during periods when SLR rates are higher. As a result, the ten-year multipliers for decades following YOIs are larger for the moderate flooding thresholds than for the minor thresholds. For the Intermediate SLR scenario, 79% of locations would experience at least a fourfold increase in the HTF frequency above the moderate threshold during a single decade (compared with 39% for the minor threshold), and 35% would experience a sixfold increase during a single decade (compared with 20% for the minor threshold).

Clustering of HTF days

The 90th percentile of the ensemble spread for annual projections (Fig. 1) is expected to be exceeded about once per decade on average. Thus, year-to-year sea-level variability unrelated to secular SLR will lead to occasional but inevitable extreme years when many HTF days cluster together[19]. The 4.4-year modulation of tidal amplitude[32] can also contribute to extreme years, apparent in the HTF projection for La Jolla (Fig. 1) and other locations, especially the Pacific Coast and Southeast-Atlantic Bight (not shown). Clustering occurs at subannual timescales as well, and there are typically one or two seasons at any location for which the number of HTF days increases more rapidly due to annual and semiannual cycles in mean sea level and tidal amplitude (Extended Data Fig. 3). In Honolulu, for example, the most likely (50th percentile) annual count of HTF days in 2047 is 63 (Fig. 1). However, splitting the analysis into monthly counts reveals that 30 of those events are expected to occur over a span of three months (October–December, Extended Data Fig. 3). The expected temporal density of HTF days during this season (ten days per month) is thus approximately double that expected from considering the annual count alone (about five days per month). Similar differences in the seasonal density of HTF days are expected for the other three locations. Note that the seasonal timing of peaks in semiannual modulations of tidal amplitude (and hence HTF frequency) vary year to year and are linked to the 4.4-year modulations mentioned above[32].

The seasonal clustering of events can be further compounded by monthly to seasonal sea-level anomalies associated with modes of internal climate variability (for example, El Niño) or other atmosphere–ocean processes. If, for example, a large monthly mean sea-level anomaly occurs during peak HTF season, the two factors produce elevated numbers of HTF days during a brief period that far exceeds the expected annual density of events[33]. To demonstrate the impact of clustering, we calculate the average number of HTF days per month in five-year periods for the four locations

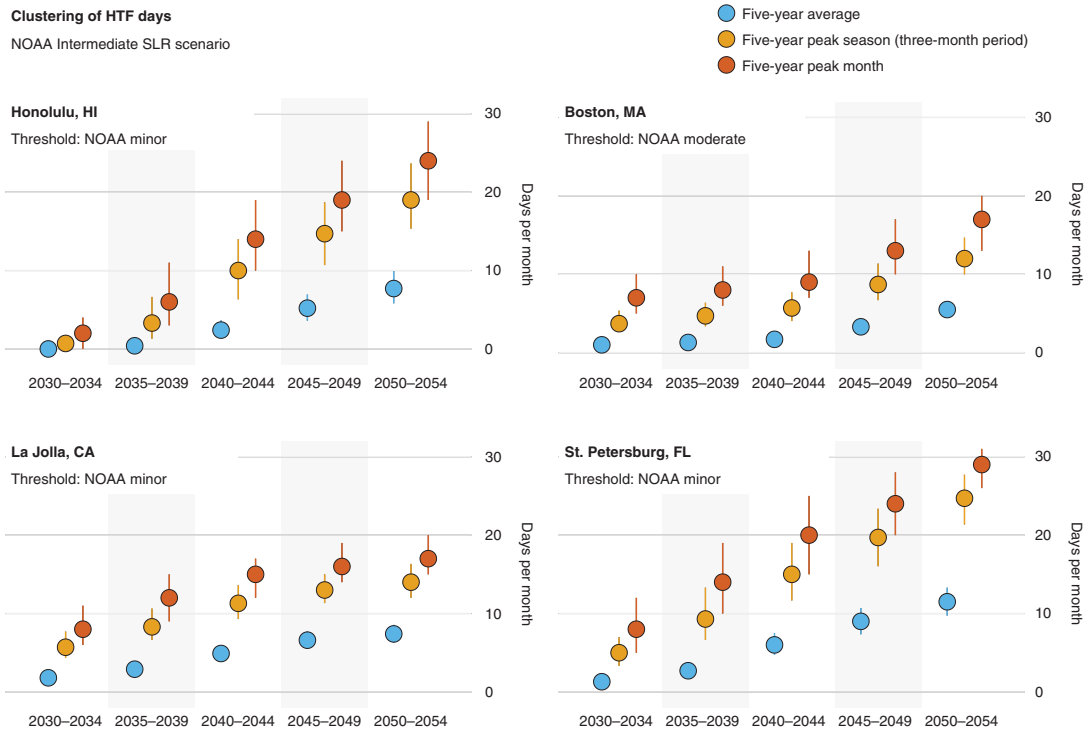

Fig. 4 | Extreme months and seasons. Projections of HTF days in five-year periods for the four US stations in Fig. 1 under the NOAA Intermediate SLR scenario, including the average number of HTF days per month in each five-year period (blue), the average number of HTF days per month during the five-year peak season (light orange) and the number of HTF days in the five-year peak month (dark orange). The circles represent the 50th percentile from the ensemble. The vertical lines show the 10th–90th percentiles of the ensemble range.

(Fig. 4). Using the ensemble projections, we also estimate the counts of HTF days during the most extreme season (that is, consecutive three-month period) and most extreme individual month over each five-year span (Fig. 4). For example, the 2040–2044 pentad in Honolulu is projected to experience ~2.5 minor HTF days per month on average (or about 150 minor HTF days over the entire five-year span). However, projected counts of minor HTF days during the most extreme season and month during this five-year span are 6–14 and 10–19 HTF days per month, respectively. Similar clustering is expected for St. Petersburg, while the effect is smaller for Boston and La Jolla. In general, using the expected number of HTF days per year (or pentad or decade) for decision-making will greatly underestimate the cumulative impact during brief periods experiencing extreme numbers of HTF days.

Another consequence of clustering is that any given HTF frequency will occur during brief periods long before it becomes expected on an annual basis. For example, consider the case for which minor flooding occurs on a majority of days during a given period. For most locations under the Intermediate scenario, this frequency of minor HTF will not occur on an annual basis until the second half of the twenty-first century[10]. Projections of minor HTF confirm this timeline for annual periods (Fig. 5, top row). However, if the focus shifts to monthly periods and includes the impact of clustering, we find that the timeline for experiencing flooding on a majority of days during a given period shifts towards the present (Fig. 5, bottom three rows). To estimate the importance of this effect, we calculated the probability that each location will experience minor flooding on a majority of days during a single month at least two decades before the year when minor flooding becomes expected on a majority of days annually. The probabilities were calculated by determining the fraction of projection ensemble members for each location that met this criterion. For the Intermediate scenario, this probability exceeds 50% (that is, it is more likely than not) at 42% of the locations analysed. The percentage increases to 81% of stations for lead times of 15 or more years. By incorporating the combined effects of month-to-month variations in mean sea level and tidal amplitude, our results suggest that planning horizons based on the emergence time[34] of a particular HTF frequency may need to be adjusted by decades towards the present to account for the clustering of HTF days during extreme months.

Discussion

Multiple strategies have been developed to identify key impact thresholds in terms of either HTF frequency[5] or the cumulative economic impact of frequent HTF events[3]. The YOI calculation here complements existing metrics by focusing on the pace of change and identifying the onset (rather than the endpoint) of rapid increases from few to many expected HTF events per year. The application of adaptation pathways requires updating policy and management strategies when predetermined environmental triggers or decision points occur[12–14]. Site-specific YOIs are candidates for such decision points, and the methodology underpinning the calculation provides important environmental context for stakeholders and decision-makers. In particular, nodal cycle modulations of tidal amplitude will suppress SLR-induced increases in HTF during certain periods and may delay the onset of environmental adaptation triggers. Such delays could produce complacency and inaction through false confidence in benign pathways. The effect of the nodal cycle is implicit in the YOI calculation, which will allow decision-makers and stakeholders to communicate that periods of little perceptible change are expected in many locations—only to be followed by periods of exponential HTF increase.

In general, if SLR approaches or exceeds the NOAA Intermediate scenario in the coming decades, the United States should expect the

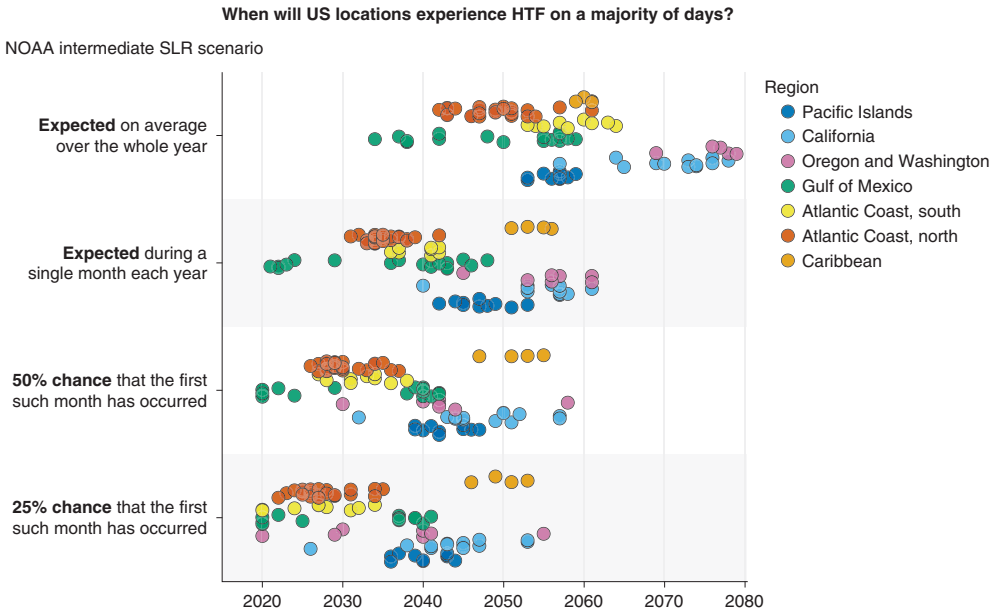

Fig. 5 | Years for which US coastal locations will experience HTF on a majority of days during annual and monthly windows. The calculations assume the NOAA Intermediate SLR scenario. Years for which HTF is expected to occur on a majority of days on average during annual and monthly periods (top two rows) are compared with years for which flooding will first occur on a majority of days during a single month (bottom two rows). The dot colours denote station regions. The vertical position of each dot within the rows is an arbitrary vertical offset to allow visual distinction between regions and individual locations. See Extended Data Fig. 4 for an analogous figure assuming the NOAA Intermediate Low SLR scenario.

onset of a rapid increase in HTF frequency during the mid-2030s corresponding to the combined effects of ongoing SLR and increasing tidal amplitude associated with nodal cycle modulations. The increase would be concentrated along the continental Pacific, Pacific Island and Gulf of Mexico coastlines, which are more vulnerable to SLR due to relatively narrow sea-level distributions[35], infrequent historical exposure to high storm surge[14] or both. Thus, under the NOAA Intermediate SLR scenario, the mid-2030s marks the onset of an expected transition in HTF from a regional issue to a national issue with a majority of US coastlines being affected. An important caveat to this result is that the YOIs represent the most likely inflection point, and decadal fluctuations in local mean sea levels may affect its timing.

The cumulative nature of impacts associated with minor HTF[1–3] suggests the need to account for severe seasons or months during which many HTF days cluster together in time. Just as engineers and coastal planners are accustomed to planning for rare, large-amplitude extreme events, adaptation and mitigation strategies focused on HTF should account for brief periods experiencing an extreme number of HTF days. The logic for basing decision-making on severe periods of HTF is the same as for basing design decisions on long (10-year or 100-year) return intervals rather than annual maxima, where the former has a planning horizon far in advance of the latter. Knowledge of the tendency for HTF days to cluster in time can aid the interpretation of HTF projections with coarse (annual and longer) temporal resolutions. On the basis of an aggregate analysis of clustering calculations across all US locations (not shown), we suggest the following rules of thumb for interpreting such projections. For a five-year period expected to experience a total of 100 HTF days, the six most severe months will experience 7–10 HTF days per month on average, while the remaining months will experience fewer than 1 HTF day per month on average. For 200 total HTF days over a five-year period, the six most severe months will experience 10–17 HTF days per month on average, while the remaining months will experience fewer than 2.5 HTF days per month on average. Importantly, this tendency for HTF days to cluster in time underscores the need for monthly-to-seasonal forecasting of sea-level anomalies to provide advance warning of periods likely to experience extreme numbers of events[36,37]. It is also possible that event clustering will be influenced by non-stationarity in the statistics of extreme non-tidal sea-level anomalies[38], which have not been considered here.

Finally, we reiterate that our analysis focused on existing and widely used NOAA SLR scenarios and derived HTF thresholds. The results are therefore unique to the specific combinations of location, SLR scenario and flooding threshold. As SLR continues and communities adapt, locally relevant flooding thresholds will evolve, and periodic reassessments will be required. Nevertheless, the concepts presented here are broadly applicable in identifying planning horizons and developing adaptation pathways for managing ongoing and future impacts of HTF. There is a need for nuanced understanding of projected increases in HTF frequency beyond quantifying, for example, bulk changes from one decade to the next. It is important to communicate to decision-makers that changes in HTF frequency will not be incremental in the coming decades but will include acute inflections in the rate of increase punctuated by extreme months and seasons during which many events will cluster together in time. These results form the basis of ongoing work to communicate projected increases in HTF to US decision-makers[39].

Online content

Any methods, additional references, Nature Research reporting summaries, source data, extended data, supplementary information, acknowledgements, peer review information; details of author contributions and competing interests; and statements of data and code availability are available at https://doi.org/10.1038/s41558-021-01077-8.

Received: 9 November 2020; Accepted: 4 May 2021;
Published online: 21 June 2021

References

1. Moftakhari, H. R., AghaKouchak, A., Sanders, B. F. & Matthew, R. A. Cumulative hazard: the case of nuisance flooding. *Earth's Future* **5**, 214–223 (2017).
2. Moftakhari, H. R., AghaKouchak, A., Sanders, B. F., Allaire, M. & Matthew, R. A. What is nuisance flooding? Defining and monitoring an emerging challenge. *Water Resour. Res.* **54**, 4218–4227 (2018).
3. Ghanbari, M., Arabi, M. & Obeysekera, J. Chronic and acute coastal flood risks to assets and communities in southeast Florida. *J. Water Resour. Plan. Manage.* **146**, 04020049 (2020).
4. Hino, M., Belanger, S. T., Field, C. B., Davies, A. R. & Mach, K. J. High-tide flooding disrupts local economic activity. *Sci. Adv.* https://doi.org/10.1126/sciadv.aau2736 (2019).
5. Sweet, W. V. & Park, J. From the extreme to the mean: acceleration and tipping points of coastal inundation from sea level rise. *Earth's Future* **2**, 579–600 (2014).
6. Wdowinski, S., Bray, R., Kirtman, B. P. & Wu, Z. Increasing flooding hazard in coastal communities due to rising sea level: case study of Miami Beach, Florida. *Ocean Coast. Manage.* **126**, 1–8 (2016).
7. Ray, R. D. & Foster, G. Future nuisance flooding at Boston caused by astronomical tides alone. *Earth's Future* **4**, 578–587 (2016).
8. Burgos, A. G., Hamlington, B. D., Thompson, P. R. & Ray, R. D. Future nuisance flooding in Norfolk, VA from astronomical tides and annual to decadal internal climate variability. *Geophys. Res. Lett.* **45**, 12432–12439 (2018).
9. Dahl, K. A., Fitzpatrick, M. F. & Spanger-Siegfried, E. Sea level rise drives increased tidal flooding frequency at tide gauges along the U.S. East and Gulf Coasts: projections for 2030 and 2045. *PLoS ONE* **12**, e0170949 (2017).
10. Sweet, W. V., Dusek, G., Obeysekera, J. & Marra, J. J. *Patterns and Projections of High Tide Flooding along the U.S. Coastline Using a Common Impact Threshold* NOAA Technical Report NOS CO-OPS 086 (US Department of Commerce, National Oceanic and Atmospheric Administration, National Ocean Service Center for Operational Oceanographic Products and Services, 2018).
11. Sweet, W. et al. *2019 State of U.S. High Tide Flooding with a 2020 Outlook* NOAA Technical Report NOS CO-OPS 092 2019 (US Department of Commerce, National Oceanic and Atmospheric Administration, National Ocean Service Center for Operational Oceanographic Products and Services, 2020).
12. Kwadijk, J. C. J. et al. Using adaptation tipping points to prepare for climate change and sea level rise: a case study in the Netherlands. *WIREs Clim. Change* **1**, 729–740 (2010).
13. Barnett, J. et al. A local coastal adaptation pathway. *Nat. Clim. Change* **4**, 1103–1108 (2014).
14. Stephens, S. A., Bell, R. G. & Lawrence, J. Developing signals to trigger adaptation to sea-level rise. *Environ. Res. Lett.* **13**, 104004 (2018).
15. Pugh, D. & Woodworth, P. *Sea-Level Science* (Cambridge Univ. Press, 2014).
16. Haigh, I. D., Eliot, M. & Pattiaratchi, C. Global influences of the 18.61 year nodal cycle and 8.85 year cycle of lunar perigee on high tidal levels. *J. Geophys. Res. Oceans* **116**, C06025 (2011).
17. Li, S. et al. Evolving tides aggravate nuisance flooding along the U.S. coastline. *Sci. Adv.* **7**, eabe2412 (2021).
18. Taherkhani, M. et al. Sea-level rise exponentially increases coastal flood frequency. *Sci. Rep.* **10**, 6466 (2020).
19. Thompson, P. R., Widlansky, M. J., Merrifield, M. A., Becker, J. M. & Marra, J. J. A statistical model for frequency of coastal flooding in Honolulu, Hawaii, during the 21st century. *J. Geophys. Res. Oceans* **124**, 2787–2802 (2019).
20. Tebaldi, C., Strauss, B. H. & Zervas, C. E. Modelling sea level rise impacts on storm surges along US coasts. *Environ. Res. Lett.* **7**, 014032 (2012).
21. Marcos, M., Calafat, F. M., Berihuete, Á. & Dangendorf, S. Long-term variations in global sea level extremes. *J. Geophys. Res. Oceans* **120**, 8115–8134 (2015).
22. Buchanan, M. K., Oppenheimer, M. & Kopp, R. E. Amplification of flood frequencies with local sea level rise and emerging flood regimes. *Environ. Res. Lett.* **12**, 064009 (2017).
23. Wahl, T. et al. Understanding extreme sea levels for broad-scale coastal impact and adaptation analysis. *Nat. Commun.* **8**, 16075 (2017).
24. Sweet, W. V. et al. *Global and Regional Sea Level Rise Scenarios for the United States* NOAA Technical Report NOS CO-OPS 083 (US Department of Commerce, National Oceanic and Atmospheric Administration, National Ocean Service Center for Operational Oceanographic Products and Services, 2017); https://doi.org/10.7289/V5/TR-NOS-COOPS-083
25. Hamlington, B. D., Leben, R. R., Strassburg, M. W., Nerem, R. S. & Kim, K. Contribution of the Pacific Decadal Oscillation to global mean sea level trends. *Geophys. Res. Lett.* **40**, 5171–5175 (2013).
26. Nerem, R. S. et al. Climate-change-driven accelerated sea-level rise detected in the altimeter era. *Proc. Natl Acad. Sci. USA* **115**, 2022–2025 (2018).
27. Han, W. et al. Impacts of basin-scale climate modes on coastal sea level: a review. *Surv. Geophys.* **40**, 1493–1541 (2019).
28. Kopp, R. E. et al. Probabilistic 21st and 22nd century sea-level projections at a global network of tide-gauge sites. *Earth's Future* **2**, 383–406 (2014).
29. IPCC *Climate Change 2013: The Physical Science Basis* (eds Stocker, T. F. et al.) (Cambridge Univ. Press, 2013).
30. Peng, D., Hill, E. M., Meltzner, A. J. & Switzer, A. D. Tide gauge records show that the 18.61-year nodal tidal cycle can change high water levels by up to 30 cm. *J. Geophys. Res. Oceans* **124**, 736–749 (2019).
31. Peltier, W. R. & Tushingham, A. M. Influence of glacial isostatic adjustment on tide gauge measurements of secular sea level change. *J. Geophys. Res. Solid Earth* **96**, 6779–6796 (1991).
32. Ray, R. D. & Merrifield, M. A. The semiannual and 4.4-year modulations of extreme high tides. *J. Geophys. Res. Oceans* **124**, 5907–5922 (2019).
33. Yoon, H., Widlansky, M. J. & Thompson, P. R. Nu'a Kai: flooding in Hawaii caused by a 'stack' of oceanographic processes [*in 'State of the Climate in 2017'*]. *Bull. Am. Meteorol. Soc.* **99**, S88–S89 (2018).
34. Hague, B. S., McGregor, S., Murphy, B. F., Reef, R. & Jones, D. A. Sea level rise driving increasingly predictable coastal inundation in Sydney, Australia. *Earth's Future* **8**, e2020EF001607 (2020).
35. Rueda, A. et al. A global classification of coastal flood hazard climates associated with large-scale oceanographic forcing. *Sci. Rep.* **7**, 5038 (2017).
36. Widlansky, M. J. et al. Multimodel ensemble sea level forecasts for tropical Pacific islands. *J. Appl. Meteorol. Climatol.* **56**, 849–862 (2017).
37. Jacox, M. G. et al. Seasonal-to-interannual prediction of North American coastal marine ecosystems: forecast methods, mechanisms of predictability, and priority developments. *Prog. Oceanogr.* **183**, 102307 (2020).
38. Widlansky, M. J., Long, X. & Schloesser, F. Increase in sea level variability with ocean warming associated with the nonlinear thermal expansion of seawater. *Commun. Earth Environ.* **1**, 9 (2020).
39. Thompson, P. R. *Flooding Days Projection Tool*. https://sealevel.nasa.gov/flooding-days-projection/ (2019).

Methods

Projections of HTF days. The projection framework is based on the idea that the number of observed hourly flooding threshold exceedances in a month—including the combined effect of tides, surge and other high-frequency contributions—is statistically related to monthly mean sea level and the amplitude of the highest tides during the month. For higher monthly mean sea level or tidal amplitude, there is a tendency to experience a greater number of flooding threshold exceedances, because the baseline sea level is higher. A higher baseline means that smaller-amplitude, more common surges can raise the total water level above the threshold.

An overview of the projection methodology is as follows:

1. Find a statistical relationship that maps monthly mean sea level, tidal amplitude and threshold height onto observed monthly counts of threshold exceedances in hourly tide-gauge data. The hourly tide-gauge data includes high-frequency surge and so on.
2. Generate ensemble projections of monthly mean sea level and tidal amplitude for the twenty-first century.
3. Map the ensemble projections of mean sea level and tidal amplitude from step 2 onto future counts of threshold exceedances using step 1. The resultant ensemble projections of threshold exceedances (that is, HTF) represent a range of possibilities for the number of exceedances a tide gauge would be expected to observe during a given future month.

The details of these steps are provided in the subsequent sections.

Relating tidal range, mean sea level and counts of HTF days. The methodology employed here builds on an approach previously developed for projecting the frequency of HTF in Honolulu, Hawai'i[19]. The fundamental assertion of this approach is that the probability distribution governing the number of HTF days at a given location during a single month is closely related to a single parameter, Δ_{99}:

$$\Delta_{99} \equiv (\zeta_{99} + \overline{\eta}) - H, \tag{1}$$

where ζ_{99} is the 99th percentile of predicted astronomical hourly tidal heights relative to current tidal datums, $\overline{\eta}$ is the monthly mean of the non-tidal sea level variability and H is the height of the flooding threshold of interest. Previous work focused on annual periods; here we calculate monthly values of ζ_{99} and $\overline{\eta}$ to produce monthly values of Δ_{99}. The term in parentheses, $\zeta_{99} + \overline{\eta}$, provides a general measure of the height of high tides during a given month. The specific role of ζ_{99} is to capture variability in high-tide levels due to seasonal-to-decadal modulations of tidal range. Note that the results herein are not sensitive to the particular percentile used. The specific role of $\overline{\eta}$ is to capture variability in high-tide levels due to changes in the mean level about which the tides oscillate. By subtracting the threshold height, H, from this sum, we can interpret variability in Δ_{99} as a measure of whether high tides are generally higher (more positive Δ_{99}) or lower (more negative Δ_{99}) than the threshold for a given month. The presence of stochastic, submonthly water level variability prevents relating Δ_{99} to a specific monthly count of threshold exceedances. Instead, we state that the Δ_{99} parameter is related to the probability mass distribution (PMD) governing the number of days during a month for which the maximum hourly water level exceeds the threshold. In other words, we cannot precisely predict the observed number of threshold exceedances on the basis of monthly quantities, because we do not know the exact number and magnitude of high-frequency anomalies that will occur in the future. We can, however, predict the likelihood of any given number of threshold exceedances on the basis of the observed historical relationships between mean sea level, tidal amplitude and threshold exceedances.

To demonstrate the relationship between Δ_{99} and monthly counts of HTF days, we first calculate observed values of ζ_{99} and $\overline{\eta}$ using hourly tide-gauge observations. We then tally the number of daily maximum water levels that exceed a range of thresholds in each month (that is, monthly counts of HTF days) and record the Δ_{99} value corresponding to each monthly count. Scatter plots of January HTF day counts versus January values of Δ_{99} for Honolulu and Boston, respectively, give insight into the functional form relating the two quantities (Extended Data Fig. 5). As expected, increasing Δ_{99} (that is, high tides rising relative to the threshold) corresponds to greater numbers of HTF days in each month. Note that the domain of Δ_{99} values is much narrower for Honolulu than for Boston, reflecting a much narrower distribution of daily maximum water levels for the former than for the latter. It is also important to note that the relationship between Δ_{99} and HTF days is nonlinear, and a unit change in Δ_{99} leads to varying increases in HTF days depending on the value of Δ_{99}.

To capture the probabilistic relationship between Δ_{99} and the monthly counts of HTF days, we model the PMD for monthly counts of HTF days as a beta-binomial distribution[40]. The beta-binomial distribution describes the probability of a discrete number of successes over N binary trials, where the probability that any single trial is a success is itself a continuous beta-distributed random variable, $p \in [0, 1]$. In this case, each of the N days in a month is a 'trial', and each time the daily maximum water level exceeds the threshold of interest is a 'success'. The beta distribution governing p can be described by its mean, μ, and variance, σ^2. Because p is beta-distributed, the beta-binomial distribution offers a general representation of binomially distributed counts that can take a variety of shapes. The flexibility of the beta-binomial distribution is useful, because the shape of the PMD for the monthly counts changes drastically depending on the value of Δ_{99}. For example, when Δ_{99} takes a large negative value (that is, when the highest tides of the month are well below the threshold), we expect a highly asymmetric, one-sided PMD with a high probability of zero exceedances and a low probability of many exceedances. As Δ_{99} increases to an expected (or mean) count of 10–20 days per month, the distribution of counts about the mean becomes approximately symmetric. As Δ_{99} increases further, the distribution becomes asymmetric and one-sided again as the counts begin to saturate at the maximum number of days per month.

We use the beta-binomial distribution to formulate a hierarchical model describing the probabilistic relationships between the vector of observed monthly counts of HTF days ($\mathbf{Y}$) and the vector of observed Δ_{99} values ($\mathbf{x}$). The model is summarized

$$\begin{aligned} \mathbf{Y} \,|\mathbf{x},\ \boldsymbol{\Theta},\ \nu\ &\sim\ \text{BetaBinomial}(N,\ \boldsymbol{\mu},\ \boldsymbol{\sigma}^2), \\ \boldsymbol{\mu}\ &=\ S(\mathbf{x};\ \boldsymbol{\Theta}), \\ \boldsymbol{\sigma}^2\ &=\ \nu\boldsymbol{\mu}(1-\boldsymbol{\mu}), \end{aligned} \tag{2}$$

where $\boldsymbol{\mu}$ and $\boldsymbol{\sigma}^2$ are vectors of μ and σ^2 that determine the shape of the beta-binomial distribution at each value in $\mathbf{x}$. The elements in $\boldsymbol{\sigma}^2$ are related to the elements in $\boldsymbol{\mu}$ by a scalar parameter, $\nu \in (0, 1)$, and the third relation in equation (2), which can be derived from the analytical function describing the distribution. This leaves only μ to be defined explicitly as a function of x (that is, Δ_{99}), which is represented by a function S requiring parameters $\boldsymbol{\Theta}$.

Since μ describes the expectation value of the probability, p, that a single day experiences a maximum hourly water level above the threshold, and since daily maximum water levels at any given station tend to be approximately normally distributed, we base the function S on the normal cumulative distribution function:

$$\Phi(x) = \frac{1}{2}\left[1 + \text{erf}\left(\frac{x-\xi}{\omega\sqrt{2}}\right)\right], \tag{3}$$

where erf(·) is the Gauss error function, and ξ and ω are parameters representing the location and scale of the function, respectively. In practice, we found that using this function alone as in prior work[19] (that is, $S(x) = \Phi(x)$) did not perform optimally in many cases due to minor deviations from a purely normal distribution—namely, slight asymmetries in the distribution of daily maximum water levels. We improved the ability of the model to describe the observed counts by defining S as the sum of two normal cumulative distribution functions blended across a change point via a logistic function:

$$S(x;\ r,\ x_0,\ \xi_1,\ \omega_1,\ \xi_2,\ \omega_2) = L(x;\ -r,\ x_0)\Phi(x;\ \xi_1,\ \omega_1) + L(x;\ r,\ x_0)\Phi(x;\ \xi_2,\ \omega_2), \tag{4}$$

where $L(x)$ is a logistic function:

$$L(x) = \frac{1}{1 + e^{-r(x-x_0)}}, \tag{5}$$

with r determining the slope of the transition—note the sign change of r from the first to the second term in equation (4)—and x_0 determining the location of the change point. This blended version of S allows the shape of the function to be determined by ω_1 and ξ_1 for $x < x_0$ and ω_2 and ξ_2 for $x > x_0$ with a narrow, smooth transition band of length scale $1/r$ to avoid discontinuity. In practice, we fix the length scale to 10% of the Δ_{99} domain and treat the change point x_0 as a free parameter. The vector of parameters required for the S in the hierarchical model is then $\boldsymbol{\Theta} = \{x_0, \xi_1, \omega_1, \xi_2, \omega_2\}$.

We estimate distributions of the free parameters in equation (2)—that is, $\boldsymbol{\Theta}$ and ν—for each station individually using Bayesian inference implemented via a Markov chain Monte Carlo (MCMC) method. Bayesian inference via MCMC was implemented by building and evaluating the hierarchical model in PyMC3 (ref. [41]), an open-source probabilistic programming framework for Python. Uninformative uniform prior distributions were assumed for all model parameters. Posterior distributions for the parameters were conditioned on vectors of observed monthly counts ($\mathbf{Y}$) and Δ_{99} values ($\mathbf{x}$) such as those represented by the scatter plots in Extended Data Fig. 5. Given the posterior distributions for the free parameters, we can then input a monthly value for Δ_{99} as $\mathbf{x}$ into equation (2) and output a probability distribution for the monthly count of HTF days above a threshold. The posterior models for Honolulu and Boston demonstrate the ability of the method to capture the probabilistic relationships underlying the scatter plots (Extended Data Fig. 5). Thus, given a projection (or ensemble of projections) of Δ_{99} during the twenty-first century, we can produce probabilistic projections for monthly counts of HTF days above a threshold.

Twenty-first-century projections of Δ_{99}. Projecting future Δ_{99} values for each station and threshold during the twenty-first century requires projections of ζ_{99} and $\overline{\eta}$ in equation (1). The latter is composed of two components: (1) secular local mean sea level (LMSL) rise related to forced climate variability and vertical land motion, and

(2) stochastic monthly LMSL variability related to atmosphere–ocean dynamics and internal climate variability. This gives three components of Δ_{99} (ζ_{99} plus two components of $\overline{\eta}$), which we project independently as discussed below.

Secular LMSL rise projections. We use the NOAA local SLR scenarios[24] obtained from the NOAA Center for Operational Oceanographic Products and Services (CO-OPS, https://tidesandcurrents.noaa.gov/publications/techrpt083.csv). These are discrete projections with predetermined amounts of LMSL rise by 2100, which are designed to provide planning scenarios corresponding to various risk tolerances. The scenarios for each site include local factors such as glacial isostatic adjustment and regional patterns of sea level change due to the gravitational and rotational effects of melting glaciers and ice sheets. We focus on the Intermediate Low and Intermediate scenarios, which correspond to twenty-first-century global mean SLR of 0.5 m and 1.0 m, respectively. The NOAA scenarios are provided with decadal resolution, which we interpolate to monthly resolution via cubic spline.

Projecting monthly LMSL variability. Gaussian processes have been used previously to model parameters relating mean sea level variability and HTF[42]. We modelled non-secular monthly LMSL variability, $m(t)$, as the weighted sum of a zero-mean Gaussian process with unit variance G and normally distributed white noise with zero mean and unit variance Σ:

$$m(t) = aG + b\Sigma\,. \tag{6}$$

Serial correlation in G is determined by an exponentiated quadratic covariance function, K:

$$K(t,t') = \exp\left[\frac{(t-t')^2}{2l^2}\right], \tag{7}$$

where l is a timescale. The distributions of the free parameters, $\{a, b, l\}$, were determined from observed monthly mean tide-gauge observations for each station via Bayesian inference and MCMC using PyMC3 (ref. [41]). Given the variance in the observed non-secular monthly mean sea level time series, σ_m^2, the parameters a and b were chosen from a multivariate beta (or Dirichlet) prior to ensure that $a^2 + b^2 = \sigma_m^2$ and for any given draw from the posterior. The parameter l was given an uninformative gamma-distributed prior. We generated an ensemble of 10^4 posterior samples of $m(t)$ spanning the twenty-first century for each US tide-gauge station.

99th percentile of astronomical tides. Tides are often treated as if they are unchanging in HTF assessments, and tide predictions are often performed and interpreted as if they are free from uncertainty. These are not good assumptions in many locations[17] due to correlations of tidal amplitude with mean sea level variability[43] and changes in the geometry of harbours and estuaries[44]. Here, we generate an ensemble of tide predictions for each location that accounts for portions of the non-stationarity in future tidal amplitudes. In particular, we include the observed relationship between mean sea level variability and constituent amplitudes and phases, and we include an extrapolation of secular trends in tidal amplitude and phase that are unrelated to mean SLR. Our method does not represent a complete accounting of the uncertainty and sources of non-stationarity—and some assumptions have been made—but the result is preferable to not considering non-stationarity and uncertainty in the tides.

Ensemble projections of ζ_{99} were determined for each location individually in a multistep process:

1. Generate an initial estimate of tidal constituents from harmonic analysis of hourly tide-gauge data. For this initial step, tidal constituents were estimated from the complete record using an implementation of UTide[45] for Python. Note that the development of UTide for Python is ongoing, but comparisons of UTide predictions to NOAA tide predictions suggest that results from the former are robust.
2. Distinguish between minor and major constituents with signal-to-noise ratios less than two and greater than two, respectively.
3. Subtract predictions of minor constituents over the observed period and perform harmonic fits on the remaining hourly variability using UTide[45] for the major constituents in each year of the record individually. Year-to-year variations in major-constituent amplitudes and phases reflect both astronomical (for example, nodal cycle) and non-astronomical (for example, correlation with mean sea level[43]) processes.
4. Model the variability in the phases and amplitudes of each constituent as a sum of Gaussian processes with periodic and linear kernels, plus a term proportional to detrended annual mean sea level variability and an additional white-noise term. The periodic kernels represent major tidal modulation periodicities (18.61, 9.305, 8.85 and 4.425 years)[16]. Linear trends in the constituent amplitudes and phases were modelled as two linear processes linked at a variable change point, which allows for an inflection in the secular trend of each constituent and ensures that extrapolated linear trends in the amplitude and phase of each constituent are representative of the most recent trend. The change point was required to be consistent for both amplitude and phase. The model parameters and the relative weight of each component were determined via Bayesian inference and MCMC using PyMC3 (ref. [41]).
5. Generate an ensemble projection of each constituent individually from the components of amplitude and phase variability in the previous step. When projecting tidal variability for the twenty-first century, we confine the relationship with mean sea level to be a relationship with steric (or density-related) changes in mean sea level. In general, the relationship between mean sea level and constituent amplitude can be related to water depth or stratification, but it is difficult to disentangle these effects in the absence of dedicated, local modelling studies[46]. The decision to confine the relationship to steric changes in mean sea level is thus a conservative choice to limit overestimating this effect. Only the steric component of the NOAA SLR scenario used in each case is added to the ensemble of monthly LMSL variability (described earlier in the Methods) to produce estimates of steric sea level variability in the twenty-first century.
6. Construct an ensemble of 10^4 hourly twenty-first-century tidal height predictions from the ensemble of annual projections for each major constituent and add a deterministic prediction of the minor constituents. The Gaussian process representations underlying each major constituent allow us to construct tidal predictions with hourly resolution that modulate smoothly from one annual window to the next. Note that in every case, our methodology for tide prediction produces a reduction in non-tidal residual variability over the observed period compared with the standard NOAA harmonic analysis.
7. From the ensemble of hourly tidal height predictions, generate an ensemble of 10^4 projections of ζ_{99}.

Ensemble projections of HTF days. To produce ensemble twenty-first-century projections of HTF days above a given threshold, we performed the following procedure for each combination of station, SLR scenario and threshold:

1. Generate 10^4 projections of Δ_{99} by adding the ensemble of $\overline{\eta}$ projections (SLR scenario plus monthly variability) to the ensemble of ζ_{99} and subtracting the threshold height, H.
2. For each value in the ensemble of Δ_{99} projections, make a draw from the posterior of the model in equation (2).
3. Generate a random positive integer representing a monthly count of HTF days from the beta-binomial distribution described by each combination of Δ_{99} value and posterior draw.

The result is an ensemble of 10^4 twenty-first-century projections of HTF days per month for each combination of station, SLR scenario and threshold. We can then leverage these ensembles of monthly counts to generate likely ranges and assess the relationship of extreme months and seasons to counts over longer periods of years to decades. Note that the spread in each ensemble grows with SLR due to the nature of counting exceedances above a threshold (for example, the 10th–90th percentile ranges in Fig. 1). For example, when a threshold is rarely exceeded, most years will experience zero HTF days, and the range of possible annual counts is narrow (for example, zero to five HTF days per year). With SLR, exceedances become more common, and the range of possible annual counts grows.

Determination of YOIs. YOIs were identified using the 50th-percentile curve from the ensemble of annual HTF projections (see below) for each combination of location, scenario and threshold. Two characteristics of the 50th-percentile curve were used. The first is the difference in the change in HTF frequency between two adjacent ten-year periods, which is analogous to the second derivative of the 50th-percentile curve and is largest when the slope of the projection changes rapidly. There can be multiple acute inflections over a single projection, however, which motivated the use of a second quantity: the ten-year multiplier (or x-fold increase) over the second of the two adjacent ten-year periods. The ten-year multiplier is largest for inflections that represent a transition from few to many expected days of HTF per year. For example, a change from 10 to 50 HTF days per year over the second ten-year period has a multiplier of 5; a change from 50 to 100 has a multiplier of 2. In practice, we computed both quantities in sliding 21-year windows centred on each year in the HTF projection curves. We identified the YOI for each combination of location, scenario and threshold as the year with the highest average rank over both quantities.

Data availability

The tide-gauge sea-level data used in this analysis are publicly accessible and were obtained from the NOAA CO-OPS Data Retrieval API (https://api.tidesandcurrents.noaa.gov/api/prod/). The NOAA SLR scenarios are publicly available and were obtained from the NOAA CO-COPS website (https://tidesandcurrents.noaa.gov/publications/techrpt083.csv).

Code availability

All code generated for the data analysis and figure creation is archived in a public repository[47] under the GNU Affero General Public License v.3.0. The repository includes the Python environment, which provides the versions of all third-party libraries and packages used in this work.

References

40. Skellam, J. G. A probability distribution derived from the binomial distribution by regarding the probability of success as variable between the sets of trials. *J. R. Stat. Soc. B* **10**, 257–261 (1948).
41. Salvatier, J., Wiecki, T. V. & Fonnesbeck, C. Probabilistic programming in Python using PyMC3. *PeerJ Comput. Sci.* https://doi.org/10.7717/peerj-cs.55 (2016).
42. Vandenberg-Rodes, A. et al. Projecting nuisance flooding in a warming climate using generalized linear models and Gaussian processes. *J. Geophys. Res. Oceans* **121**, 8008–8020 (2016).
43. Devlin, A. T. et al. Coupling of sea level and tidal range changes, with implications for future water levels. *Sci. Rep.* **7**, 17021 (2017).
44. Familkhalili, R. & Talke, S. A. The effect of channel deepening on tides and storm surge: a case study of Wilmington, NC. *Geophys. Res. Lett.* **43**, 9138–9147 (2016).
45. Codiga, D. L. *Unified Tidal Analysis and Prediction Using the UTide Matlab Functions* Technical Report No. 2011-01 (Graduate School of Oceanography, University of Rhode Island, 2011); https://doi.org/10.13140/RG.2.1.3761.2008
46. Haigh, I. D. et al. The tides they are a-changin': a comprehensive review of past and future nonastronomical changes in tides, their driving mechanisms, and future implications. *Rev. Geophys.* **58**, e2018RG000636 (2020).
47. Thompson, P. R. Code repository for 'Rapid increases and extreme months in projections of United States high-tide flooding'. *Zenodo* https://doi.org/10.5281/zenodo.4723019 (2021).

Acknowledgements

P.R.T. acknowledges support from NASA grant no. 80NSSC17K0564 and NOAA grant no. NA16NMF4320058. M.J.W. acknowledges support from NOAA grant nos NA17OAR4310110 and NA19OAR4310292. B.D.H. acknowledges support from the NASA Sea-Level Change Team (N-SLCT, WBS no. 105393).

Author contributions

P.R.T. designed the approach, performed the analyses and drafted the paper. M.J.W., B.D.H. and M.A.M. made substantive revisions. All authors made substantive contributions to the interpretation and communication of the results.

Competing interests

The authors declare no competing interests.

Additional information

Extended data is available for this paper at https://doi.org/10.1038/s41558-021-01077-8.

Supplementary information The online version contains supplementary material available at https://doi.org/10.1038/s41558-021-01077-8.

Correspondence and requests for materials should be addressed to P.R.T.

Peer review information *Nature Climate Change* thanks Kristina Dahl, Ben Hague and Hamed Moftakhari for their contribution to the peer review of this work.

Reprints and permissions information is available at www.nature.com/reprints.

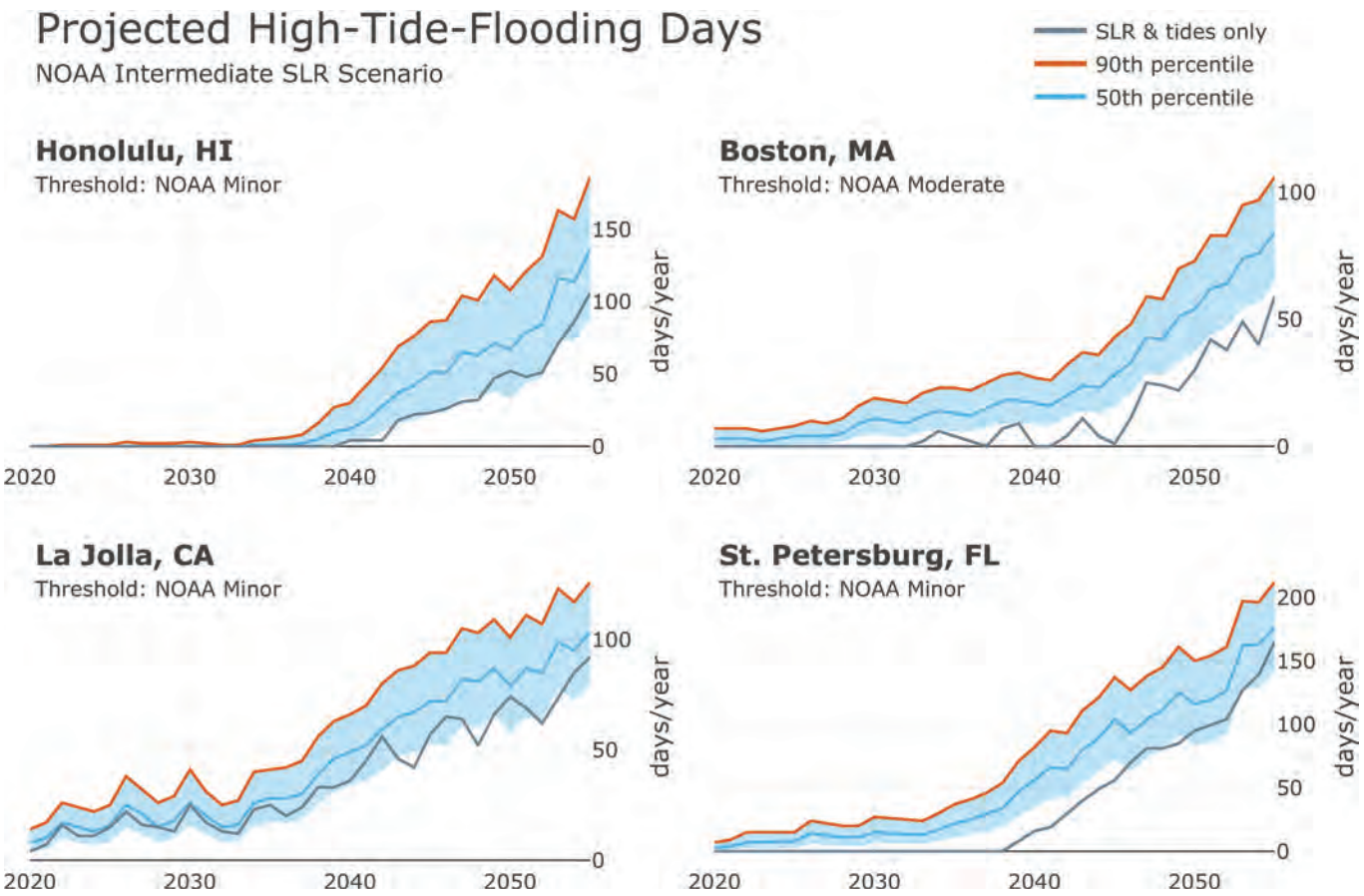

Extended Data Fig. 1 | Projections of annual counts of high-tide-flooding (HTF) days compared to expectations from SLR and tides alone. The four ensemble projections (blue) are identical to Fig. 1. The simple projection of HTF frequency based only on the SLR scenario and predictions of astronomical tides (gray) underestimates the frequency of HTF due to the exclusion of local mean sea level variability across a variety of time scales from high-frequency surge to decadal climate variability.

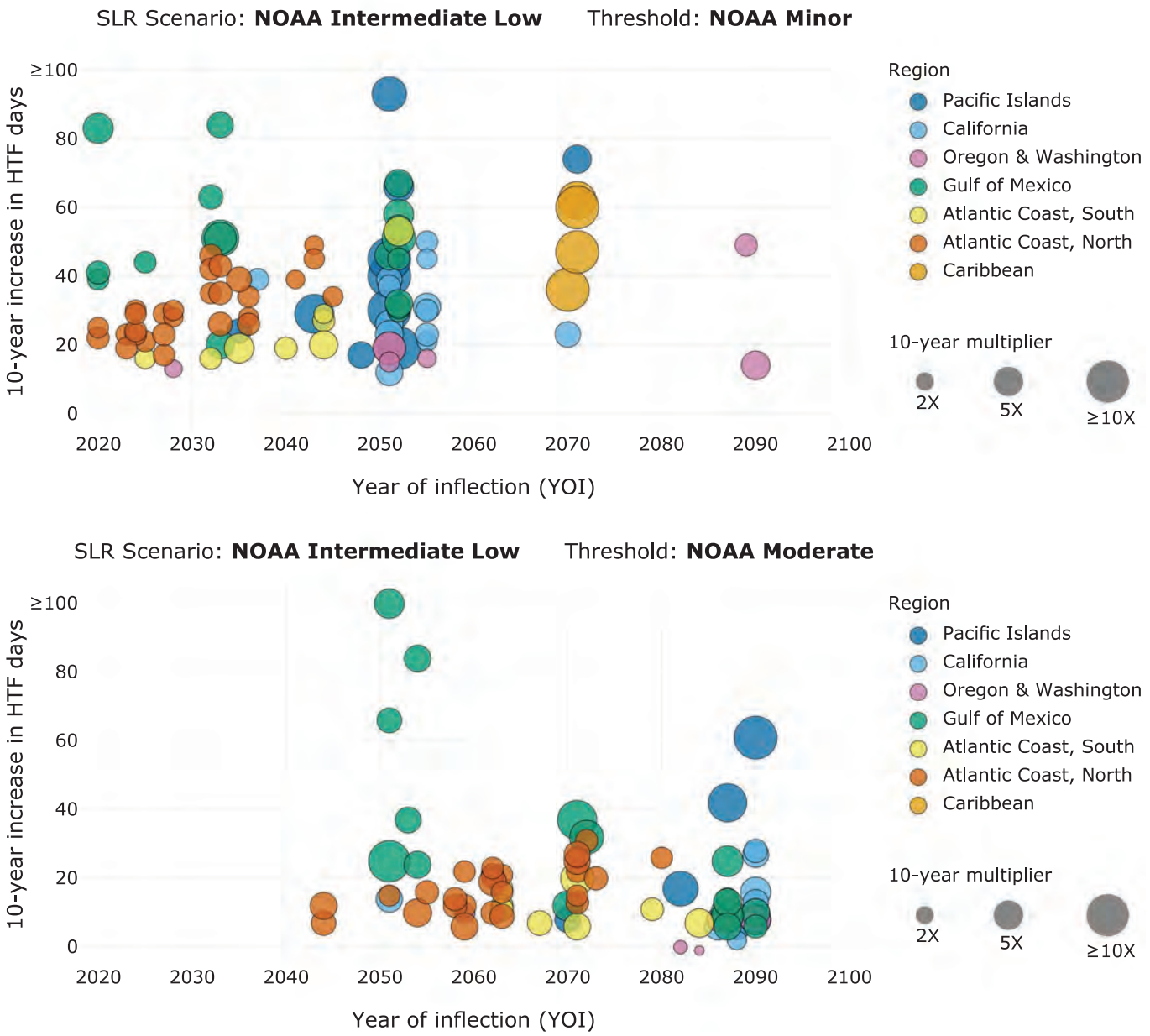

Extended Data Fig. 2 | Years of inflection (YOIs) for the NOAA Intermediate Low SLR scenario. The upper and lower panels correspond to the NOAA Minor and Moderate flooding thresholds, respectively. Position along the horizontal axis corresponds to the timing of the YOI. The vertical axis is projected ten-year increases in annual counts of HTF days following YOIs. Marker size corresponds to ten-year multipliers following the YOIs. Color denotes geographic region.

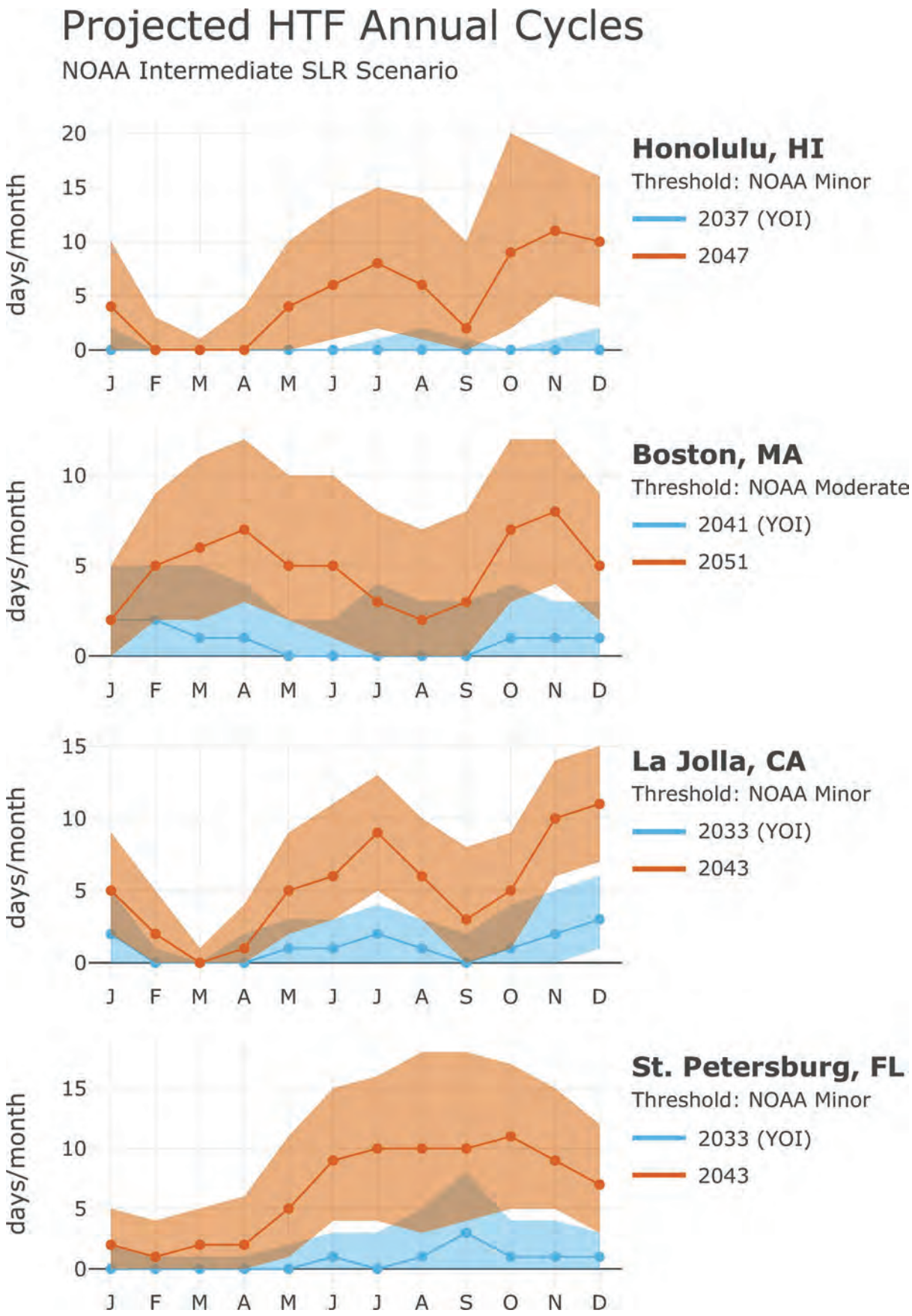

Extended Data Fig. 3 | Projected changes in the seasonal cycle of HTF frequency. Projections correspond to the YOI (blue) and 10 years later (orange) for the four US locations in Fig. 1 assuming the NOAA Intermediate SLR scenario. Shading shows the 10th–90th percentile intervals for each year and month.

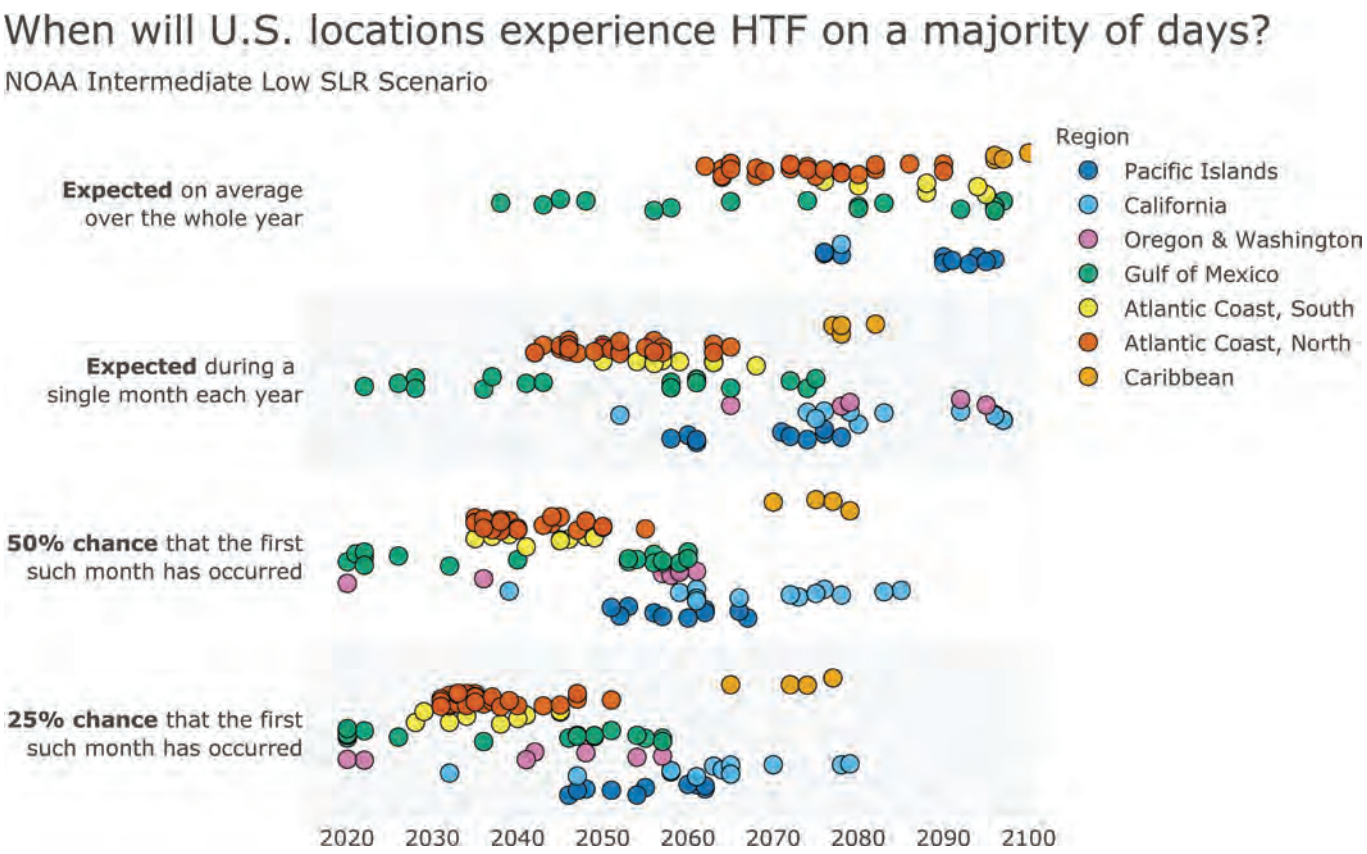

Extended Data Fig. 4 | Years for which U.S. coastal locations will experience HTF on a majority of days during annual and monthly windows. Calculations assume the Intermediate Low SLR scenario. Years for which HTF is expected to occur on a majority of days on average during annual and monthly periods (top two rows) are compared to years for which flooding will first occur on a majority of days during a single month (bottom two rows). Marker colors denote station region. The vertical position of each marker within the rows is an arbitrary vertical offset to allow visual distinction between regions and individual locations.

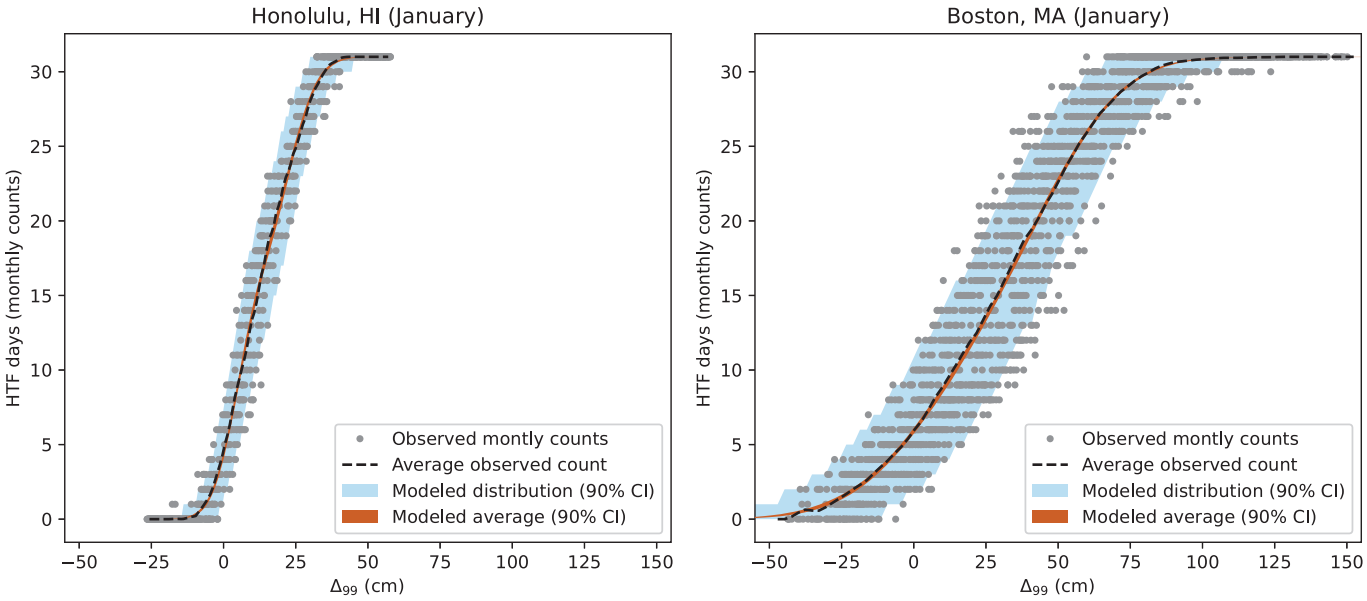

Extended Data Fig. 5 | Relationships between Δ_{99} and monthly counts of HTF days. Examples correspond to the observed (gray and black) and fitted (orange and red) relationships for the month of January in (a) Honolulu and (b) Boston.

DOI: 10.1111/jiec.13084

RESEARCH AND ANALYSIS

JOURNAL OF INDUSTRIAL ECOLOGY WILEY

Update to limits to growth

Comparing the World3 model with empirical data

Gaya Herrington

KPMG LLP, Los Angeles, California

Correspondence
Gaya Herrington (née Branderhorst), KPMG LLP, 550 South Hope Street, Los Angeles, CA 90071, USA.
Email: gayabranderhorst@gmail.com

Editor Managing Review: Heinz Schandl

Abstract

In the 1972 bestseller *Limits to Growth* (LtG), the authors concluded that, if global society kept pursuing economic growth, it would experience a decline in food production, industrial output, and ultimately population, within this century. The LtG authors used a system dynamics model to study interactions between global variables, varying model assumptions to generate different scenarios. Previous empirical-data comparisons since then by Turner showed closest alignment with a scenario that ended in collapse. This research constitutes a data update to LtG, by examining to what extent empirical data aligned with four LtG scenarios spanning a range of technological, resource, and societal assumptions. The research benefited from improved data availability since the previous updates and included a scenario and two variables that had not been part of previous comparisons. The two scenarios aligning most closely with observed data indicate a halt in welfare, food, and industrial production over the next decade or so, which puts into question the suitability of continuous economic growth as humanity's goal in the twenty-first century. Both scenarios also indicate subsequent declines in these variables, but only one—where declines are caused by pollution—depicts a collapse. The scenario that aligned most closely in earlier comparisons was not amongst the two closest aligning scenarios in this research. The scenario with the smallest declines aligned least with empirical data; however, absolute differences were often not yet large. The four scenarios diverge significantly more after 2020, suggesting that the window to align with this last scenario is closing.

KEYWORDS
collapse, industrial ecology, limits to growth, system dynamics modeling, systems thinking, World3

1 | INTRODUCTION

1.1 | Limits to growth

In the 1972 bestseller *Limits to Growth* (LtG), the authors concluded that if humanity kept pursuing economic growth without regard for environmental and social costs, global society would experience a sharp decline (i.e., collapse) in economic, social, and environmental conditions within the twenty-first century. They used a model called World3 to study key interactions between variables for global population, birth rate, mortality, industrial output, food production, health and education services, non-renewable natural resources, and pollution. The LtG team generated different World3 scenarios by varying assumptions about technological development, amounts of non-renewable resources, and societal priorities. The

few comparisons of empirical data with the scenarios since then, most recently from 2014 (Turner), indicated that the world was still following the "business as usual" (BAU) scenario. BAU showed a halt in the hitherto continuous increase in welfare indicators around the present day and a sharp decline starting around 2030.

This article describes the research into whether humanity was still following BAU and whether there seemed opportunity left to change course to become more aligned with another LtG scenario, perhaps one in which collapse is avoided. World3 scenarios were quantitatively compared with empirical data. The research thus constitutes an update to previous comparisons but also adds to them in several ways. Earlier data comparisons used scenarios from the 1972 LtG book. The scenarios in this research were created with the latest, revised and recalibrated, World3 version. This data comparison also included a scenario and two variables that had not been part of such research before, and benefited from better empirical proxies thanks to improved data availability.

1.2 | Limits to growth message

The LtG message was that continuous growth in industrial output cannot be sustained indefinitely (Meadows, Meadows, Randers, & Behrens, 1972). Effectively, humanity can either choose its own limit or at some point reach an imposed limit, at which time a decline in human welfare will have become unavoidable. An often missed, but key point in the LtG message is the plural of "limits" (Meadows & Meadows, 2007; Meadows, Meadows, & Randers, 2004). In an interconnected system like our global society, a solution to one limit inevitably causes interactions with other parts of the system, giving rise to a new limit which then becomes the binding constraint to growth (Meadows & Meadows, 2007). To illustrate this point, the LtG authors created various scenarios with World3. World3 was based on the work of Forrester (1971, 1975), the founder of system dynamics: a modeling approach for interactions between objects in a system, often characterized by non-linear behavior like delays, feedback loops, and exponential growth or decline. The LtG scenarios were thus not meant to produce point predictions, but rather to help us understand the behavior of systems in the world over time.

1.3 | LtG publications

The first book (Meadows et al., 1972) was commissioned by the Club of Rome and introduced World3 together with 12 scenarios. The most widely discussed scenario has been the BAU. It maintained parameters at historic levels from the latter part of the twentieth century, without imposing any additional assumptions. In BAU, standards of living would at some point stop rising along with industrial growth once the accompanying depletion of non-renewable resources had started to render these a limiting factor in industrial and agricultural production. Continuation of standard economic operation without adapting to the constraint of growing resource scarcity would then require increasingly more industrial capital to be diverted toward extracting non-renewable resources. This would leave less for food production, citizen services and industrial re-investment, causing declines in these factors and, subsequently, in population (Meadows et al., 1972).

There were 11 other scenarios in the first book, including "comprehensive technology" (CT) and "stabilized world" (SW). CT assumes a range of technological solutions, including reductions in pollution generation, increases in agricultural land yields, and resource efficiency improvements that are significantly above historic averages (Meadows et al., 1972, p. 147). The SW scenario assumes that in addition to the technological solutions, global societal priorities changed from a certain year onward (Meadows et al., 1972). A change in values and policies translates into, amongst other things, low desired family size, perfect birth control availability, and a deliberate choice to limit industrial output and prioritize health and education services. SW was the only scenario in which declines were avoided.

The second book, Beyond the Limits, was published in 1992 (Meadows, Meadows, & Randers). The LtG team had recalibrated World3 to two decades of additional data. The authors concluded that while humankind had had the opportunity to act during the 20 years after the first LtG book, society had now reached overshoot (i.e., exceeds the earth's carrying capacity).

The third and last book, *Limits to Growth: The 30-Year Update*, dates from 2004 (Meadows et al.). It described 10 new scenarios which were similar to those from the first two books in assumptions, but made with a revised World3 model: World3-03. The model revisions included incorporation of two new variables: the human ecological footprint (EF) and human welfare. The assumptions regarding technological progress were also intensified, going above historic rates even further, making the CT scenario more optimistic compared to its 1972 version.

1.4 | Criticism

The LtG books and World3 received much criticism at the time (e.g., Bardi, 2011; Norgard, Peet, & Ragnarsdóttir, 2010). Much of this was focused on the economic and technological assumptions underlying the World3 model. Additionally, there was technical criticism of World3 and the new modeling technique (system dynamics) itself. There were also misconceptions about the scenarios and LtG message, some of which have proven

persistent and influential in the public debate. An example is the claim that the first book predicted resource depletion by 1990 (Passell, Roberts, & Ross, 1972). This misconception spread to the point of being repeated by organizations like the United Nations Environment Programme (2002). It was actively revived by analysts ("Plenty of Gloom", 1997; Bailey, 1989; Lomborg & Olivier, 2009), who subsequently dismissed LtG because depletion and collapse had not taken place. Reversal points lie beyond 2000 in all the scenario graphs in the LtG books, however.

Criticism on World3's underlying assumptions focused mostly on those concerning technological progress and market correction. Some regarded the absence of a corrective price mechanism as a fatal flaw, contending that increased prices would spur substitutions between resources and other technological solutions (Kaysen, 1972; Solow, 1973). Economist Solow (1973), for example, argued that increased scarcity would drive up prices of non-renewable resources, and also that pollution externalities would drive more regulation and higher taxes. Research by the Organisation for Economic Co-operation and Development (OECD, 2017, 2018), amongst others, suggests; however, that the social costs of pollution and natural resource depletion are currently not fully reflected in taxes. Fossil fuels alone still carry large indirect after-tax government subsidies (Coady, Parry, Le, & Shang, 2019), totaling 6.4% of global gross domestic product (GDP). Others argued in a reaction to the first LtG book that World3 did not give enough credence to humanity's ability to invent technological solutions to environmental challenges (Cole, Freeman, Jahoda, & Pavitt, 1973; Kaysen, 1972). The LtG authors have since pointed out (Meadows et al., 2004; Meadows et al., 1992) that their books contained several scenarios other than the BAU, which were based on assumptions about technological innovation and adoption that are significantly higher than historic averages. These optimistic assumptions on humankind's ingenuity and willingness to share technological solutions do not prevent declines in an LtG scenario, unless it is paired with societal value and policy changes (as in SW).

Technical criticism included the claim that World3 model can be sensitive; relatively small parameter changes will in some cases significantly alter a scenario's trajectory (Castro, 2012; de Jongh, 1978; Vermeulen & de Jongh, 1976). Recreation of runs with the same parameter changes as in these critical studies confirmed that finding, although it also showed that the parameter changes did not avoid an overshoot and collapse pattern (Turner, 2013). A 1973 review of World3 by Cole, Freeman, Jahoda, & Pavitt, concluded that the model was inadequate from the perspective of linear modeling. Sterman (2000) has since pointed out that adequacy as a linear model is not the right criterion for a system dynamics model.

1.5 | Updates to LtG

Several qualitative reviews of the LtG publications have described how dynamics in World3 could be observed in the real world (Bardi, 2014; Jackson & Weber, 2016; Simmons, 2000). One such review was from LtG author Randers (2000). Around 1990, it became clear that non-renewable resources, particularly fossil fuels, had turned out to be more plentiful than assumed in the 1972 BAU scenario. Randers therefore postulated that not resource scarcity, but pollution, especially from greenhouse gases, would cause the halt in growth. This aligns with the second scenario in the LtG books. This scenario has the same assumptions as the BAU, except that it assumes double the amount of non-renewable resources. This scenario is referred to as BAU2, and received more focus than the BAU scenario in the second and third LtG books. More natural resources do not avoid collapse in World3; the cause changes from resource depletion to a pollution crisis.

BAU2 was quantitatively assessed in a 2015 recalibration study of World3-03 (Pasqualino, Jones, Monasterolo, & Phillips, 2015). Results indicated that society had invested more to abate pollution, increase food productivity, and invest in services compared to BAU2. However, the authors did not compare their calibration with SW, nor did they use their recalibrated version of World3 to run the scenario beyond the present to see if collapse was avoided. Thus, their findings could not be taken as an indication that humanity had done enough to avoid declines, as the authors themselves made sure to point out.

Quantitative comparisons between LtG scenarios and empirical data were conducted by Turner (2008, 2012, 2014). He compared global observed data for the LtG variables with 3 of the 12 scenarios from the first book: BAU, CT, and SW. Turner concluded that world data compared favorably to key features of BAU, and much more so than for the other two scenarios.

1.6 | This research: A data comparison to LtG

In this research, data available in 2019 was compared with the recalibrated World3-03 to examine whether this produced the same outcomes as Turner had found. Because he used the 1972 variables, Turner did not include the two that were added in 2004, human welfare and EF. Another open question therefore was to what extent these variables aligned with their real-world counterparts. Lastly, given the attention that BAU2 had received and that its pollution crisis can be interpreted as depicting climate change (i.e., collapse from greenhouse gas pollution), this scenario ought to be included in a comparison.

The research goal was to determine to what extent empirical data aligned with selected scenarios of World3-03 (henceforth called "World3"). Data was compiled from various official databases, as indicators for what the following 10 variables represented: population, fertility (birth rate), mortality (death rate), industrial output per capita (p.c.), food p.c., services p.c., non-renewable resources, persistent pollution, human welfare, and

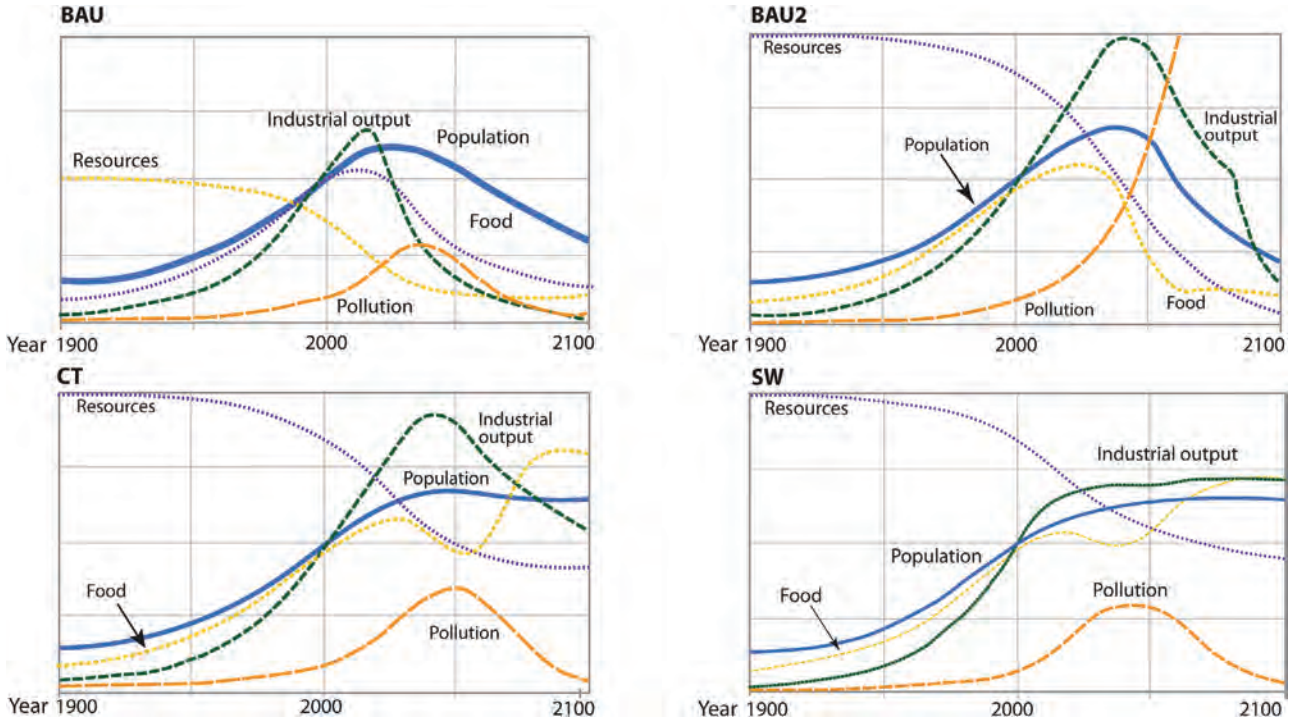

FIGURE 1 The BAU, BAU2, CT, and SW scenarios. Adapted from *Limits to Growth: The 30-Year Update* (p. 169, 173, 219, 245), by Meadows, D. H., Meadows, D. L., and Randers, J., 2004, Chelsea Green Publishing Co. Copyright 2004 by Dennis Meadows. Adapted with permission

TABLE 1 Description and cause of halt in growth and/or decline per scenario

Scenario	Description	Cause
BAU	No assumptions added to historic averages	Collapse due to natural resource depletion.
BAU2	Double the natural resources of BAU	Collapse due to pollution (climate change equivalent).
CT	BAU2 + exceptionally high technological development and adoption rates	Rising costs for technology eventually cause declines, but no collapse.
SW	CT + changes in societal values and priorities	Population stabilizes in the twenty-first century, as does human welfare on a high level.

ecological footprint (EF). This data was plotted along with four World3 scenarios: BAU, BAU2, CT, and SW. These were the 2004 LtG book equivalents of the three scenarios in Turner's earlier work, plus BAU2.

Figure 1 shows how some of the LtG variables behave in each of these four scenarios. It should be noted that the numerical scales of the World3 output differ widely between variables. They are scaled in Figure 1 (as in the LtG books) to fit in one plot. This means that relative positions to each other on the *y*-axis have no meaning whatsoever. What is relevant is the movement of the variables over time in each of the four scenarios. These movements together depict the storyline of that scenario, which unfolds based on the specific scenario assumptions.

The assumptions underlying each scenario differ in technological, social, or resource conditions. The cause of decline, varying from a temporary dip to societal collapse, also differs for each scenario (Table 1).

2 | METHODS

2.1 | Scenario data

BAU, BAU2, CT, and SW, correspond to scenarios 1, 2, 6, and 9 in the 2004 LtG book. This means that for the SW scenario, policy changes are assumed to start in 2002. To create the scenarios, the original CD-ROM that came with the 2004 book was used. The CD-ROM contains simulations of the scenarios and numerical output of the variables. A zip file of World3-03 is also available from MetaSD (2020) and it can be run on free software from Vensim (2020).

2.2 | Determination of accuracy

To quantify how closely the LtG scenarios compare with observed data, the same two measures as in Turner (2008) were used:

1. the combination of
   a. the value difference (between the model output and empirical data), and
   b. the difference (between the model output and empirical data) in rate of change (ROC)

   –both applied at the time point of the most recent empirical data,

2 the normalized root mean square difference (NRMSD).

These two measures do not provide the level of precision of some statistical tests, which is not possible given World3's global scope and aggregation. Rather, the measures are meant to be combined with visual inspection to gauge the scenarios' accuracy. In other words, the accuracy measures are meant to determine World3's merit, not for point predictions, but as an analysis tool for general global dynamics.

2.2.1 | Formulas

The calculations of the two measures are done for 5-year intervals ending in the final year of the data series. The 5-year interval aligns with the LtG team's practice in the plots in their books. World3 provides output in half-year increments, but the LtG team did not consider changes over smaller periods significant (Meadows et al., 1972). In the equations below, the final year is assumed to be 2015 for ease of interpretation. The final year varied per data source, from 2015 to 2020 (see Supporting Information S2). It is straightforward to adjust the formulas for data series ending in another year.

Measure 1: value change and rate of change

$$\Delta\text{Value} = \frac{\text{Variable}_{2015} - \text{Observed Data}_{2015}}{\text{Observed Data}_{2015}}$$

$$\Delta\text{Rate of Change} = \frac{(\text{Variable}_{2015} - \text{Variable}_{2010}) - (\text{Observed Data}_{2015} - \text{Observed Data}_{2010})}{\text{Observed Data}_{2015} - \text{Observed Data}_{2010}}$$

Measure 2: NRMSD

In the formula below, the start of the calculation is assumed to be 1990. This year is what was used for each variable where this was possible; however, some series did not go back as far, in which case the equation below would have to be adapted accordingly.

$$\text{NRMSD}_{2015} = \frac{\sqrt{\frac{\sum_{t=0}^{5}(\text{Variable}_{1990+5t} - \text{Observed Data}_{1990+5t})^2}{6}}}{\left(\frac{\sum_{t=0}^{5}\text{Observed Data}_{1990+5t}}{6}\right)}$$

2.2.2 | Uncertainty ranges

It was necessary to establish suitable uncertainty ranges for each of these measures, given World3's low precision and the error margins one can expect in the empirical data. The same uncertainty ranges as suggested in Turner's comparisons were used, that is, 20%, 50%, and 20% for the value difference, ROC and NRMSD, respectively. This recognizes that global data are unlikely to have a very high accuracy due to measurement difficulties, and many variables are combinations of factors. At the same time the uncertainty ranges are still narrow enough to be a meaningful indication of agreement between observed and simulated data. It is not suggested to interpret the 20% and 50% as strictly as, say, one would use α as a cut-off point in statistical analysis. As mentioned, the accuracy measures and uncertainty ranges complement a visual inspection of the graphs by quantifying the alignment error.

2.3 | Closest fit count

Apart from a measure of absolute fit, the above-mentioned uncertainty range, it was also necessary to distinguish amongst the four scenarios in terms of relative fit. This can be done with a simple tally over the variables for each scenario. A scenario was counted as a closest fit when it aligned more closely than other scenarios and at least one of that variable's proxies was within the uncertainty bounds for both accuracy measures. Another option would have been to count a scenario as a closest fit if either measure 1 or measure 2 was within the uncertainty range for at least one proxy. The choice to only count a scenario when both accuracy measures were within range was made because it's more conservative. When all scenarios were outside of uncertainty bounds for at least one measure, they were counted as inconclusive. For cases where two or more scenarios aligned to the same extent, they were all counted.

2.4 | Data sources

Below follows a list of the source(s) of empirical data used for each variable in this comparison. Reliability of each source is briefly discussed in Supporting Information S1.

Some variables required proxies because the variable in World3 is not directly observable or quantifiable in the real world. The same data sources as Turner were often chosen; however, in several cases it was possible to improve on previous proxies thanks to new or recently enhanced indices and databases. When empirical data was expressed in different units than the LtG scenarios, they were normalized to the 1990 scenario value, because that is the year that World3 was recalibrated to last (Meadows et al., 1992).

2.4.1 | Population

Figures from the Population Division of the United Nations Department of Economic & Social Affairs (UN DESA PD, 2019) were used for this variable. Their population series includes estimates for 2020, which were compared against the LtG 2020 values. Annual population figures can also be found on the World Bank Open Data website (WB, 2019a). Both sites mention national agencies and international organizations as their sources, such as Eurostat, the US Census Bureau, and census publications from national statistical offices.

2.4.2 | Fertility and mortality (two variables)

The data series from the WB Open Data site (2019b, 2019c) were used for both of these variables. The WB mentions as its sources the same organizations and publications as for its population series.

2.4.3 | Food per capita

Total energy available per person per day was used to approximate this variable. The daily caloric value per capita can be found in the Food Balance Sheets on FAOSTAT (2019), the database of the Food and Agriculture Organization of the UN.

2.4.4 | Industrial output per capita

The industrial output p.c. variable represented citizens' material and technological standard of living and was a factor in the World3 society's ability to grow food and deliver services (Meadows et al., 2004). The index of industrial production (IIP) and gross fixed capital formation (GFCF) were used as proxies. Both proxy series were divided by population to arrive at per capita numbers.

IIP is a standardized macroeconomic indicator of an economy's real output in manufacturing, mining, and energy (e.g., Moles & Terry, 1997). Unlike GDP, IIP excludes retail and professional services, making it a useful proxy for industrial output. The IIP series can be retrieved as "INSTAT2" on the data portal of the UN Industrial Development Organization (UNIDO, 2019a). UNIDO does not provide a global IIP, so one was created with a weighted average of country IIPs. National manufacturing value added, also sourced from UNIDO (2019b), was used for weighting.

The WB (2019d) provides a global GFCF series. GFCF includes land improvements (e.g., fences and drains), infrastructure (e.g., roads), buildings and construction (e.g., schools, offices, hospitals, and industrial buildings), machinery, and equipment purchases. This aligns closely with the definition of the industrial output variable in World3, especially as it relates to a society's ability to deliver services and grow food.

2.4.5 | Services per capita

In World3, services p.c. represents education and health services (Meadows et al., 2004). The Education Index (EI), spending on health, and spending on education were used as proxies.

The EI is constructed by the UN Development Programme (UNDP, 2019a). It is calculated using mean years of schooling and expected years of schooling (UNDP, 2019b). These two figures can be quite different, especially in developing countries, and combined thus provide a good indication of currently available education services (UNDP, 2019c).

The WB provides global figures for both government spending on education (2019e) and health expenditure (2019f). The two series are expressed as a percentage of GDP. The LtG authors described several collapse patterns as resources being diverted away from these citizen services to industrial capital in order to keep extracting natural resources, abate pollution, and/or produce food. Fraction of GDP is an indication of how resources are allocated toward something on a macro level, as expressed by the WB's statement that a "high percentage to GDP suggests a high priority for education" (2019e). Therefore, tracking the fraction of global GDP spent on education or health can help reveal whether the mechanism described by LtG is indeed observable.

2.4.6 | Pollution

World3 assumes pollution to be globally distributed, persistent, and damaging to human health and agricultural production. CO_2 concentrations and plastic production were used as proxies.

Atmospheric CO_2 data (Tans & Keeling, 2019) were obtained from the National Oceanic & Atmospheric Administration (NOAA). The 1900 CO_2 level of 297 parts per million (Etheridge et al., 1996) was subtracted from the NOAA data, because the LtG scenarios put pollution at 0 in 1900. Although CO_2 is not the only persistent pollutant—NO_x, SO_x, heavy metals, and ozone-depleting substances are other examples—it is an adequate proxy because of the global impacts that climate change brings for human health, the environment, and our ability to grow food, and because there exist accurate time series data.

Global plastic production data was sourced from Geyer, Jambeck, and Law (2017). The data was adjusted downwards to the share of plastic that gets discarded, which reportedly went from 100% in 1980 to 55% in 2015 (Geyer et al., 2017). Not all plastic is considered pollution; however, plastic's persistence and ubiquity in today's society, and documented impacts on human health, aligns with World3's assumptions on the pollution variable. Various kinds of plastics can be found throughout the entire consumer product and food supply chain, from oceans and marine wildlife (Smillie, 2017; van Sebille et al., 2015) to tap water (Kosuth, Wattenberg, Mason, Tyree, & Morrison, 2017), from agricultural land (Nizzetto, Langaas, & Futter, 2016) to dietary components and the air we breathe (Wright & Kelly, 2017a), prompting a growing body of scientific literature on a wide range of possible negative human health effects (Halden, 2010; Wright & Kelly, 2017b).

2.4.7 | Non-renewable resources

Two proxies were used for this variable, both based on different expert estimates of fossil fuel resources. Full substitution between energy resources is assumed, which is conservative given the current state of technology (Brathwaite, Horst, & Iacobucci, 2010; Driessen, Henckens, van Ierland, & Worrell, 2016; Graedel, Harper, Nassar, & Reck, 2015). The proxy data series were not normalized to 1990 values because they represent fractions (i.e., they run on a scale from 1 to 0) and so scaling them would distort the comparison. Because BAU and BAU2 differed only in amount of resources and these were set to 1 at 1900, the two scenarios show the same curve.

Both fossil energy proxies consisted of estimates of remaining coal, natural gas, and oil. The first fossil fuel proxy was the same as in Turner's earlier work. His 2008 paper lists all the sources he used to determine high and low expert estimates for fossil energy resources in 1900. Annual production of each resource was sourced from the World Watch Institute, which in turn had compiled the data from organizations including the UN, British Petroleum (BP), and the US Energy Information Administration. Turner's series were updated with production data from BP's Statistical Review of World Energy (2019) and summed over the three fossil resources to arrive at the total annual production series. These production data were cumulatively subtracted from the total high and low resource estimates, resulting in an upper and lower bound for the fraction of nonrenewable resources remaining over time. The second proxy was constructed using the same method, but with fossil energy resource estimates from a Geochemical Perspective (GP) publication (Sverdrup & Ragnarsdóttir, 2014), and production data from the World Bank (WB) (2019g). For that reason, this proxy is indicated with "WB" at the end in the results.

TABLE 2 Accuracy measure 1: Value difference and rate of change (ROC) difference (both in %) for each scenario and variable

Scenario		Population	Fertility	Mortality	Food p.c.	Industrial output p.c.	Services p.c.	Pollution	Natural cap	Welfare	EF
BAU	Δ value	−6	−17	15	−15	−11; 3	5; 8; 9	−20; 64	−15; −11; −2; 15	−4	15
	ΔROC	−42	55	−12	−342	−107; −90	−7; −5; 33	−14; 68	12; 55; 121; 179	−152	593
BAU2	Δ value	−5	−10	8	−14	−7; 13	10; 11; 13	−20; 65	−15; −11; −2; 15	−2	19
	ΔROC	−28	−4	−6	−279	−64; 5	57; 85; 97	−14; 73	12; 55; 121; 179	−62	940
CT	Δ value	−5	−10	6	−12	−6; 13	10; 11; 13	−20; 64	−15; −11; −2; 16	−1	18
	ΔROC	−25	−3	−7	−193	−62; 8	57; 86; 97	−14; 69	7; 50; 113; 166	−40	841
SW	Δ value	−11	−22	11	−10	−9; 2	18; 20; 22	−19; 68	−15; −11; −2; 16	−1	13
	ΔROC	−52	−61	−9	−275	−108; −95	22; 32; 68	−8; 78	−3; 39; 97; 143	−67	247

2.4.8 | Human welfare

The HDI data series can be found on the website of UNDP (2019a). The HDI has undergone methodological changes over the years (UNDP, 2019d), which have led to significant retroactive adjustment to the series. The 2004 LtG book (Meadows et al.) notes that the World3 welfare variable was very close to the UNDP value as at 1999, but this was no longer the case for the latest version of the HDI data series. The UNDP (2019d) states: "The difference between HDI values (…) published in HD Reports for different years represents a combined effect of data revision, change in methodology, and the real change in achievements in indicators". UNDP (2019d) therefore advises not to source HDI numbers from Reports, but to use the "data series available in the on-line database". Therefore, the current HDI data were scaled with a factor 1.106 to line up with the World3 scenarios value as at 2000.

2.4.9 | Human ecological footprint

The LtG team created this variable after Wackernagels' Ecological Footprint (Meadows et al., 2004). The Global Footprint Network (GFN, 2019a) publishes the EF on its website. The EF series were scaled to scenario values between 1990 and 2000 (with a factor of 1.17), because the LtG team would have calibrated World3 to line up with EF figures at the time. The reason that today's EF data did not exactly line up is most likely the several revisions to the EF calculation over the past two decades (GFN, 2019b), similar to the HDI.

3 | RESULTS

3.1 | Overview for each accuracy measure

The table and graph below provide an overview of the two accuracy measures for each variable and scenario. Graphs for each variable plotted with the scenarios are provided in Supporting Information S1. Table 2 shows the results for accuracy measure 1, the graph in Figure 2 shows accuracy measure 2. Some variables had more than one data series for comparison with the scenario (i.e., more than one proxy). These data are listed in one cell per variable in the table and displayed separately in the graph.

The numbers in Table 2 that were within the uncertainty ranges (20% for the value difference and 50% for the ROC) are printed in green, the ones outside the range in red. The uncertainty boundaries were left in black. The 20% line is easily identified in Figure 2 and marked by a dashed green line.

3.2 | Closest fit counts per scenario

Table 3 contains a count per scenario for each time it was the closest fit. As mentioned in Section 2, for variables where two or more scenarios aligned to the same extent, each scenario was counted. This is why Table 3 shows 22 total counts over 10 variables. The use of more than one proxy for some variables did not lead to contradictory counts; although different proxies for the same variable sometimes had different numerical results, they led to the same outcomes in terms of alignment (or not) to a certain scenario.

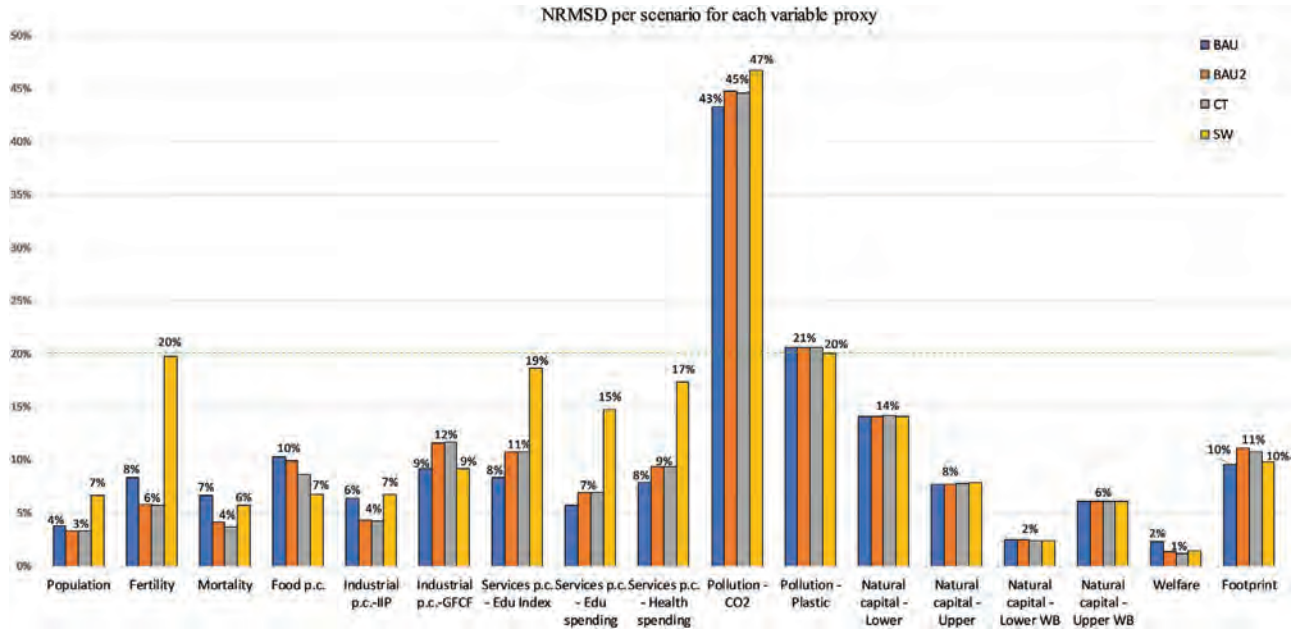

FIGURE 2 Accuracy measure 2: NRMSD. Plotted for each scenario and variable proxy. Underlying data used to create this figure can be found in Supporting Information S2. Data visualization was aided by Daniel's XL Toolbox addin for Excel, version 7.3.4, by Daniel Kraus, Würzburg, Germany (www.xltoolbox.net)

TABLE 3 Count per scenario of closest agreement with empirical data

Scenario	BAU	BAU2	CT	SW	None
Count of closest alignment with data	4	6	7	3	2

Even when scenarios showed close alignment, in some cases choosing a closest fit scenario was not possible because they all aligned to a similar extent. This is because scenarios start to deviate later in World3-03 than was the case in the 1972 version of World3. Such was the case with non-renewable resources, for example, and with the plastics proxy for the pollution variable. In particular, the BAU2 and the CT scenarios do not deviate significantly before 2020, resulting in both being closest fits for several variables. Because scenarios often aligned closely in value, a decisive factor in determining the closest fit was the difference in ROC. This means that even in cases where one scenario could be picked as a closest fit, this outcome could change in future updates because additional datapoints can change a ROC significantly. For example, the accuracy measures for the welfare variable indicated CT as the closest fit, but this is only because its ROC difference was below the 50% uncertainty range. The other scenarios agree closely in value too, and mathematically speaking it's entirely possible that next years' datapoints will cause their rates of change (now 62% and 67%) to dip below 50%. This should be kept in mind with Table 3.

4 | DISCUSSION

4.1 | Close alignment

When it comes to value, both measures indicate an overall close alignment between the LtG scenarios and empirical data. Measure 2 (the NRMSD) was not greater than 20% for all variables (Figure 2), except for pollution. Table 2 shows that most differences in value were also within the 20% range, except for pollution and for fertility (i.e., birth rate) in SW.

The ROC showed more and larger deviations between scenarios and empirical data. Sometimes this was due to little movement in the variable itself, leading to a low difference between observed datapoints. This low difference meant that the numerator (see Section 2.2.1) would get inflated, even though value differences were not large. This was the case for the EF and welfare variables, and to a lesser extent for services p.c., food p.c., and natural capital.

4.2 | The end of growth

Despite all scenarios showing a relatively close track in value, there were differences between them for some variables. Unlike previous comparisons, this research did not reveal the BAU scenario aligning with empirical data more closely than the others. Like in Turner's work, however, the lowest count for closest fit was for SW, the scenario that the LtG work models as eventually following a sustainable path. When it was possible to distinguish between scenarios, the CT and BAU2 aligned closest most often. BAU2 and CT scenarios show a halt in growth within a decade or so from now. Both scenarios thus indicate that continuing business as usual, that is, pursuing continuous growth, is not possible. Even when paired with unprecedented technological development and adoption, business as usual as modeled by LtG would inevitably lead to declines in industrial capital, agricultural output, and welfare levels within this century. These forecasts put in perspective the recent low economic predictions (e.g., OECD, 2020; WB, 2019h), and talks from organizations like the IMF about a "synchronized slowdown" of global growth (Lawder, 2019) and "uncertain recovery" from the COVID-19 pandemic (IMF, 2020).

4.3 | Collapse?

The CT and BAU2 scenarios show distinctly different decline patterns, and one cannot simply "take the midway" between two scenarios produced by a complex, non-linear model like World3. Although the steepness of a scenario's decline cannot be used for predictive purposes (Meadows et al., 2004), it can be said that BAU2 shows a clear collapse pattern, whereas CT suggests the possibility of future declines being relatively soft landings, at least for humanity in general. The moderate declines in CT would align with a global forecast made in 2012 by LtG author Randers. Randers' forecast (2012) was made with a different model than World3 and so it cannot be compared with CT in most ways. However, the overall developments are not dissimilar, as the forecast includes consumption and GDP stagnation around the middle of the century followed by declines but not a collapse pattern.

4.4 | About tipping points

The BAU2 and CT scenarios seem to align quite closely not just with observed data, but also with contemporary debate. On one hand, the BAU2 scenario resonates with messages from climate scientists that we currently might be at the "climate tipping point" (Cai, Lenton, & Lontzek, 2016; Intergovernmental Panel on Climate Change, 2019; Lenton et al., 2019; Pearce, 2019). On the other hand, CT is the scenario of those who believe in humanity's ingenuity to innovate ourselves out of any limit. The assumptions underlying CT are highly optimistic given historic figures. For example, CT assumes technological progress rates of 4% a year which, amongst other things, should lead to reductions in pollution emissions of 10% from their 2000 values by 2020 and 48% by 2040. Given the rising trend in global CO_2 emissions so far, halving these within the next 20 years seems unrealistic. However, the technologist could argue that history is full of "technological tipping points" (Montresor, 2014; World Economic Forum, 2015), where innovations disrupted trends and revolutionized society beyond what conventional wisdom deemed possible.

Detailing this discussion goes beyond the scope of this article. More important, the findings and LtG work indicate an altogether different question to ask than whether society could be following the CT. Two best fit scenarios that marginally align closer than the other two, point to the fact that it's not yet too late for humankind to purposefully change course to significantly alter the trajectory of future data points. The fact that the SW scenario shows the smallest declines, suggests that if we are to bet our future on the possibility of tipping points, rather than just the technological ones, we should also aim for the "social tipping points" (David Tàbara et al., 2018; Otto et al., 2020; Westley et al., 2011): A transformation of societal priorities which, together with technological innovations specifically aimed at furthering these new priorities, can bring humanity back on the path of the SW scenario.

5 | CONCLUSION

Empirical world data was compared against scenarios from the last LtG book, created by the World3 model. The data comparison, which used the latest World3 version, included four scenarios: BAU, BAU2, CT, and SW. Empirical data showed a relatively close fit for most of the variables. This was true to some extent for all scenarios, because in several cases the scenarios do nott significantly diverge until 2020. When scenarios had started to diverge, the ones that aligned closest with empirical data most often were BAU2 and CT. This result is different to previous comparisons that used the earlier World3 version, and which indicated BAU as the most closely followed scenario. The scenario that depicts the smallest declines in economic output, SW, is also the one that aligned least closely with observed data. Furthermore, the two closest aligning scenarios BAU2 and CT, respectively, predict a collapse pattern and moderate decline in output. At this point therefore, the data most aligns with the CT and BAU2 scenarios which indicate a slowdown and eventual halt in growth within the next decade or so, but World3 leaves open whether the subsequent decline will

constitute a collapse. World3 also indicates the possibility, for now, of limiting declines to less than in the CT. Although SW tracks least closely, a deliberate trajectory change brought about by society turning toward another goal than growth is still possible. The LtG work implies that this window of opportunity is closing fast.

ACKNOWLEDGMENTS

This research was based on my Master of Liberal Arts thesis in Sustainability at Harvard University Extension School, graduation March 2020 (Branderhorst 2020). I am grateful to Graham Turner for sharing his previous work with me and giving me his support. It was a pleasure and honor to discuss my research with him. I would like to thank Esther G. Naikal and Giovanni Ruta from the World Bank for providing me with the underlying data on natural capital calculations. I am also very appreciative of John Sterman for meeting with me at short notice in January 2019 while he was on sabbatical. That talk in his MIT office provided me with exactly the right insights to nudge my research in the right direction.

CONFLICT OF INTEREST

The author declares no conflict of interest.

ORCID

Gaya Herrington https://orcid.org/0000-0002-9284-9129

REFERENCES

Bailey, R. (1989). Dr. Doom. *Forbes*, *144*, 44.

Bardi, U. (2011). *Cassandra's curse: How "the limits to growth" was demonized*. Retrieved from https://www.resilience.org/stories/2011-09-15/cassandras-curse-how-limits-growth-was-demonized/

Bardi, U. (2014). *Extracted: How the quest for mineral wealth is plundering the planet*. White River Junction, Vermont: Chelsea Green Publishing Co.

Branderhorst, G. (2020). *Update to limits to growth: Comparing the World3 model with empirical data* (Master's thesis, Harvard Extension School). Retrieved from https://dash.harvard.edu/handle/1/37364868

Brathwaite, J., Horst, S., & Iacobucci, J. (2010). Maximizing efficiency in the transition to a coal-based economy. *Energy Policy*, *38*(10), 6084–6091.

British Petroleum (BP). (2019). *Statistical review of world energy*. Retrieved from https://www.bp.com/en/global/corporate/energy-economics/statistical-review-of-world-energy.html

Cai, Y., Lenton, T. M., & Lontzek, T. S. (2016). Risk of multiple interacting tipping points should encourage rapid CO_2 emission reduction. *Nature Climate Change*, *6*(5), 520–525.

Castro, R (2012). Arguments on the imminence of global collapse are premature when based on simulation models. *GAIA*, *21*, 271–273.

Coady, D., Parry, I., Le, N.-P., & Shang, B. (2019). *Global fossil fuel subsidies remain large: An update based on country-level estimates*. Retrieved from https://www.imf.org/en/Publications/WP/Issues/2019/05/02/Global-Fossil-Fuel-Subsidies-Remain-Large-An-Update-Based-on-Country-Level-Estimates-46509

Cole, H. S. D., Freeman, C., Jahoda, M., & Pavitt, K. L. R. (1973). *Models of doom: A critique of the limits to growth*. New York: Universe Publishing.

David Tàbara, J., Frantzeskaki, N., Hölscher, K., Pedde, S., Kok, K., Lamperti, F., … Berry, P. (2018). Positive tipping points in a rapidly warming world. *Current Opinion in Environmental Sustainability*, *31*(C), 120–129.

de Jongh, D. C. (1978). Structural parameter sensitivity of the limits to growth world model. *Applied Mathematical Modelling*, *2*, 77–80.

Driessen, P. P. J., Henckens, M. L. C. M., van Ierland, E. C., & Worrell, E. (2016). Mineral resources: Geological scarcity, market price trends, and future generations. *Resources Policy*, *49*, 102–111. https://doi.org/10.1016/j.resourpol.2016.04.012

Etheridge, D. M., Steele, L. P., Langenfelds, R. L., Francey, R. J., Barnola, J.-M., & Morgan, V. I. (1996). Natural and anthropogenic changes in atmospheric CO_2 over the last 1000 years from air in Antarctic ice and firn. *Journal of Geophysical Research*, *101*(D2), 4115–4128.

FAOSTAT. (2019). *Food balance sheets*. Retrieved from http://www.fao.org/faostat/en/#data/FBS

Forrester, J. W. (1971). *World dynamics*. Cambridge, MA: Wright-Allen Press.

Forrester, J. W. (1975). *Collected papers*. Waltham, MA: Pegasus Communications.

Geyer, R., Jambeck, J. R., & Law, K. L. (2017). Production, use, and fate of all plastics ever made. *Science Advances*, *3*(7), e1700782.

Global Footprint Network (GFN). (2019a). *Country trends*. Retrieved from http://data.footprintnetwork.org/#/countryTrends?cn=5001&type=earth

Global Footprint Network (GFN). (2019b). *FAQs*. Retrieved from https://www.footprintnetwork.org/faq/

Graedel, T. E., Harper, E. M., Nassar, N. T., & Reck, B. K. (2015). On the materials basis of modern society. *Proceedings of the National Academy of Sciences*, *112*, 6295. https://doi.org/10.1073/pnas.1312752110

Halden, R. U. (2010). Plastics and health risks. *Annual Review of Public Health*, *31*(7), 179–194.

Intergovernmental Panel on Climate Change. (2019). *IPCC special report on the ocean and cryosphere in a changing climate*. Retrieved from https://www.ipcc.ch/srocc/

International Monetary Fund (IMF). (2020). *World economic outlook update*. Retrieved from https://www.imf.org/en/Publications/WEO/Issues/2020/06/24/WEOUpdateJune2020

Jackson, T., & Weber, R. (2016). *Limits revisited: A review of the limits to growth debate*. Retrieved from http://limits2growth.org.uk/revisited

Kaysen, C. (1972). The computer that printed out W*O*L*F*. *Foreign Affairs*, *50*, 660–668. https://doi.org/10.2307/20037939.

Kosuth, M., Wattenberg, E. V., Mason, S. A., Tyree, C., & Morrison, D. (2017). Synthetic polymer contamination in global drinking water. *Orb Media*. Retrieved from https://orbmedia.org/stories/Invisibles_final_report/multimedia

Lawder, D. (2019). New IMF chief Georgieva warns of "synchronized slowdown" in global growth. *Nasdaq*. Retrieved from https://www.nasdaq.com/articles/new-imf-chief-georgieva-warns-of-synchronized-slowdown-in-global-growth-2019-10-08

Lenton, T., Rockström, J., Gaffney, O., Rahmstorf, S., Richardson, K., Steffen, W., & Schellnhuber, H. (2019). Climate tipping points – Too risky to bet against. *Nature*, *575*(7784), 592–595.

Lomborg, B., & Olivier, R. (2009). The dustbin of history: Limits to growth. *Foreign Policy*, *103*, 34–48. Retrieved from https://foreignpolicy.com/2009/11/09/the-dustbin-of-history-limits-to-growth/

Meadows, D. H., & Meadows, D. L. (2007). The history and conclusions of the limits to growth. *System Dynamics Review*, *23*, 191–197. https://doi.org/10.1002/sdr.371

Meadows, D. H., Meadows, D. L., & Randers, J. (1992). *Beyond the limits: Confronting global collapse, envisioning a sustainable future*. White River Junction, VT: Chelsea Green Publishing Co.

Meadows, D. H., Meadows, D. L., & Randers, J. (2004). *The limits to growth: The 30-year update*. White River Junction, VT: Chelsea Green Publishing Co.

Meadows, D. H., Meadows, D. L., Randers, J., & Behrens, W. W. (1972). *The limits to growth: A report for the Club of Rome's project on the predicament of mankind*. New York: Universe Books.

MetaSD. (2020). *World3-03*. Retrieved from https://metasd.com/tag/world3/

Moles, P., & Terry, N. (1997). *The handbook of international financial terms*. Oxford: Oxford University Press.

Montresor, F. (2014, August 14). *14 tech predictions for our world in 2020*. Retrieved from https://www.weforum.org/agenda/2014/08/14-technology-predictions-2020/

Nizzetto, L., Langaas, S., & Futter, M. (2016). Pollution: Do microplastics spill on to farm soils? *Nature*, *537*, 488. https://doi.org/10.1038/537488b

Norgard, J., Peet, J., & Ragnarsdóttir, K. (2010). The history of limits to growth. *Solutions*, *1*(2), 59–63. Retrieved from https://www.thesolutionsjournal.com/article/the-history-of-the-limits-to-growth/

Organisation for Economic Co-operation and Development (OECD). (2017). *Environmental fiscal reform: Progress, prospects, and pitfalls*. Retrieved from http://www.oecd.org/tax/tax-policy/environmental-fiscal-reform-progress-prospects-and-pitfalls.htm

Organisation for Economic Co-operation and Development (OECD). (2018). *Effective carbon rates 2018: Pricing carbon emissions through taxes and emissions trading*. Paris: OECD Publishing. https://doi.org/10.1787/9789264305304-en.

Organisation for Economic Co-operation and Development (OECD). (2020). *OECD economic outlook, interim report March 2020*. Retrieved from https://www.oecd-ilibrary.org/economics/oecd-economic-outlook/volume-2019/issue-2_7969896b-en

Otto, I., Donges, J., Cremades, R., Bhowmik, A., Hewitt, R., Lucht, W., … Schellnhuber, H. (2020). Social tipping dynamics for stabilizing Earth's climate by 2050. *Proceedings of the National Academy of Sciences of the United States of America*, *117*(5), 2354–2365.

Passell, P., Roberts, M., & Ross, L. (1972). The limits to growth. *The New York Times*. Retrieved from https://www.nytimes.com/1972/04/02/archives/the-limits-to-growth-a-report-for-the-club-of-romes-project-on-the.html

Pasqualino, R., Jones, A., Monasterolo, I., & Phillips, A. (2015). Understanding global systems today—A calibration of the World3-03 model between 1995 and 2012. *Sustainability*, *7*, 9864–9889. https://doi.org/10.3390/su7089864

Pearce, F. (2019). *As climate change worsens, a cascade of tipping points looms*. Retrieved from https://e360.yale.edu/features/as-climate-changes-worsens-a-cascade-of-tipping-points-looms

Plenty of gloom. (1997, December 18). *The Economist*. Retrieved from https://www.economist.com/christmas-specials/1997/12/18/plenty-of-gloom

Randers, J. (2000). From limits to growth to sustainable development or SD (sustainable development) in a SD (system dynamics) perspective. *System Dynamics Review*, *16*, 213–224.

Randers, J. (2012). *2052: A global forecast for the next forty years*. White River Junction, VT: Chelsea Green Publishing Co.

Simmons, M. R. (2000). *Revisiting the limits to growth: Could the Club of Rome have been correct, after all?* Eugene, OR: Mud City Press. Retrieved from http://www.mudcitypress.com/PDF/clubofrome.pdf

Smillie, S. (2017). From sea to plate: How plastic got into our fish. *The Guardian*. Retrieved from https://www.theguardian.com/lifeandstyle/2017/feb/14/sea-to-plate-plastic-got-into-fish

Solow, R. M. (1973). Is the end of the world at hand? *Challenge*, *16*, 39–50. https://doi.org/10.1080/05775132.1973.11469961

Sterman, J. (2000). *Business dynamics: Systems thinking and modeling for a complex world*. Boston, MA: Irwin/McGraw-Hill.

Sverdrup, H., & Ragnarsdóttir, K. (2014). Natural resources in a planetary perspective. *Geochemical Perspectives*, *3*, 129–341. Retrieved from https://doi.org/10.7185/geochempersp.3.2

Tans, P., & Keeling, R. (2019). *Globally averaged marine surface annual mean data* [Data file]. Retrieved from https://www.esrl.noaa.gov/gmd/ccgg/trends/data.html

Turner, G. M. (2008). A comparison of the limits to growth with 30 years of reality. *Global Environmental Change*, *18*, 397–411.

Turner, G. M. (2012). On the cusp of global collapse? Updated comparison of the limits to growth with historical data. *GAIA*, *21*(2), 116–124. Retrieved from https://www.ethz.ch/content/dam/ethz/special-interest/usys/ites/ecosystem-management-dam/documents/EducationDOC/Readings_DOC/Turner_2012_GAIA_LimitsToGrowth.pdf

Turner, G. (2013). The limits to growth model is more than a mathematical exercise: Reaction to R. Castro. 2012. Arguments on the imminence of global collapse are premature when based on simulation models. GAIA, 21/4: 271–274. *GAIA*, *22*, 18–19.

Turner, G. (2014). *Is global collapse imminent?* Parkville, VIC: Melbourne Sustainable Society Institute, The University of Melbourne. Retrieved from http://sustainable.unimelb.edu.au/sites/default/files/docs/MSSI-ResearchPaper-4_Turner_2014.pdf

United Nations Department of Economic & Social Affairs, Population Division (UN DESA PD). (2019). *Total population – Both sexes* [Datafile]. Retrieved from https://population.un.org/wpp/Download/Files/1_Indicators%20(Standard)/EXCEL_FILES/1_Population/WPP2019_POP_F01_1_TOTAL_POPULATION_BOTH_SEXES.xlsx

United Nations Development Programme (UNDP). (2019a). *Human development data (1990–2017)*. Retrieved from http://hdr.undp.org/en/data

United Nations Development Programme (UNDP). (2019b). *Education index (1990–2017)*. Retrieved from http://hdr.undp.org/en/content/education-index

United Nations Development Programme (UNDP). (2019c). *Technical notes*. (Human development indices and indicators: 2018 statistical update). Retrieved from http://hdr.undp.org/sites/default/files/hdr2018_technical_notes.pdf

United Nations Development Programme (UNDP). (2019d). *Frequently asked questions – Human development index (HDI)*. Retrieved from http://hdr.undp.org/en/faq-page/human-development-index-hdi#t292n2872

United Nations Environment Programme. (2002). *Global environment outlook 3*. Retrieved from https://www.unenvironment.org/resources/global-environment-outlook-3

United Nations Industrial Development Organization (UNIDO). (2019a). Selected database: INDSTAT 2 2019, ISIC Revision 3. Retrieved from https://stat.unido.org/database/INDSTAT%202%202019,%20ISIC%20Revision%203

United Nations Industrial Development Organization (UNIDO). (2019b). *Selected database: MVA 2019, manufacturing*. Retrieved from https://stat.unido.org/database/MVA%202019,%20Manufacturing

van Sebille, E., Wilcox, C., Lebreton, L., Maximenko, N., Hardesty, B. D., van Franeker, J. A., … Law, K. L. (2015). A global inventory of small floating plastic debris. *Environmental Research Letters*, *10*(12), 124006.

Vensim. (2020). *Free downloads*. Retrieved from https://vensim.com/free-download/

Vermeulen, P. J., & de Jongh, D. C. J. (1976). "Dynamics of growth in a finite world" – Comprehensive sensitivity analysis. *IFAC Proceedings Volumes*, *9*, 133–145. Retrieved from https://www.sciencedirect.com/science/article/pii/S1474667017673336

Westley, F., Olsson, P., Folke, C., Homer-Dixon, T., Vredenburg, H., Loorbach, D., … Leeuw, S. (2011). Tipping toward sustainability: Emerging pathways of transformation. *AMBIO*, *40*(7), 762–780.

World Bank (WB). (2019a). *Population, total*. Retrieved from https://data.worldbank.org/indicator/SP.POP.TOTL

World Bank (WB). (2019b). *Birth rate, crude (per 1,000 people)*. Retrieved from https://data.worldbank.org/indicator/SP.DYN.CBRT.IN

World Bank (WB). (2019c). *Death rate, crude (per 1,000 people)*. Retrieved from https://data.worldbank.org/indicator/SP.DYN.CDRT.IN

World Bank (WB). (2019d). *Gross fixed capital formation (constant 2010 US$)*. Retrieved from https://data.worldbank.org/indicator/NE.GDI.FTOT.KD

World Bank (WB). (2019e). *Government expenditure on education, total (% of GDP)*. Retrieved from https://data.worldbank.org/indicator/SE.XPD.TOTL.GD.ZS

World Bank (WB). (2019f). *Government expenditure on health, total (% of GDP)*. Retrieved from https://data.worldbank.org/indicator/SH.XPD.CHEX.GD.ZS

World Bank (WB). (2019g). *Unpublished Excel files* [Data files]. Retrievable from World Bank at request.

World Bank (WB). (2019h). *Global economic prospects: Slow growth, policy challenges*. Retrieved from https://www.worldbank.org/en/publication/global-economic-prospects#overview

World Economic Forum. (2015). *Deep shift: Technology tipping points and societal impact*. Retrieved from http://www3.weforum.org/docs/WEF_GAC15_Technological_Tipping_Points_report_2015.pdf

Wright, S. L., & Kelly, F. J. (2017a). Plastic and human health: A micro issue? *Environmental Science & Technology*, *51*, 6634–6647. https://doi.org/10.1021/acs.est.7b00423pmid:28531345

Wright, S. L., & Kelly, F. J. (2017b). Threat to human health from environmental plastics. *BMJ*, *358*(4334), j4334. Retrieved from https://doi-org.ezp-prod1.hul.harvard.edu/10.1136/bmj.j4334

SUPPORTING INFORMATION

Additional supporting information may be found online in the Supporting Information section at the end of the article.

How to cite this article: Herrington G. Update to limits to growth: Comparing the world3 model with empirical data. *J Ind Ecol*. 2020;1–13. https://doi.org/10.1111/jiec.13084